Order Number 9312195

Sedimentary and tectonic processes along the Peru-Chile Trench

Hagen, Ricky Allen, Ph.D.

University of Hawaii, 1992

U·M·I

300 N. Zeeb Rd.
Ann Arbor, MI 48106

SEDIMENTARY AND TECTONIC PROCESSES ALONG THE PERU-CHILE TRENCH

A DISSERTATION SUBMITTED TO THE GRADUATE DIVISION OF THE UNIVERSITY OF HAWAII IN PARTIAL FULFILLMENT OF THE REQUIREMENTS FOR THE DEGREE OF

DOCTOR OF PHILOSOPHY

IN

GEOLOGY AND GEOPHYSICS

DECEMBER 1992

By

Ricky A. Hagen

Dissertation Committee:

Ralph Moberly, Chairperson
Patricia Cooper
Frederick Duennebier
Gregory Moore
Alexander Shor
Alexander Malahoff

ACKNOWLEDGMENTS

A large part of the person I am today (for better or worse) was formed in a small town in Wisconsin by a large and close extended family and a caring community of friends and neighbors. My parents encouraged me to do well in school, with the thought, I believe, that I might someday be the first in the family to go to college. Well, I certainly accomplished that goal, and I think that they must have wondered over the years if I were ever going to stop going to school and get a "real" job! I know that in many cases it was hard for my family to understand what I was doing and why, but their love and support never wavered, and I thank them for all that they have given and done for me.

I realized just the other day, that I have spent almost 1/4 of my life here in Hawaii. I know that I am not the same person who stepped off the plane 8 years ago. I have learned a lot in the intervening time - both about the world and about myself, and most of this growing and learning process occurred within the ever-changing community of friendly, caring people that make up HIG/SOEST. When I sat down to list all of the people I want to thank (for help, friendship, and support), I realized that it would comprise a chapter in itself. I thank Lisa Petersen for her love and all that she has shared with me. For the rest, I will issue a blanket THANK YOU to everyone who has touched my life and made my time in Hawaii so special - know that I thought of you all as I wrote these words.

There are people I want to thank by name, however, people who are not only friends and colleagues, but who also provided research opportunities, guidance, and advice in this research project (and other side projects), and who supported me financially these many years. Ralph Moberly and Bill Coulbourn allowed me to be involved in their research on the Peru - Chile forearc, on which this dissertation is based, and supported me financially. Ralph also served as my research advisor, and I thank him for being there when I had problems, for encouraging me to get involved in other projects, and for letting

me set my own course to the completion of this dissertation. Bill Coulbourn was the main instigator of our studies of the Peru - Chile forearc, and his untimely death in 1990 deprived us all of a good friend and colleague. Sandy Shor allowed me to use SeaMARC/HMRG computers, equipment, supplies, and expertise while I processed the SeaMARC II data used in my research, and also provided financial support.

One of the reasons it took me so long to finish this project is that I kept allowing people to sidetrack me on interesting projects unrelated to my dissertation. They may have taken some of my time, but they also contributed greatly to my education (and fattened my vitae!). Fred Duennebier took me along on an interesting cruise in the Marshall Islands. Dick Hey and Dave Naar invited me to work with them on the Easter Microplate data. Loren Kroenke gave me a tour of the Ontong Java Plateau on ODP Leg 130. Sandy Shor sent me to the north Atlantic and also let me turn a comprehensive exam question into a paper on the Mariana Trough. I thank all of these people for the opportunities they have given me to work with and learn from them.

The research presented in this dissertation was supported by the National Science Foundation (grant OCE-8610056). I was also an Achievement Rewards for College Scientists (ARCS) scholarship recipient in 1987.

ABSTRACT

Geophysical data collected in several areas along the Peru-Chile Trench are used to examine sedimentary and tectonic processes occurring at this plate boundary.

A survey of the Peru forearc using the SeaMARC II seafloor mapping system reveals that subduction of the Nazca Ridge caused uplift of the forearc by as much as 1500 m. This uplift is seen in the varied depths of two forearc terraces opposite the subducting ridge. Oblique lineaments on the forearc may be faults with a strike-slip component of motion caused by the oblique subduction of the Nazca Ridge. The trench in this area is nearly linear, with no re-entrant in the forearc due to subduction of the Nazca Ridge. Compressional deformation of the forearc due to subduction of the ridge is relatively minor; the gently sloping Nazca Ridge is able to slide beneath the forearc without significantly deforming it.

The subducting plate at the Peru-Chile trench is pervasively faulted as the plate is bent into the subduction zone. Normal faulting is dominant and begins about 50 km from the trench axis, increasing in frequency and offset toward the trench. In the Lima Basin, Arica Bight, and Iquique Basin areas, fault trends on the outer wall of the trench parallel the trend of magnetic anomalies on the Nazca Plate. In the Nazca Ridge area, faulting parallels the trench, probably because of a lack of spreading fabric on the ridge. In the Yaquina Basin area faulting follows neither the trench nor the spreading fabric trend. This may be caused by extension across the nearby Mendaña Fracture Zone. These results generally agree with a previous study, which concluded that faulting follows the trend of the spreading fabric as long as it differs from the strike of the trench by less than 30°.

Intrusive and extrusive volcanic areas are observed on the subducting plate in several areas. These volcanic features appear to have formed well after the seafloor was

created at the ridge crest. Many of the areas are cut by faulting, however, indicating that they formed before the seafloor entered the zone of subduction-induced faulting.

Side-scan sonar data collected in the Arica Bight area reveal an extensive submarine canyon system in the East Arequipa Basin. The main branch of this canyon system extends for more than 100 km along the axis of the basin, is 350 to 1100 m wide, and has relief of 160 to 230 m through most of this distance. The canyon is highly meandering, with an overall sinuosity of almost 2, comparable to highly meandering subaerial rivers.

This canyon probably developed from channelized turbidity flows that moved down the axis of the basin from the north. As the basin filled, the main distributary channel within the basin became a conduit to bypass sediment onto lower forearc. The canyon appears to extend upslope to the mouth of the Rio Tambo in southern Peru and may have been fed by turbidity currents from its delta front. Terraces along the submarine canyon developed as meander belts during periods of canyon stability. Downcutting of the canyon and entrenchment of the meanders may have been caused by faulting of the forearc seaward of the structural high, or piracy of the lower canyon.

Extension of the forearc of southern Peru and northern Chile has produced a series of en-echelon forearc slope basins. The basins form north-south oriented troughs that are oblique to the curving subduction zone in the Arica Bight area. The faults that define the forearc slope basins break the middle forearc slope into large blocks that are visible in side-scan and bathymetry data. These north-south trending faults interact with trench-parallel faults to create embayments visible in the forearc bathymetry. Growth of these embayments continues through surface erosion and slumping.

A prominent angular unconformity is visible in seismic profiles across the East and West Arequipa basins. The unconformity and the sediments beneath it dip to the west, indicating subsidence of the leading edge of the forearc. A model is proposed in which

extension of the forearc produced block-faulted depressions into which sediment was deposited. Faulting was later concentrated along the margins of these basins and they developed half-graben forms. Following this rotational motion, deposition of sediment was concentrated in the deep portions of the basins next to the boundary faults. Sediment loading and uplift of the bounding structural highs cause the basin sediments to dip toward the center of the basins. The extension observed in the offshore portion of the forearc in the Arica Bight area is consistent with structures observed on land, and fits into a pattern of tectonic erosion of the forearc that has been observed at other places along the Peru-Chile Trench. This extension may also result from lateral motion of lower forearc slivers along trench-parallel strike-slip faults. This could remove support at the base of the forearc slope, causing faulting and westward extension on the upper slope.

TABLE OF CONTENTS

LIST OF TABLES

LIST OF ILLUSTRATIONS

CHAPTER 1

INTRODUCTION

The existence of a deep trench along the west coast of South America was first reported by ships laying submarine telegraph cables in the late 1800s. The first bathymetric maps of the southeast Pacific delineating the trench were published by Murray in 1895 based on results of the CHALLENGER expedition. Charts of this area remained essentially unchanged until the Shellback expedition of 1952 and the ATLANTIS cruise of 1955 [*Ziegler et al.*, 1957] made several crossings of the trench area with precision depth recorders. The Downwind expedition of 1957-58 collected 5400 miles of echosounding traverses over the trench as well as several seismic refraction stations. *Fisher and Raitt* [1962] combined these data with results from the earlier cruises to produce fairly detailed bathymetric maps.

By this point in time the available bathymetric, seismic, and gravity data from this region showed all of the features that plate tectonics would later recognize as evidence for a subduction zone: a deep oceanic trench; a large negative gravity anomaly along and slightly shoreward of the trench; a line of Tertiary to Recent volcanoes to the east; and seismic activity at depths of 70-300 km, also to the east of the trench. With the advent of plate tectonics in the late 1960s, the Peru-Chile trench was recognized as the prime example of an "Andean type" subduction zone where an oceanic plate is being subducted beneath a continental plate.

The Nazca Plate Project, a multidisciplinary effort by scientists from the Hawaii Institute of Geophysics (HIG) and Oregon State University (OSU) in the 1970s, collected thousands of kilometers of geophysical data over nearly the whole length of the trench and forearc. These data sets were used by several authors [*Coulbourn and Moberly*, 1977;

Schweller et al., 1981; *Johnson and Ness*, 1981; *Couch and Whitsett*, 1981; and *Coulbourn*, 1981] to define the tectonics, structure, and sedimentary framework of the Nazca plate and the continental margin. Subsequent studies utilizing multi-beam bathymetric and side-scan sonar systems such as GLORIA [*Warsi et al.*, 1983], Sea Beam [*Bourgois et al.*, 1988], and SeaMARC II [*Bartlett*, 1987; *Hussong et al.*, 1988], have refined our models of the subduction process and revealed a wealth of new information on small-scale features.

In August 1987 SeaMARC II, single-channel seismic, and standard underway geophysical data were collected near the intersection of the Nazca Ridge with the trench and in the Arica Bight region (Figure 1.1). The Nazca Ridge survey was conducted primarily to investigate the collision of this large aseismic ridge with the forearc. The Arica Bight region was surveyed to determine the pathways of sediment transport and the relationship between sedimentation and basin evolution.

The continental margin of southern Peru and northern Chile

The coastline of South America trends roughly 130° from Lima, Peru, to Arica in northern Chile. At this point the coast swings in a broad curve to trend nearly north-south. This broad seaward concavity in the coast has been termed the Arica Bight [*Coulbourn and Moberly*, 1977]. The Peru-Chile trench closely mimics the trend of the coast throughout this area (Figure 1.1).

The Nazca Plate is subducting beneath the South American plate along the trench at a rate of about 90 mm/yr on an azimuth of about 081° in southern Peru and northern Chile. The distribution of earthquake hypocenters clearly defines a generally shallow-dipping Wadati-Benioff zone beneath Peru and Chile [*Barazangi and Isacks*, 1976; 1979]. The hypocenters appear to define a tear or bend in the subducting plate that separates the

Figure 1.1 Location map showing SeaMARC II surveys along the Peru-Chile forearc. The Yaquina and Lima Basin surveys were conducted in 1985 and served as site surveys for drilling on ODP Leg 112 [*Hussong et al.*, 1988]. The Nazca Ridge, Arica Bight, and Iquique Basin surveys were conducted in 1987.

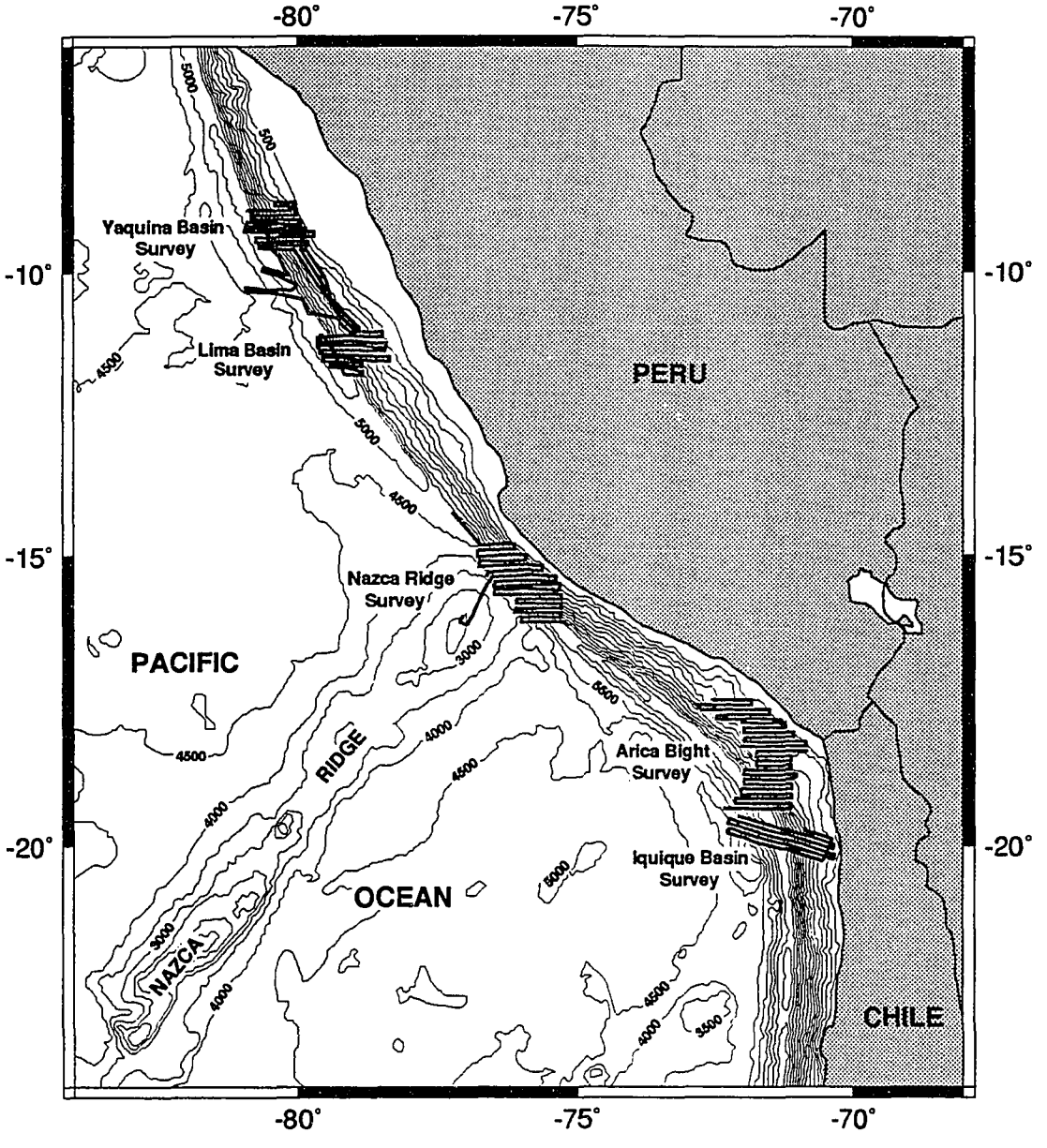
-80°
-75°
-70°
-10°
-15°
-20°
Yaquina Basin Survey
Lima Basin Survey
Nazca Ridge Survey
Arica Bight Survey
Iquique Basin Survey
PERU
CHILE
PACIFIC
OCEAN
NAZCA
RIDGE
5000
4500
4000
3500
3000

shallow dipping (about 10°) seismic zone beneath central Peru from the more steeply dipping (about 30°) zone beneath southern Peru and northern Chile. The portion of the plate currently being subducted along southern Peru and northern Chile is at least 36 Ma [*Handschumacher,* 1976] and has a NNW-SSE magnetic lineation fabric that was created at a spreading center.

The subducting plate is broken by a network of normal faults as it moves over the outer swell into the trench and may develop horsts and reverse faults as it undergoes compression in the trench axis [*Coulbourn and Moberly,* 1977; *Schweller and Kulm,* 1978; *Schweller et al.,* 1981; *Coulbourn,* 1981; and *Warsi et al.,* 1983]. Relief of the outer swell in this area is less than normal for most island arc trenches in the western Pacific with the exception of the Arica Bight where a rise of nearly 1 km occurs seaward of the trench [*Schweller et al.,*1981]. The Nazca Plate near the trench in this region is covered by a relatively thin (generally less than 125 ms) blanket of sediment.

The Nazca Ridge is a large linear aseismic ridge which rises to an average depth of 2 to 3 km from the 4 to 4.5 km depths of the surrounding seafloor. The ridge intersects the trench at about 15° S, is oriented northeast-southwest, is more than 200 km wide, and extends for over 1100 km to the southwest (Figure 1.1). The Nazca Ridge is believed to result from the interaction of a hotspot with a spreading center and is therefore thought to be the same age as the surrounding seafloor [*Cutler,* 1977; *Pilger and Handschumacher,* 1981]. The direction of convergence of the Nazca and South American plates is approximately east-west in this area. Because of the 130° trend of the Peruvian coast, the Nazca Ridge is believed to have swept down the coast from the north. This movement has been recognized as uplift and subsidence in the geologic record along the coast [*von Huene et al.,* 1988].

The Peru-Chile trench is shallower than most island-arc trenches in the western Pacific, some of which reach depths of more than 8 km. Axial depths off Peru and

southern Chile are 6.5 km or less; off northern Chile the trench is deeper than 7.5 km. Where the Nazca Ridge intersects the trench the trench axis shoals to less than 5 km. The trench axis north of the Nazca Ridge contains minor amounts of ponded turbidites supplied from the forearc and transported along axis from the north. The Nazca Ridge apparently acts as a barrier to further southward flow. Immediately south of the ridge the trench is essentially free of sediment [*Schweller et al.*, 1981]. This lack of sediment reflects the arid climate of the coast in this area. No permanent streams reach the shoreline between 18° S and 30° S and much of the sediment eroded from the Andes is trapped inland [*Galli-Olivier*, 1969].

The forearc of the Peru-Chile trench is commonly divided into the lower, middle, and upper slopes. The lower slope rises fairly steeply (7°-10°) from the trench axis to about 4 km water depth. This region appears chaotic and no discernable layering is observed in seismic records. Narrow ledges on the lower slope appear to be laterally continuous on SeaMARC II data collected to the north of the Nazca Ridge [*Bartlett*, 1987; *Hussong et al.*, 1988] and have been interpreted as the surface expression of accreted imbricate sediment packets. The upper levels of these small benches are often covered by a veneer of presumably terrigenous sediments [*Coulbourn*, 1981].

The mid-slope area is transitional between the lower slope and the nearly flat upper slope basins. The mid-slope generally extends from 4 to 2 km depth and has a regional slope of 3° to 5°. This level of the forearc is commonly characterized by a series of small sediment filled benches and basins that are fed by debris flows and channels from higher on the slope. The mid-slope area is separated from the upper slope by a structural high that appears to consist of outcropping layers of lithified terrigenous sediment. The structural high appears to be deformed along strike in some areas into a series of cumulations and depressions that divide the forearc laterally into a series of discrete basins [*Coulbourn*, 1981].

The upper slope is generally characterized by gentle slopes of 1° to 3°. Seismic sections through these basins commonly show an increasing landward dip of the seismic layers with increasing depth. This has been interpreted as indicating progressive uplift of the structural high with time or downthrow and rotation along faults bounding the basins [*Coulbourn and Moberly,* 1977].

Data used in this study

The primary dataset used in this study was collected aboard the R/V MOANA WAVE in August 1987. These data consist of: SeaMARC II side-scan sonar reflectivity and swath bathymetry, single-channel seismic reflection profiles, gravity, 3.5 kHz echosounder profiles, and dredge hauls. Additional bathymetric and gravity data from other cruises in the area were aquired through the National Geophysical Data Center (NGDC). SeaMARC II and single-channel seismic reflection data from the Lima Basin and Yaquina Basin areas of the Peru coast were collected by Don Hussong in 1985 and are used with his permission. Multichannel seismic lines from offshore in the Arica Bight region were funded by the United Nations and collected by Western Geophysical Company for Empresa Nacional del Petroleo (ENAP). These lines, and important onshore geological information, were provided by Ricardo Fuenzalida of ENAP.

Single-channel seismic reflection data collected during the 1987 surveys are of poor quality. The data suffer from a variety of problems including a balky and under-powered source (a single 40 in^3 airgun) and problems with a newly installed digital recording system. As a result, penetration is poor (particularly in deep water) and there are numerous gaps in the digital data due to computer crashes and tape changes. Nevertheless, the seismic data provides important structural and stratigraphic information.

SeaMARC II was a shallow towed (50 to 150 m) side-scan sonar mapping system that collected sonar backscatter data in swaths up to 10 km wide and bathymetric data with a swath width equal to 3.4 times the water depth. The system operated at frequencies of 11 kHz on the port side and 12 kHz on the starboard side. Survey speed was generally about 8 kts. At this speed nearly 3500 km^2 of seafloor can be surveyed per day.

SeaMARC II swath bathymetry is determined by measuring phase differences of acoustic arrivals at a pair of transducer arrays on either side of the tow vehicle. The acoustic angle is converted to an electrical angle that is then compared to a lookup table (generated from data collected over flat ground) to arrive at a depth. Bathymetric resolution is limited to about 2% of water depth [*Blackinton*, 1986; *Matsumoto*, 1990].

The SeaMARC II bathymetry used in this study is of somewhat variable quality. At the time of the survey, the system was transmitting weakly on the port side. This power problem does not significantly affect the quality of the side-scan backscatter images. The port side bathymetry, however, is noticeably noisier than the starboard side, particularly in the deep water over the trench axis. The bathymetry was processed following the cruise to facilitate computer manipulation and display of the images. The bathymetric phase data were first filtered to reduce system noise and converted to across-track depths. The resulting depth data were then gridded into longitude, latitude, and depth triples (at 200 to 250 m horizontal spacings) using a nearest-neighbor gridding algorithm. The resulting data are displayed as computer-generated contour plots and shaded relief images.

Side-scan resolution is a function of many variables and is both range- and orientation-dependent. The resolution of the SeaMARC II system is on the order of several tens of meters [*Johnson and Helferty,* 1990]. The backscatter data were corrected for slant range (based on water depth below the tow vehicle), beam-pattern errors, bottom-tracking errors, and gain variations. The individual image swaths for the various tracks were then gridded and assembled into a mosaic of the survey area. The side-scan data are displayed

with areas of high reflectivity represented by dark gray to black tones and low reflectivity areas plotted as shades of light gray to white.

Two types of processing [*Sender et al.*, 1989; *Shor*, 1990] are presently used to produce side-scan images by the SeaMARC II group at HIG. The first, the "age" presentation, attempts to preserve relative backscatter intensity (displayed graphically as gray levels, with dark showing the highest backscatter). This is done by removing the effects of gain steps (caused by operator adjustments during data collection) and recalculating the data back to a uniform gain amplification. Once the data have been corrected in this manner, a table of display levels is calculated, uniformly distributing all the data values into sixteen gray shades. The objective is to maximize contrast while simultaneously preserving, to the degree possible, the relative regional backscatter characteristics.

The disadvantage of the "age" processing technique for interpreting tectonics is that the limited dynamic range of grayscale presentation prevents one from observing the details of structure in the data, as the local contrasts are overwhelmed by the regional crustal backscatter variations. Additionally, in some data sets the "age" method results in clipping at either the high or low end (or both), as the 256 data intensity levels recorded do not provide a dynamic range which is adequate to fully represent the backscatter intensity of all seafloor terrain at constant amplification.

The technique used to enhance the local backscatter variations we call the "structure" presentation. In the "structure" technique of processing, the operator-applied gain steps in the data are smoothed by comparing data levels on both sides of the step and applying a ramp of gain factors over a 15-minute interval to either side of the gain step. This technique smooths out the offset, and maintains the data levels as a well-behaved histogram (assuming operators have monitored data acquisition well, and collected data without clipping, and also that the local dynamic range of returns does not exceed that of

the system). The second step, and the one that enhances the local backscatter variations (i.e. structure), is to calculate tables of display levels at closely-spaced intervals from the data itself for conversion of backscatter amplitude values to grayscale levels. For this study, tables of display levels were calculated every 15 minutes, with a smooth interpolation of table values from one table to the next over a 10-minute interval. The resulting image removes most of the regional (long wavelength) backscatter variation, and emphasizes the finer scale changes (structure).

The "age" presentation is most useful when long-wavelength regional backscatter information is needed or, in mid-ocean ridge and other volcanic areas, when a sense of relative age of volcanic features is desired. The "structure" presentation is useful when one is interested in small-scale structural or sedimentological features of the seafloor. The "structure" method is the technique that was used to process all of the side-scan data presented here.

Dissertation Organization

Chapter 2 of this dissertation presents the results of a study of the Peru-Chile Trench at about 15° S where the Nazca Ridge is currently being subducted. This study uses SeaMARC II side-scan and swath bathymetry and single-channel seismic reflection data to examine the effect that subduction of the ridge has on the forearc. Some of the results of this study were presented at the 1991 fall meeting of the American Geophysical Union in San Francisco, California [*Hagen*, 1991]. A paper based on this chapter has been submitted to *Marine Geophysical Researches* for publication.

Chapter 3 is a short study that examines the faulting of the subducting Nazca Plate that is observed in five SeaMARC II surveys along the Peru-Chile Trench. The faulting is observed to be oblique to the trend of the trench and appears to follow the trend of the pre-

existing seafloor spreading fabric. A paper based on this chapter has been submitted to *Geo-Marine Letters* for publication.

Chapter 4 examines a large submarine canyon system in the East Arequipa Basin of southern Peru. The canyon system is highly meandering and I propose that it did not form by headward erosion, but evolved from channelized turbidity flows that filled the basin. A paper based on this chapter has been submitted to *Marine Geology* for publication.

In Chapter 5, I examine the morphology and structure of the forearc in the Arica Bight area. I show that the forearc has undergone extension and rifting and present a model for the evolution of the forearc slope basins that is consistent with tectonic erosion of the forearc. This study will be presented at the 1992 fall meeting of the American Geophysical Union in San Francisco, California in early December.

CHAPTER 2

TECTONIC EFFECTS OF A SUBDUCTING ASEISMIC RIDGE: THE SUBDUCTION OF THE NAZCA RIDGE AT THE PERU TRENCH

Abstract

A 1987 survey of the offshore Peru forearc using the SeaMARC II seafloor mapping system reveals that subduction of the Nazca Ridge has resulted in uplift of the lowermost forearc by as much as 1500 m. This uplift is seen in the varied depths of two forearc terraces opposite the subducting ridge. Uplift of the forearc has caused fracturing, minor surficial slumping, and increased erosion through debris channels. Oblique trending linear features on the forearc may be faults with a strike-slip component of motion caused by the oblique subduction of the Nazca Ridge. The trench in the zone of ridge subduction is nearly linear, with no re-entrant in the forearc due to subduction of the Nazca Ridge. Compressional deformation of the forearc due to subduction of the ridge is relatively minor, suggesting that the gently sloping Nazca Ridge is able to slide beneath the forearc without significantly deforming it. The structure of the forearc is similar to that revealed by other SeaMARC II surveys to the north, consisting of (1) a narrow (10 to 15 km wide) zone of accreted material making up the lowermost forearc, (2) a chaotic middle forearc, (3) outcropping consolidated material and draping sediment on the upper forearc, and (4) the smooth, sedimented forearc shelf.

The subducting Nazca plate and the Nazca Ridge are fractured by subduction-induced faults with offsets of up to 500 m. Normal faulting is dominant and begins about 50 km from the trench axis, increasing in frequency and offset toward the trench. These faults are predominantly trench-parallel. Reverse faults become more common in the deepest portion of the trench and often form at slight angles to the trench axis.

Intrusive and extrusive volcanic areas on the Nazca plate appear to have formed well after the seafloor was created at the ridge crest. Many of the areas show evidence of current scour and are cut by faulting, however, indicating that they formed before the seafloor entered the zone of subduction-induced faulting.

Introduction

In August 1987 geophysical surveys of the Peru Trench and forearc were conducted aboard the *R/V Moana Wave*, operated by the Hawaii Institute of Geophysics. SeaMARC II side-scan sonar backscatter images and swath bathymetry, gravity, single-channel seismic reflection, and 3.5 kHz echosounder data were collected over the forearc, trench, and subducting plate at the point where the Nazca Ridge is currently subducting beneath South America (Figure 1.1). The side-scan sonar reflectivity images and swath bathymetry provide continuous coverage of an area greater than 18,000 km^2.

The Nazca Ridge is a large linear aseismic ridge which rises to an average depth of less than 3 km from the 4 to 4.5 km depths of the surrounding seafloor. The ridge intersects the trench at about 15° S, is oriented northeast-southwest (about 055°), is more than 200 km wide, and extends for more than 1100 km to the southwest where it intersects the Easter Seamount Chain (Figure 2.1). The Nazca Ridge is believed to have formed by the interaction of a hotspot with a spreading center, in a manner similar to the present interaction of the Iceland hotspot with the mid-Atlantic Ridge, and is therefore thought to be the same age as the adjacent seafloor [*Cutler*, 1977; *Pilger and Handschumacher*, 1981]. Seismic refraction and gravity studies [*Cutler*, 1977; *Couch and Whitsett*, 1981] indicate that the crust beneath the ridge is at least twice as thick as the surrounding seafloor. The present direction of convergence of the Nazca and South American plates is approximately E-W (about 90 mm/yr toward 081°) in this area [*Cande*, 1986]. Because of the 310° trend

of the Peruvian coast, the Nazca Ridge is believed to have swept down the coast from the north at a rate of about 55 km/my. Evidence for this movement has been recognized in the geologic record along the coast as a migrating period of uplift and subsidence [*von Huene et al.*, 1988; *von Huene*, in press] and has also been observed in the sedimentary history recorded in ODP Leg 112 cores [*Suess et al.*, 1988].

Data Interpretation

Figure 2.1 shows the SeaMARC II side-scan sonar mosaic of the main Nazca Ridge survey area. The area shown includes portions of the forearc, the trench axis, and the central and southern portions of the Nazca Ridge on the subducting Nazca Plate (Figure 2.2). The seafloor surveyed ranges in depth from about 370 m on the edge of the shelf to almost 6400 m in the trench axis (Figure 2.3).

The Nazca Plate and the Nazca Ridge

One of the most striking features of the side-scan mosaic is the pattern of dark stripes on the subducting Nazca plate (Figure 2.1). These stripes are generally parallel to the trench axis and vary in length from less than 5 km to more than 50 km. Seismic reflection and 3.5 kHz echosounder profiles show that these features are fault scarps. The high backscatter of the faults is caused by the rough surface of the scarps and their high angle to the sonar vehicle. They thus stand out in sharp contrast to the 200 to 300 m of smooth pelagic sediment that covers the rest of the plate. Faulting of this type is a common feature of the subducting plate at many subduction zones [*Jones et al.*, 1978; *Masson*,

Figure 2.1 SeaMARC II side-scan sonar backscatter mosaic of the Nazca Ridge survey area. The data are presented with high backscatter areas displayed as dark tones and low backscatter areas as light grays. Individual side-scan swaths are 10 km wide. The boundary between the Nazca and South America plates runs diagonally through the survey from northwest to southeast. The subducting Nazca plate is broken by numerous trench-parallel faults and scattered small volcanoes and lava flows.

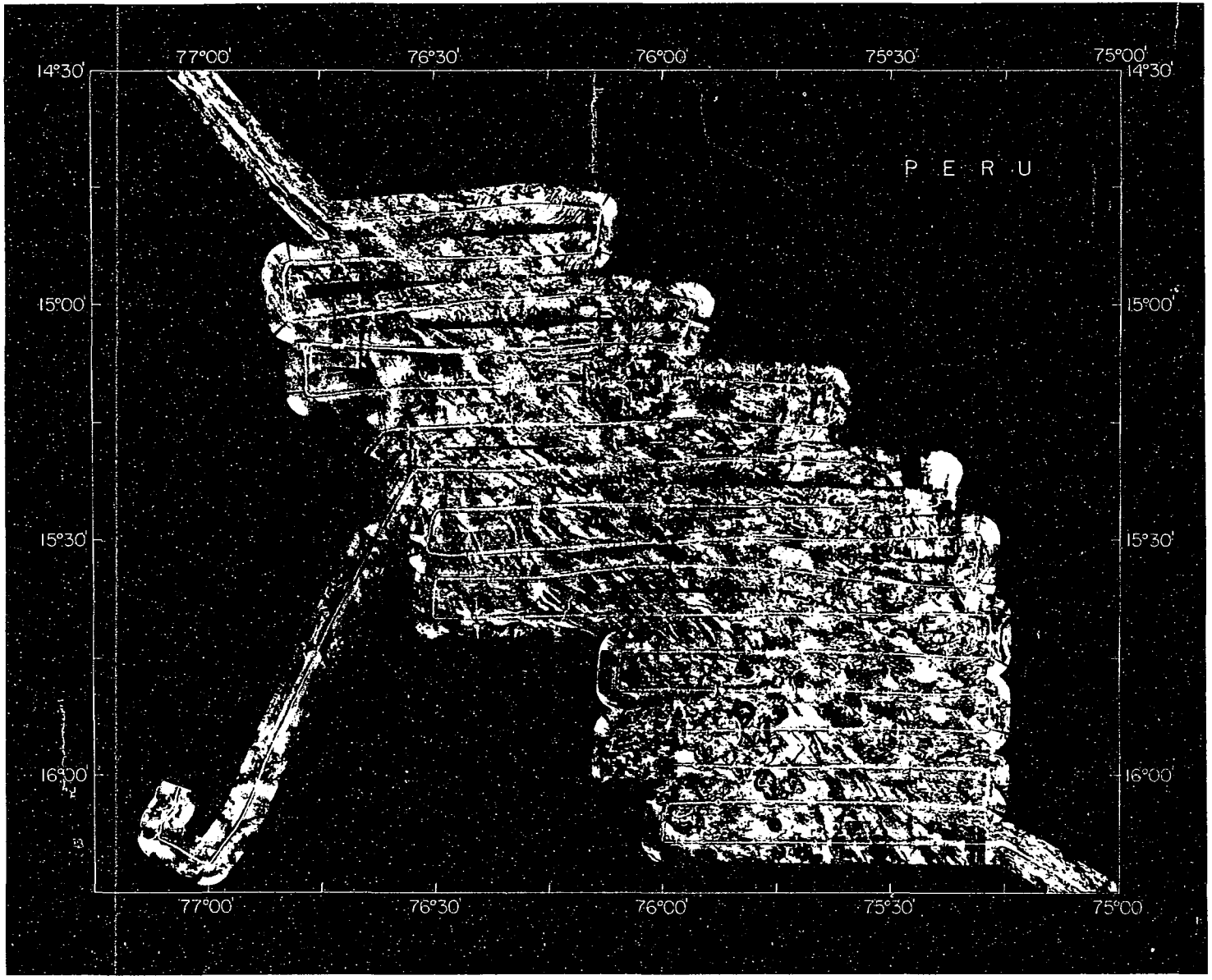
77°00'
76°30'
76°00'
75°30'
75°00'
14°30'
15°00'
15°30'
16°00'
P E R U

Figure 2.2 Geologic interpretation of SeaMARC II side-scan and bathymetry data from the Nazca Ridge survey area. Normal faults on the subducting Nazca plate are indicated by thin solid lines. Reverse faults are shown by thicker solid lines. Heavily sedimented volcanic areas on the Nazca plate are shown by the "v" pattern, lightly sedimented volcanic areas are shown by the gray pattern. Individual volcanoes and lava flows are shown in black. Terraces on the forearc are stippled. Diagonal dashed lines separate the lower and middle forearc and the upper forearc and the shelf. Faults, fractures, and other lineations on the forearc are shown by dashed lines.

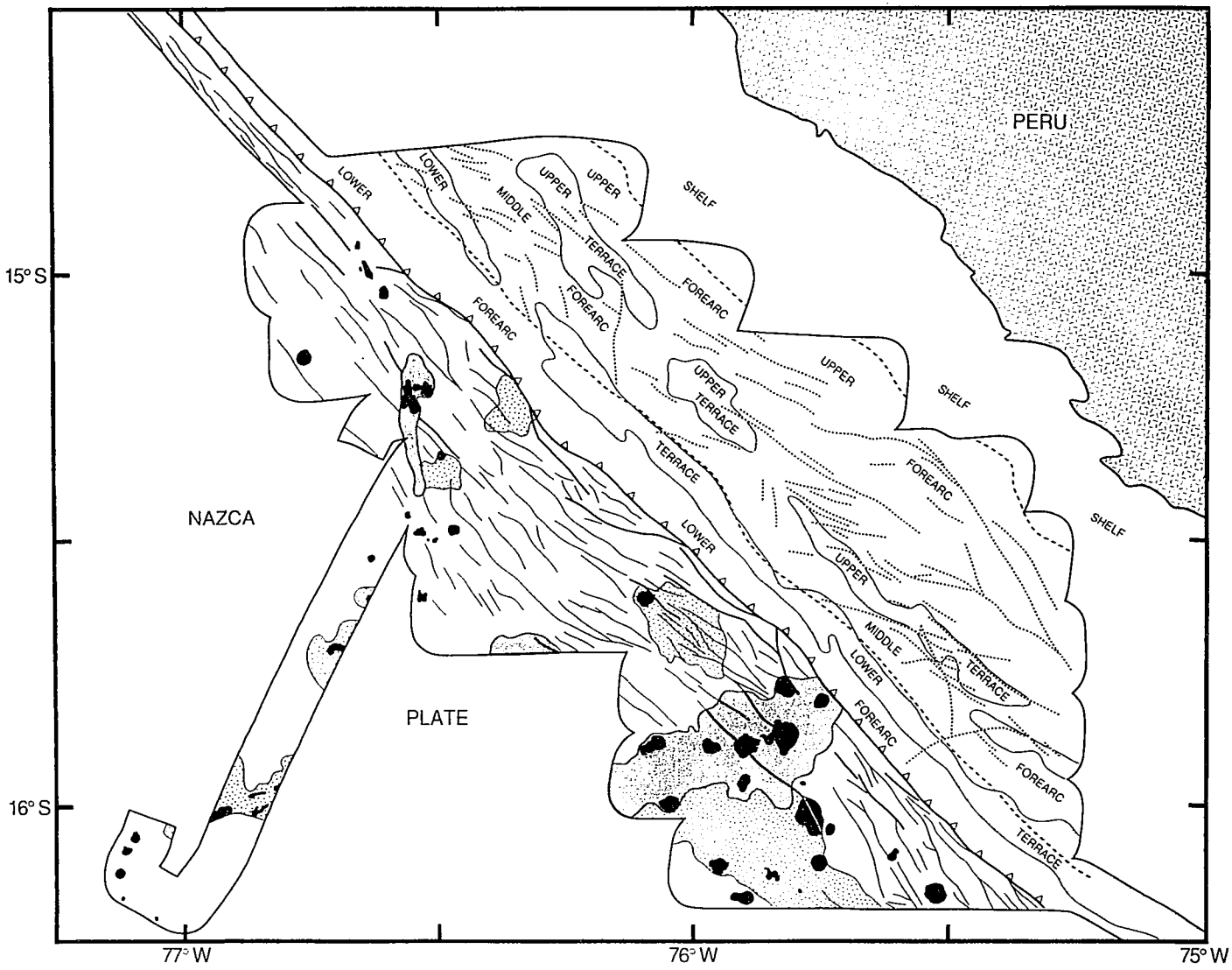
PERU
NAZCA
PLATE
15° S
16° S
77° W
76° W
75° W
LOWER
MIDDLE
UPPER
TERRACE
FOREARC
SHELF

Figure 2.3 Hand-contoured SeaMARC II bathymetry of the Nazca Ridge survey area. Contour interval is 100 m. The terraced nature of the forearc is seen in the varied spacing of the contour lines. The dashed boxes show the locations of side-scan closeup figures 2.4, 2.5, 2.6, and 2.7. The location of seismic reflection profile A - A' (Figure 2.9) is also indicated.

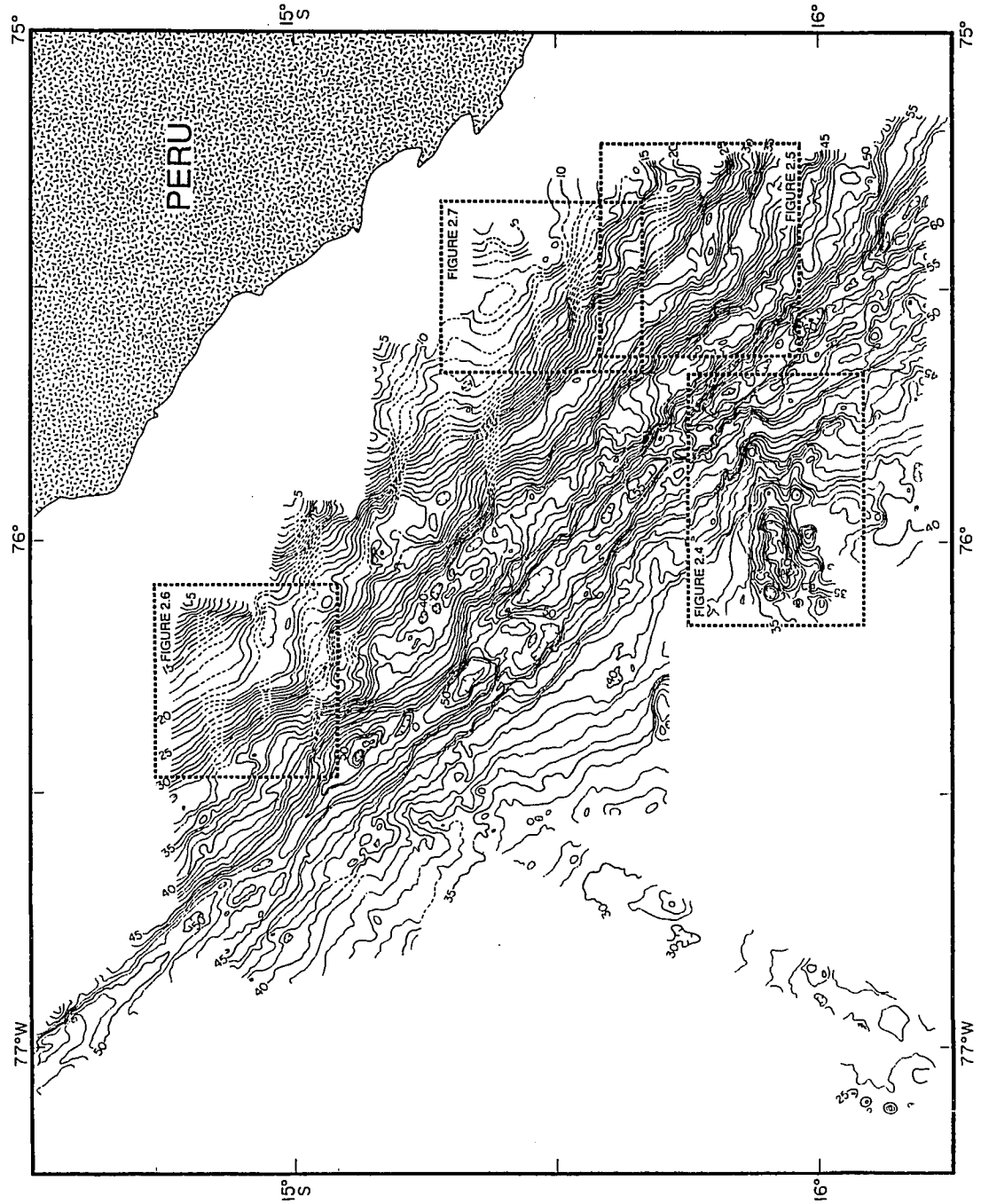
PERU
FIGURE 2.4
FIGURE 2.5
FIGURE 2.6
FIGURE 2.7
75°
76°
77°W
15°S
16°

1991] and is believed to be caused by tension in the surface of the plate as it bends into the subduction zone.

Fault offsets were determined from seismic and 3.5 kHz echosounder profiles, SeaMARC II bathymetry, and side-scan backscatter look directions. Faulting begins approximately 50 km west of the trench and increases in both frequency and offset toward the trench axis. Normal faults predominate throughout this area; reverse faults are usually confined to the deeper portions of the trench (Figure 2.2). The offset along each fault varies along strike, but, in general, fault offsets increase toward the trench axis, reaching more than 500 m in some places.

Other prominent features on the subducting Nazca plate are the scattered dark areas of high backscatter that stand out in sharp contrast to the smooth, sedimented seafloor (Figure 2.1). These areas occur as low, irregularly shaped regions and as small sub-circular conical features with relief of 200 to 300 m. We interpret these areas as small volcanoes and lava flows (Figure 2.2). These volcanic features do not appear to be genetically related to the faulting of the subducting plate as there is no evidence in the seismic or side-scan data of volcanics erupting along a fault. Many of the volcanoes and lava flows are cut by subduction-induced faulting, however, indicating that they formed before the seafloor entered the stress field associated with the subduction zone. Current scour around some of these features also suggests that they are older, sediment-covered volcanoes that have been recently exposed by bottom currents.

Figure 2.4 shows the largest of these volcanic features, a small volcanic ridge on the southeast flank of the Nazca Ridge. This ridge trends about 065°, nearly perpendicular to the trench axis, and is cut by several trench-parallel faults. The ridge is about 800 m high and is about 40 km long and 15 to 20 km wide. It is topped by several small (3 to 5 km diameter), semi-circular volcanoes that are 200 to 300 m high. A single dredge of one of these volcanoes recovered mildly alkalic basaltic glass with TiO_2, Na_2O, and K_2O levels

Figure 2.4. SeaMARC II side-scan sonar image of a small volcanic ridge on the subducting Nazca plate. The ridge rises about 800 m above the surrounding seafloor. The ridge is capped by several small volcanoes and is cut by subduction-induced faulting. High backscatter lava flows are exposed at the western end of the ridge, whereas the eastern portion of the ridge has more sediment cover. The east-west oriented gray lines are areas of no data beneath the shiptrack. Bottom detect and crosstalk are data acquisition errors. Figure location is shown on Figure 2.3.


VOLCANO
FAULTS
TRENCH AXIS
VOLCANO
VOLCANO
FAULTS
LAVA FLOW
VOLCANIC RIDGE
FAULT
CROSSTALK
BOTTOM DETECT
ERROR
FAULTS
VOLCANO
-15° 50'
-16° 00'
-76° 10'
-76° 00'
-75° 50'

that are too high to be related to a mid-ocean ridge basalt parent magma (Table 2.1) [M. Garcia, *pers. comm.*]. This supports the hypothesis that these features were created by off-ridge volcanism after the underlying seafloor was created at the mid-ocean ridge.

The intersection of the Nazca Ridge with the Peru Trench creates a shallowing of the trench axis, where the axial depth rises to less than 4800 m (Figure 2.3). The trench to the north is deeper than 5300 m, whereas to the south depths quickly become greater than 6200 m. The trench in this area is nearly devoid of terrigenous sediment, with the width of the trench axis controlled by the width of the individual fault block currently being subducted. The contact between the subducting plate and the over-riding plate is clearly visible as a distinct change in backscatter character (Figure 2.1). The backscatter of the subducting plate is generally low (light grays) indicating a relatively smooth, evenly sedimented surface. The lower forearc, however, has a variable backscatter, indicating a more complex morphology. The plate contact in this area trends approximately 315° and is essentially linear, with only minor local perturbations. This is somewhat surprising considering the amount of anomalously thick oceanic crust (the Nazca Ridge) that is currently being subducted.

The Peru Forearc

The submarine portion of the forearc in the Nazca Ridge survey area can be divided into the lower forearc, the middle forearc, the upper forearc, and the forearc shelf (Figure 2.2). These divisions are based primarily on side-scan backscatter characteristics that separate the forearc into discrete morphotectonic divisions. Divisions of the forearc based on bathymetry, a common method of interpreting forearcs, is probably inappropriate here due to the influence of the subducting Nazca Ridge on the forearc (see discussion later). In addition to the morphotectonic divisions outlined above, two levels of terraces or

TABLE 2.1 CHEMISTRY OF NAZCA RIDGE SEAMOUNT GLASSES

Sample	P-1	P-2
SiO_2	49.85	49.79
TiO_2	2.64	2.48
Al_2O_3	16.23	16.16
FeO	8.69	8.61
MgO	5.75	6.27
CaO	9.99	10.26
Na_2O	3.37	3.19
K_2O	1.38	1.26
P_2O_5	0.52	0.46
Total	98.42	98.48

Note: Glasses are nearly non-vesicular (< 1 vol %) and have a high alkali content. This may indicate that volatiles did not exsolve from the samples and they may be present in high concentration. This would explain the apparent low totals [M. Garcia, *pers. comm.*].

benches occur on the forearc in this area. A lower terrace occurs on the upper part of the lower forearc. Another terrace occurs higher on the forearc, at the base of the upper forearc slope (Figure 2.2). The terraces vary in shape and width along strike but are generally 5 to 10 km wide and are horizontal to slightly dipping. These terraces are about half the width of those seen to the north at 11.5° S in the Lima Basin area [*Hussong et al.*, 1988].

The lower forearc is 10 to 15 km wide in the survey area and consists of a zone of trench-parallel fabric made up of small ridges and ledges that are laterally continuous (Figure 2.1). This type of terrain has been observed on side-scan images of other portions of the Peru forearc [*Hussong et al.*, 1988], where it has been interpreted as a zone of accreted sediment packets. The landward margin of this zone is a distinct morphologic boundary throughout most of the survey area (Figures 2.1 and 2.2). It is, however, not as clearly seen as it is in the Lima Basin area to the north [*Hussong et al.*, 1988]. This boundary is generally linear and parallels the trench axis. It occurs at about 3500 m depth at the northern edge of the survey, but is found below 5000 m at the southeast margin. The 5 to 10 km wide lower terrace occurs along the upper part of the lower forearc in the southern portion of the survey area. This narrow terrace is at approximately 5000 m depth in the southern part of the survey area but rises to about 3200 m in the north where it crosses onto the middle forearc.

The structural boundaries of the middle and upper forearc are less distinct than those of the lower forearc and are chosen here based on similarities to the Lima Basin area where subsurface structural information is more complete [*Moore and Taylor*, 1988; *von Huene and Miller*, 1988]. The middle forearc extends from the landward boundary of the lower forearc to the base of the upper forearc, where high backscatter indicates that consolidated material is exposed (Figure 2.1). The middle forearc exhibits a chaotic backscatter character. Small sediment ponds and low backscatter areas indicating sediment draping are intermixed with rough areas of higher backscatter. In the northern portion of

the survey, numerous small debris channels extend across the middle forearc from the upper slope.

At the upslope edge of the middle forearc a second, discontinuous terrace occurs (Figure 2.2). This upper terrace lies at the base of the upper forearc slope and contains thin accumulations of ponded sediment. Like the lower forearc terrace, this terrace increases in depth to the south across the survey area. In the north the terrace is at about the 2000 m level, whereas to the south it lies at about 3500 m depth. In the southern portion of the middle forearc the upper terrace consists of small sediment ponds. At the eastern edge of the survey faulting has apparently offset a portion of one of these ponds by about 500 m, forming a small shelf at about 3700 m depth (Figure 2.5). This pond contains about 0.2 s of layered sediment that dips slightly landward.

The upper forearc rises from the upper terrace to the edge of the forearc shelf at about 500 m depth. This area of the forearc is characterized by high backscatter outcrops of lithified sediment. Dredging of similar outcrops in the Yaquina and Lima Basin areas recovered high-grade metamorphic rocks (quartz-biotite gneiss and schist) [*Kulm et al.*, 1988]. Portions of the area are mantled by a thin layer of unconsolidated sediment. Debris channels cut across the upper forearc and are particularly common in the northern part of the survey area (Figure 2.1). These channels are arranged in a parallel pattern that extends only as far as the upper level of terraces and sediment ponds on the middle forearc (Figure 2.6).

Numerous structural lineations are visible in the side-scan images of the middle and upper forearc (Figures 2.1 and 2.2). These lineations may arise from faults, fractures, outcropping strata, or slump blocks. Because of the poor quality of our seismic reflection data we are, in most cases, unable to determine the cause of these various linear features. Rather than having a trench-parallel (315°) trend, many of these lineations trend down toward the trench axis at about 300° (Figure 2.2). Some of these WNW-trending lineations

Figure 2.5. SeaMARC II side-scan sonar image of the southern middle forearc. The upper terrace in this area consists of small basins occupying ledges that may have been formed by faulting. Forearc structural lineations trend slightly more westerly than the northwest-trending plate boundary seen in the lower left corner of the figure. Figure location is shown on Figure 2.3.

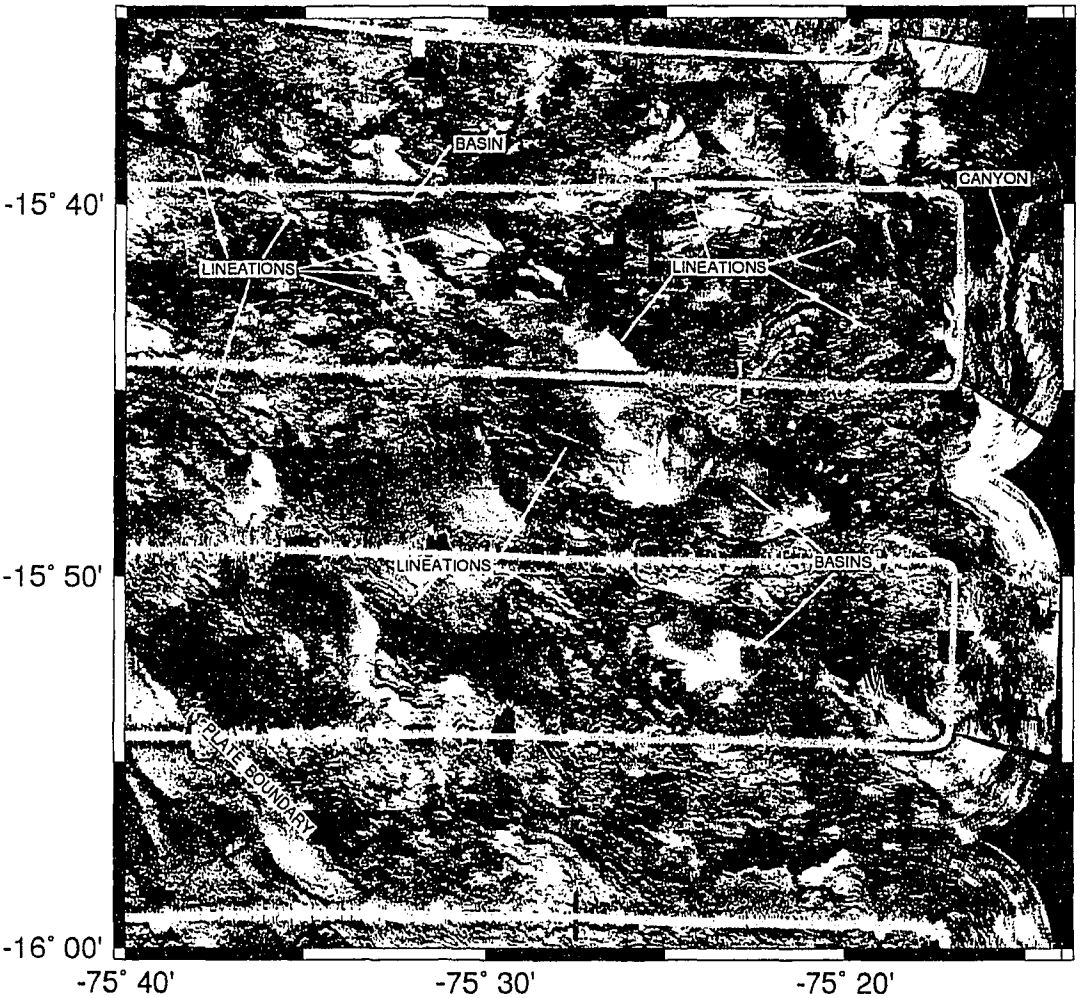
BASIN
CANYON
LINEATIONS
LINEATIONS
LINEATIONS
BASINS
PLATE BOUNDARY
-15° 40'
-15° 50'
-16° 00'
-75° 40'
-75° 30'
-75° 20'

Figure 2.6. SeaMARC II side-scan sonar image of the upper and middle forearc in the northern portion of the survey area. Debris channels are well developed in this area and extend from the edge of the forearc shelf to the middle forearc. Structural lineations trend at about 300° down across the forearc. Small high backscatter areas at the base of the upper forearc may be mud volcanoes formed above fractures in the forearc. Figure location is shown on Figure 2.3.

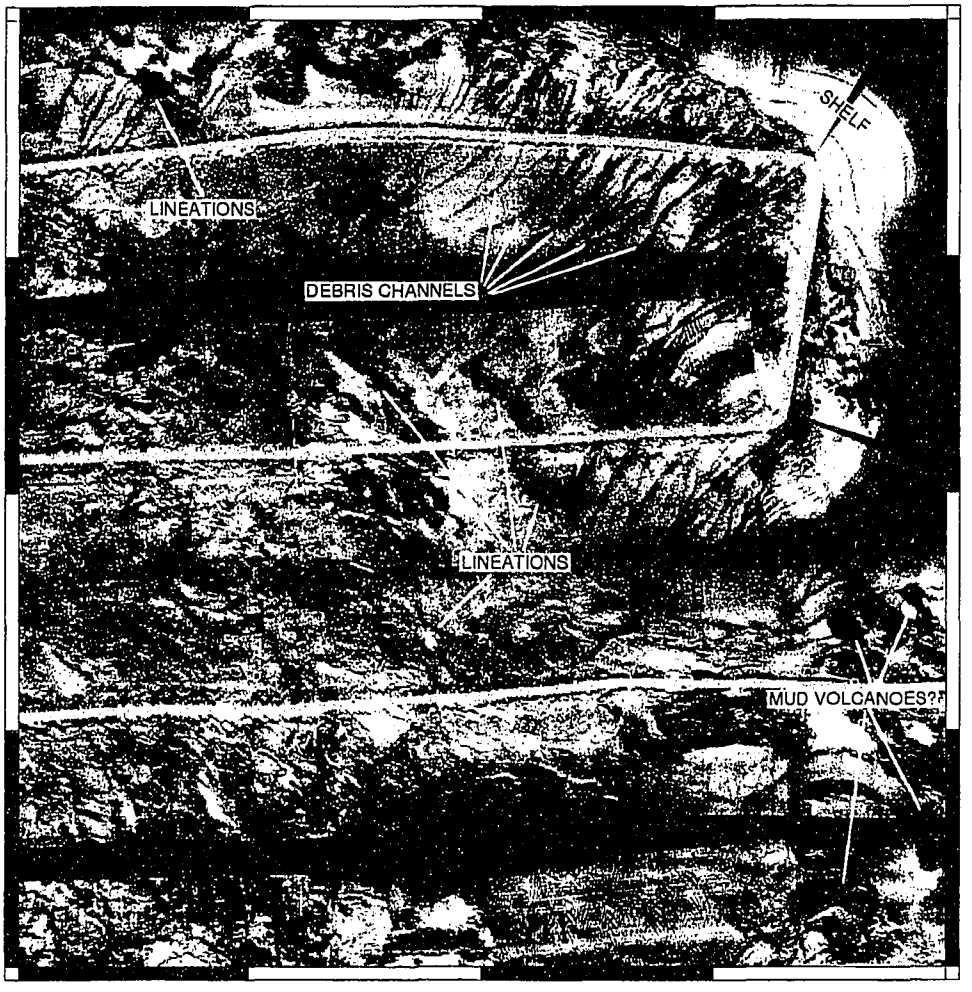
SHELF
LINEATIONS
DEBRIS CHANNELS
LINEATIONS
MUD VOLCANOES??
-14° 50'
-15° 00'
-76° 20'
-76° 10'

appear to be branches of trench-parallel lineations higher on the forearc (Figure 2.7). As discussed later, this pattern of structural elements in the forearc may result from the oblique subduction of the Nazca Ridge.

Discussion

The Nazca Plate

Fault orientations on the subducting Nazca plate, although somewhat variable, generally parallel the trench axis which trends about 315° (Figure 2.8). Normal faulting in this area thus does not seem to be occurring by re-activation of the pre-existing seafloor spreading fabric, which trends at about 335° in this area [*Hilde and Warsi*, 1986].

A GLORIA survey across the Nazca plate to the north (between 10° and 12° S) found large numbers of small volcanoes on the central Nazca plate [*Searle*, 1983]. The small volcanoes seen in the GLORIA images are very similar to those observed in the Nazca Ridge survey area. Erlandson et al. [*1981*] reported an extensive region seaward of the Peru Trench that exhibits sediment thinning and rough basement topography. They hypothesized that off-ridge volcanism had produced sills and lava flows, causing the apparent sediment thinning. Seismic reflection profiles collected across the subducting Nazca plate during our SeaMARC II survey show clear examples of sills and intrusions (Figure 2.9).

These data show that the intrusive and extrusive volcanic areas visible in the side-scan images and seismic reflection profiles formed well after the surrounding seafloor was created at a spreading center since a significant amount of sediment was deposited before the sills (or lava flows) were emplaced. Faulting of these volcanic areas and current scour around several of the volcanoes indicates that this period of volcanism ended before the

Figure 2.7 SeaMARC II side-scan image of the upper forearc in the central portion of the survey area. This figure shows a long trench-parallel fault on the upper forearc that splays into several branches trending down across the forearc toward the trench. The sense of offset across this fault is inconsistent on 3.5 kHz echosounder profiles, suggesting that it has a significant component of strike-slip motion. Figure location is shown on Figure 2.3.

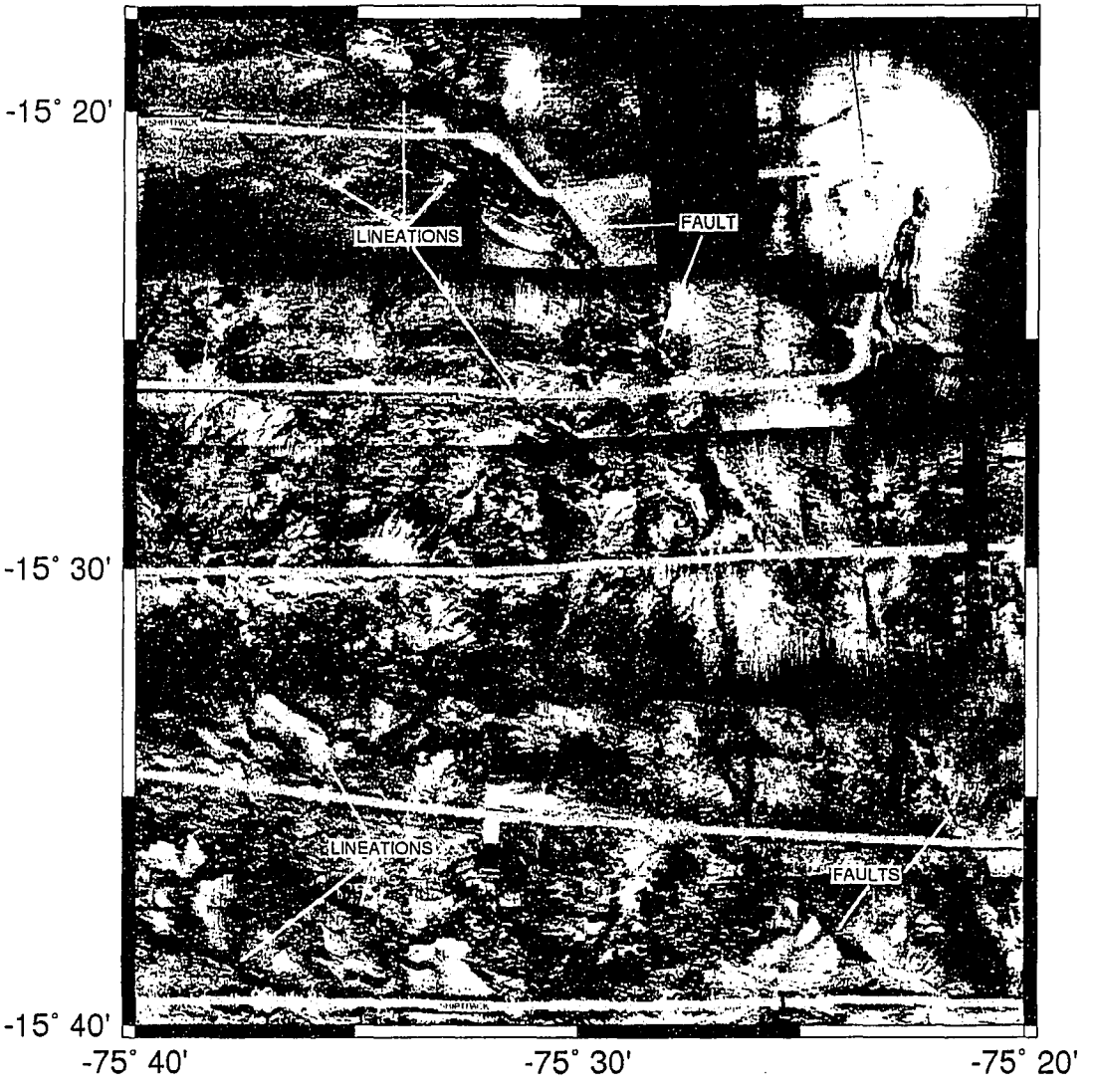
-15° 20'
-15° 30'
-15° 40'
-75° 40'
-75° 30'
-75° 20'
LINEATIONS
FAULT
LINEATIONS
FAULTS

Figure 2.8. Sector diagram showing fault azimuths on the Nazca plate and the forearc in the Nazca Ridge survey area. Faults were digitized from the side-scan mosaic and are plotted as cumulative fault length vs. azimuth. This weights the measurements by the length of the fault segments. In the upper diagram, the smaller sector plot overlying the fault azimuths represents the trend of the trench axis. T is the trend of the trench, M is the trend of magnetic anomalies on the nearby Nazca Plate [*Cande*, 1986], and C is the plate convergence direction.

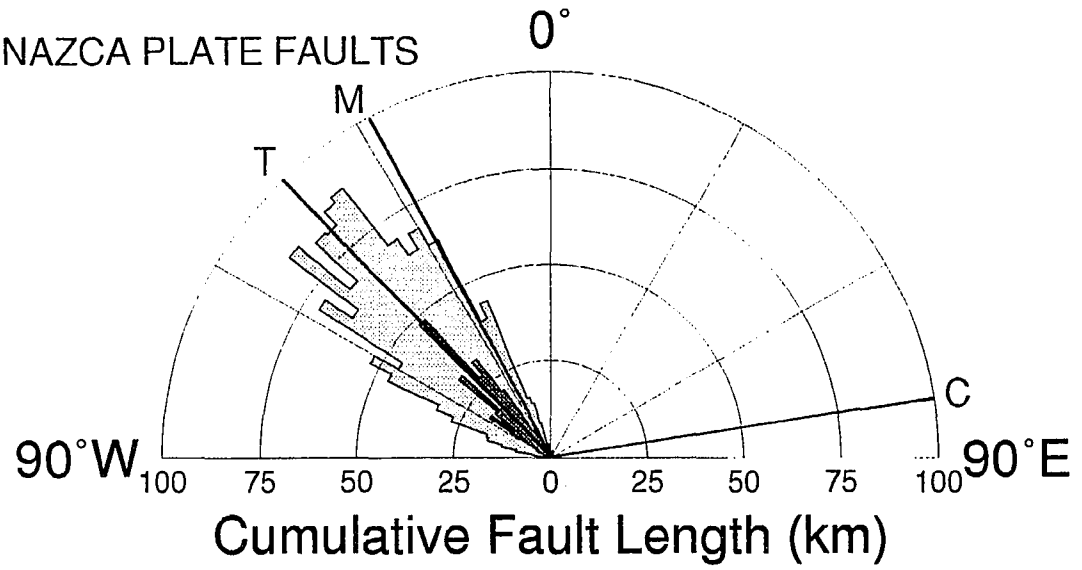
NAZCA PLATE FAULTS
0°
M
T
C
90°W
90°E
100
75
50
25
0
25
50
75
100
Cumulative Fault Length (km)

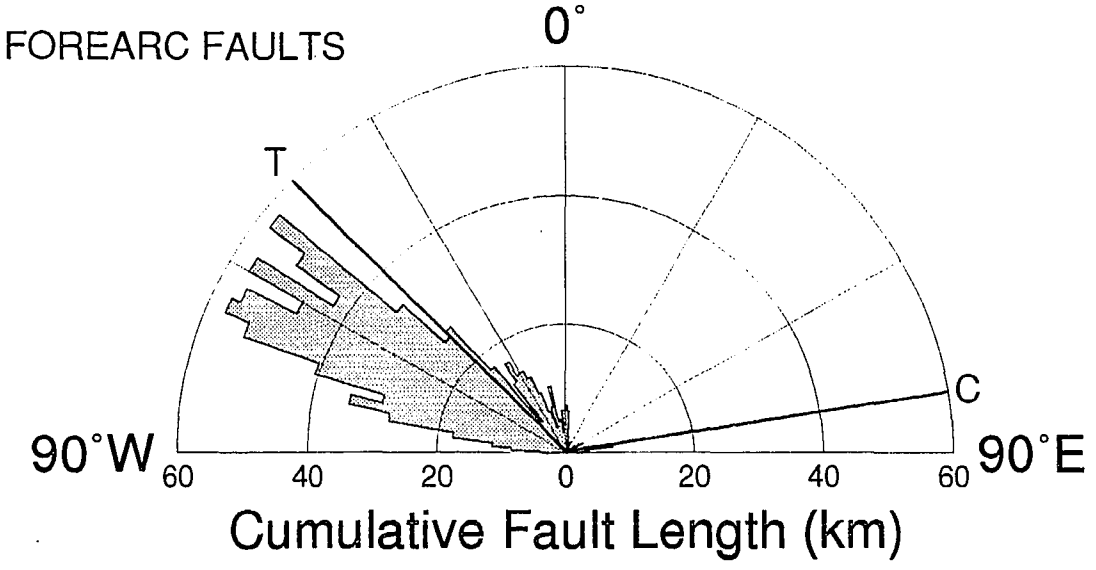
FOREARC FAULTS
0°
T
C
90°W
90°E
60
40
20
0
20
40
60
Cumulative Fault Length (km)

Figure 2.9 Single-channel seismic reflection profile along the crest of the Nazca Ridge showing small volcanoes and sills within the sediment column. B, the acoustic basement reflection, is clearly seen to extend beneath the strong reflectors in the sediment column. This indicates that the strong mid-section reflectors are not caused by faulted basement blocks. The strength and levelness of the mid-section reflectors shows that they are not side-echoes from out of the plane of the profile. Profile location is shown on Figure 2.3.

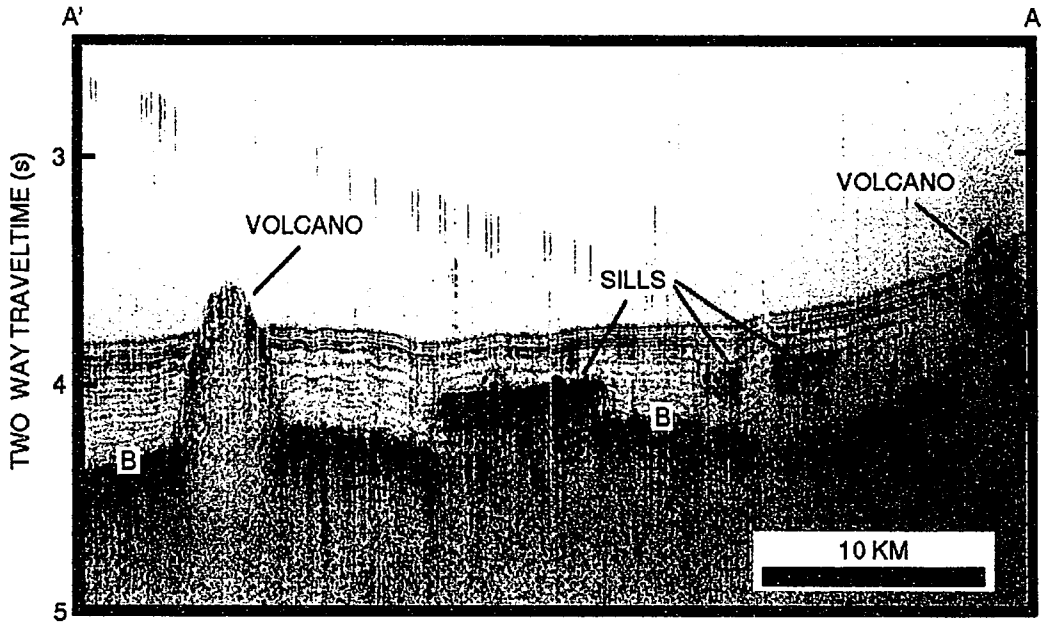
A'
A
3
4
5
TWO WAY TRAVELTIME (s)
VOLCANO
VOLCANO
SILLS
B
B
10 KM

seafloor entered the zone of subduction-induced faulting at the outer slope of the trench. It is difficult to conceive of a mechanism to explain these observations. It is possible that cooling stresses may fracture the Nazca plate as it moves away from the spreading center, resulting in small amounts of decompressional melting and forming the observed sills, lava flows, and small volcanoes. Alternately, some type of broad thermal anomaly may affect the plate, causing a broad region of low level tectonic and volcanic activity.

The Peru Forearc

The terraced nature of the Peru-Chile forearc was recognized in previous studies [*Kulm et al.*, 1977; *Thornburg and Kulm*, 1981]. Terraces and slope basins are common features of forearcs in general [*Dickinson and Seely*, 1979] and are thought to represent periods of imbricate thrusting due to discrete pulses in accretion of material to the forearc [*Kulm et al.*, 1977; *Johnson and Ness*, 1981]. These terraces generally maintain a fairly constant depth parallel to structural boundaries.

In the Lima Basin area to the north of our survey, the lower terrace lies at about 3800 m depth, along the upper edge of the lower forearc [*Hussong et al.*, 1988]. Multichannel seismic reflection profiles through the Lima Basin indicate that this terrace overlies the boundary between the narrow wedge of accreted material, and older accreted material or thinned continental crust [*Moore and Taylor*, 1988; *von Huene and Miller*, 1988].

In the Nazca Ridge survey area both the upper and lower terraces vary in depth, becoming more than 1500 m deeper to the southeast along the forearc. As in the Lima Basin area, the lower terrace lies along the upper edge of the accretionary zone through most of the survey area. At the northern edge of the survey area, however, where the thickest portion of the Nazca Ridge is subducting, the lower terrace is "pushed" upward to

the level of the middle forearc (Figure 2.2). The morphology of the entire forearc is also changed from steep slopes and narrow terraces in the south, to gentler slopes and broad terraces in the northern part of the survey area where subduction of the Nazca Ridge is at its peak (Figure 2.10). The bathymetric features of the forearc in this area thus reflect the effects of the subducting Nazca Ridge but are not reliable indicators of the underlying structure of the forearc.

In addition to the observed uplift of the forearc in the northern portion of the survey area, forearc structural lineations on the middle and upper forearc may result from oblique compressional stresses. Compression of the forearc by the collision with the Nazca Ridge (convergence at about 90 mm/y toward 081°) could produce conjugate strike-slip faulting of the forearc on approximately 035° and 305° trends. No 035° trends are observed in the data presented here. The trend of the trench and trench-parallel structures is about 315° in this area, which makes it difficult to clearly delineate any 305° trends caused by collision. Most of the lineations in the middle and upper forearc do, however, have trends that are not trench-parallel, but are closer to 305° (Figure 2.8). These features begin as trench-parallel lineations on the upper forearc in the southern part of the survey and splay into branches that trend at about 300° across the middle forearc toward the trench. These data suggest that the oblique collision of the Nazca Ridge may cause trench-parallel faults and fractures to develop oblique strike-slip extensions as the collision progresses. Offset across these faults is minor; uplift of the forearc is the dominant response to the subduction of the Nazca Ridge.

These data suggest that subduction of the Nazca Ridge has not significantly altered the structure of the forearc by lateral deformation, but has uplifted the northern portion of the survey area. This uplift may cause steeper, unstable slopes that are more susceptable to

Figure 2.10 Gridded SeaMARC II bathymetry from the Nazca Ridge survey area. The data were gridded at a 200 m horizontal spacing and are displayed with illumination from the northeast. This illumination highlights the terraces on the forearc as well as reverse faults on the subducting Nazca plate. In the lower portion of the figure the data are viewed from the south at an elevation of 40° with illumination from the northeast. The changes in shape and elevation of the lower forearc caused by subduction of the Nazca ridge are clearly shown in this image.

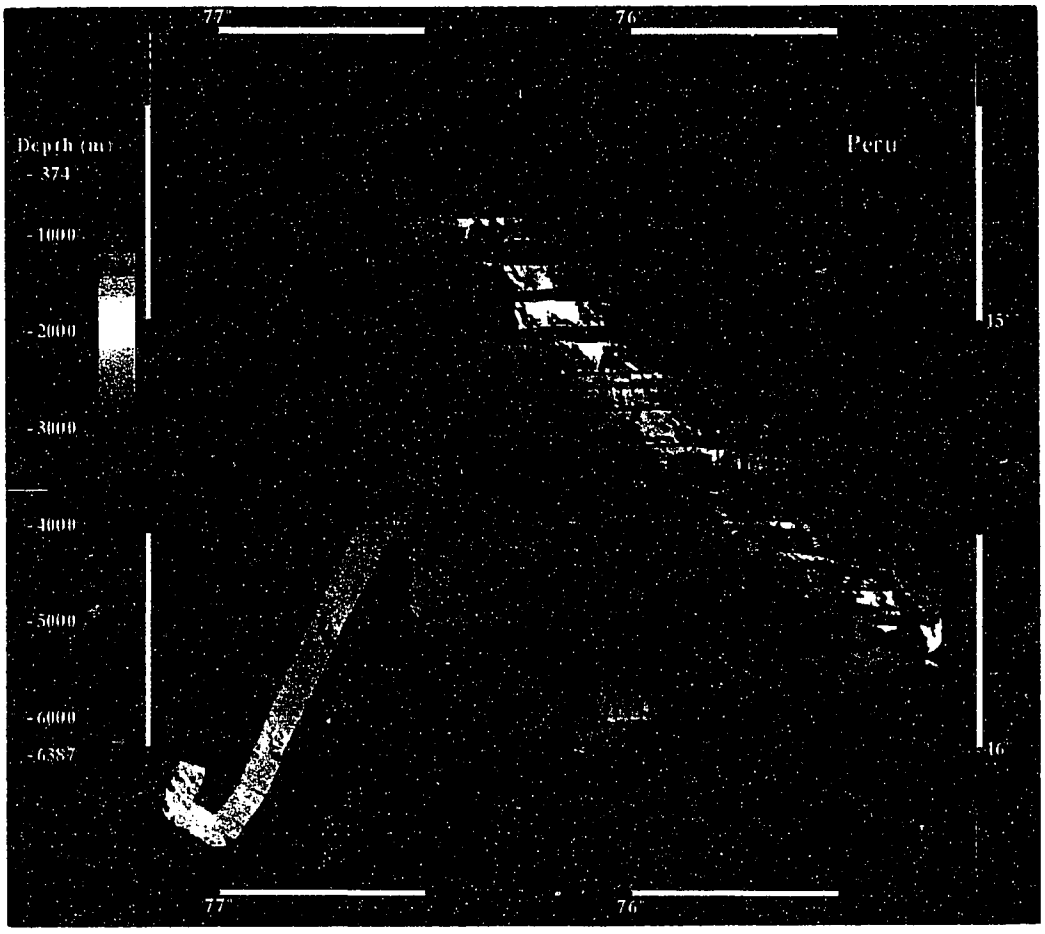
77°
76°
Depth (m)
-374
-1000
-2000
-3000
-4000
-5000
-6000
-6387
Peru
15°
16°
77°
76°

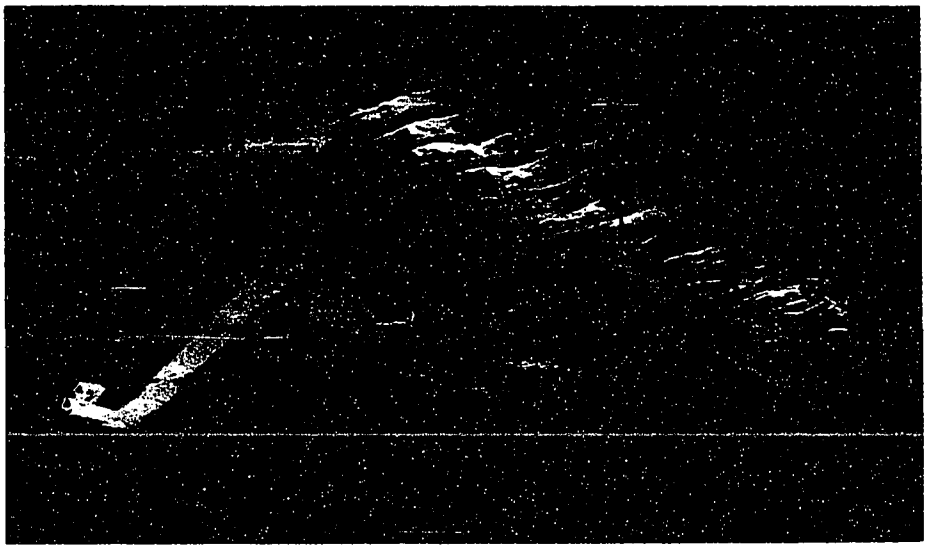

erosion. The northern part of the survey area exhibits a large number of well-developed debris channels that may have formed in this way (Figure 2.1).

Many other subducting ridges, seamount chains, and fracture zones that are presently being subducted result in significant compressional deformation of the forearc. A notable example of forearc deformation, in a setting similar to the subduction of the Nazca Ridge, can be seen in SeaMARC II data from southern Panama [*Moore and Sender*, in press]. In this area three narrow fracture zone ridges with relief of 1200 to 2200 m are sweeping along the forearc as they are being subducted. Unlike the Nazca Ridge, however, the ridges are plowing into the lower forearc, uplifting and deforming the accretionary prism and creating large re-entrants.

The relatively subdued response of the forearc to the subduction of the Nazca Ridge probably results from the shape of the colliding ridge. The Nazca Ridge has a broad, dome-shaped cross-section with slopes of only 1 to 2 degrees. This apparently allows the ridge to slip beneath the forearc with little compressional deformation of the overlying material.

Conclusions

The forearc of southern Peru near 15° S latitude consists of four major structural divisions: (1) the narrow (10 to 15 km wide) lower forearc consisting of thin packets of accreted sediment, (2) the middle forearc, a chaotic zone of rough terrain draped by sediment, (3) the upper forearc with outcrops of consolidated sediment cut by debris channels, and (4) the gently sloping and sedimented forearc shelf.

Subduction of the Nazca Ridge beneath the South American continent in southern Peru has resulted in uplift of the lower forearc by as much as 1500 m. This uplift has caused faulting and surficial slumping on the forearc and has led to increased erosion

through debris channels. Forearc structural lineations show no major surface offsets but trend at oblique angles to the trench, suggesting that they may be conjugate strike-slip faults caused by the oblique subduction of the Nazca Ridge. The trench in the zone of ridge subduction is generally linear, with no large re-entrants such as are seen at other ridge-trench intersections. Only minor compressional deformation, in the form of fracturing and strike-slip faulting, is observed, suggesting that the broad, gently sloping ridge is able to slide beneath the forearc without significantly disturbing the typical slope and terrace morphology in this area.

The Nazca plate and the Nazca Ridge itself are heavily faulted by subduction-induced normal and reverse faults with offsets of up to 500 m. Trench-parallel normal faults predominate; reverse faults generally occur near the trench axis. Faulting begins about 50 km west of the trench axis and increases in both frequency and offset toward the trench.

Intrusive and extrusive volcanic areas on the subducting Nazca plate appear to have formed well after the seafloor was created at the ridge crest, but before subduction-induced faulting of the plate began. A dredge from one of these volcanoes recovered mildly alkalic basaltic glass with a chemistry that appears to be unrelated to a mid-ocean ridge parent magma, supporting the hypothesis that this volcanism occurred off-ridge.

CHAPTER 3

FAULT PATTERNS ON THE OUTER WALL OF THE PERU-CHILE TRENCH

Abstract

We examine fault patterns in the outer trench wall of the Peru-Chile trench as revealed by five SeaMARC II surveys. Like most oceanic trenches, the subducting plate at the Peru-Chile trench is pervasively faulted as the plate is bent into the subduction zone. In three of the five survey areas studied (Lima Basin, Arica Bight, Iquique Basin), fault trends on the outer wall of the Peru-Chile trench parallel the trend of magnetic anomalies on the Nazca plate. In the Nazca Ridge survey area, faulting parallels the trench trend, probably because of a lack of spreading fabric on the ridge. In the Yaquina Basin survey area faulting follows neither the trench nor the spreading fabric trend. This is probably caused by stress changes in the subducting plate resulting from extension along the nearby Mendaña fracture zone.

These results generally agree with a previous review of subduction-related faulting which concluded that faulting will follow the trend of the spreading fabric as long as it differs from the strike of the dipping slab by less than 30°. The angle between the trench and the spreading fabric is less than 10° in all five of the surveys examined here, and the preference for faulting to follow the spreading fabric is clear, particularly in the Arica Bight and Iquique Basin survey areas.

Introduction

Early echosounder and seismic reflection profiles across subduction zones revealed that the surfaces of subducting oceanic plates are commonly extensively faulted [*Raitt et al.*,

1955; *Fisher and Hess*, 1963; *Ludwig et al.*, 1966]. This faulting was thought to be predominantly tensional and trench-parallel [*Ludwig et al.*, 1966; *Jones et al.*, 1978]. The faults are believed to form by bending of the plate into the trench and by loading of the subducting plate by the forearc [*Ludwig et al.*, 1966; *Jones et al.*, 1978].

In some instances faults trending obliquely to the trench have been observed and have commonly been attributed to re-activation of the seafloor spreading fabric [*Coulbourn*, 1977; *Honza*, 1978]. Since faults were observed both parallel to and oblique to both the spreading fabrics and the subduction zone trends, Hilde [*1983*] concluded that no faulting pattern was apparent and that faulting was probably related only to the bending of the subducting plate.

A recent study [*Masson*, 1991] re-examined the question of tectonic controls of faulting on subducting plates using GLORIA long-range side-scan sonar and Seabeam swath bathymetric data from several subduction zones. Masson [*1991*] concluded that faulting is nearly always controlled by the strike of the subducting slab or by the seafloor spreading fabric. He proposed that re-activation of seafloor spreading fabric occurs when the angle between the spreading fabric and the strike of the subducting slab is less than 30°. He also found that other subduction zone parameters, such as convergence direction and age of the subducting plate, have no apparent effect on subduction-induced faulting.

This chapter examines data from five SeaMARC II surveys of the Peru-Chile trench (Figure 3.1). Although the focus of these studies was the forearc, significant areas of the subducting Nazca plate were included in the surveys. The side-scan sonar data reveal a pervasively faulted subducting plate, allowing us to compare the faulting along this trench to that seen at other subduction zones.

Figure 3.1 Location map showing SeaMARC II surveys along the Peru-Chile forearc. The Yaquina and Lima Basin surveys were conducted in 1985 and served as site surveys for drilling on ODP Leg 112 [*Hussong et al.*, 1988]. The Nazca Ridge, Arica Bight, and Iquique Basin surveys were conducted in 1987. Magnetic anomalies and fracture zones are from Cande et al. [*1989*].

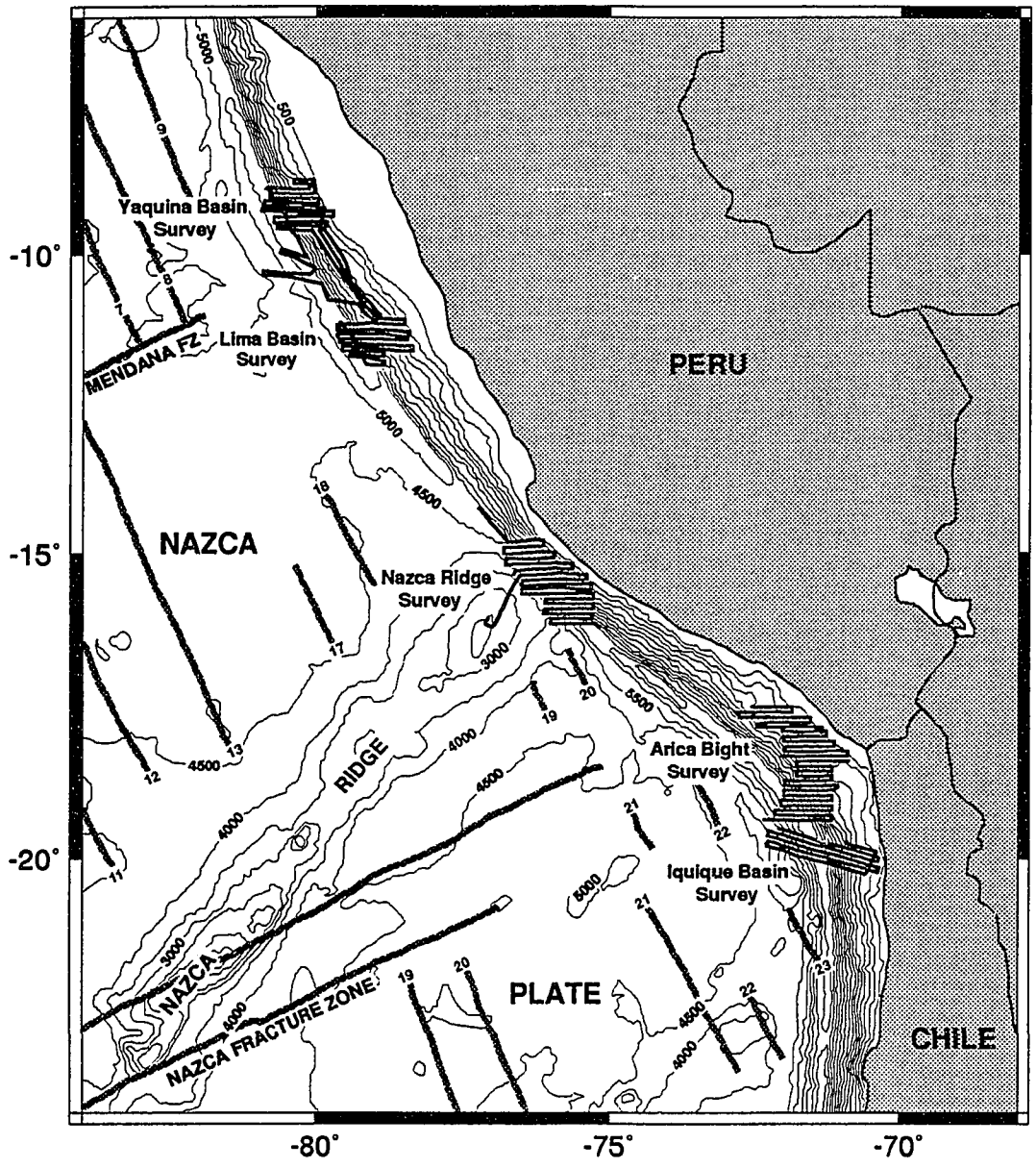
Yaquina Basin Survey
Lima Basin Survey
MENDANA FZ
PERU
NAZCA
Nazca Ridge Survey
RIDGE
Arica Bight Survey
Iquique Basin Survey
NAZCA PLATE
NAZCA FRACTURE ZONE
CHILE
-10°
-15°
-20°
-80°
-75°
-70°

Data Description

Figure 3.2 shows the portions of the five SeaMARC II side-scan sonar surveys along the Peru-Chile margin that lie on the subducting Nazca plate. The side-scan images consist of 10-km-wide swaths assembled into mosaics. The side-scan data are presented with high backscatter as dark gray to black and low backscatter areas as light gray to white. Rough surfaces such as fault scarps, lava flows, and volcanoes have high backscatter and appear dark. Smooth, sedimented seafloor appears as various shades of lighter gray.

With the exception of a single GLORIA side-scan sonar swath across the Nazca plate near 10° S [*Warsi et al.*, 1983], the orientation of seafloor spreading fabric on the older portions of the Nazca plate is poorly known. In this paper we will use the trend of magnetic anomalies determined by Cande et al. [*1989*] as an approximation of seafloor fabric trends.

Fault azimuths were approximated by digitizing a series of straight line segments. The fault segments were plotted as sector diagrams using the cumulative length of the segments as a weighting factor. The unweighted data were also plotted as histograms of fault azimuth. There is little difference in the trends displayed by the two data presentations, although peak trends are usually more pronounced in the weighted sector diagrams. The trend of the trench in each survey area was also determined by the method described above.

Fault azimuths measured from the side-scan sonar mosaics are subject to distortion if the side-scan pixels are not relocated using the bathymetry. The distortion is caused by positioning side-scan pixels on the basis of a flat-bottom assumption when the seafloor actually has significant slope [*Johnson and Helferty*, 1990]. The magnitude of this relocation error depends on topography and the orientation of survey lines. The distortion

Figure3.2 SeaMARC II side-scan sonar backscatter data from surveys along the Peru-Chile trench. Only the portions of the surveys over the subducting Nazca plate are shown. See Figure 3.1 for survey locations.

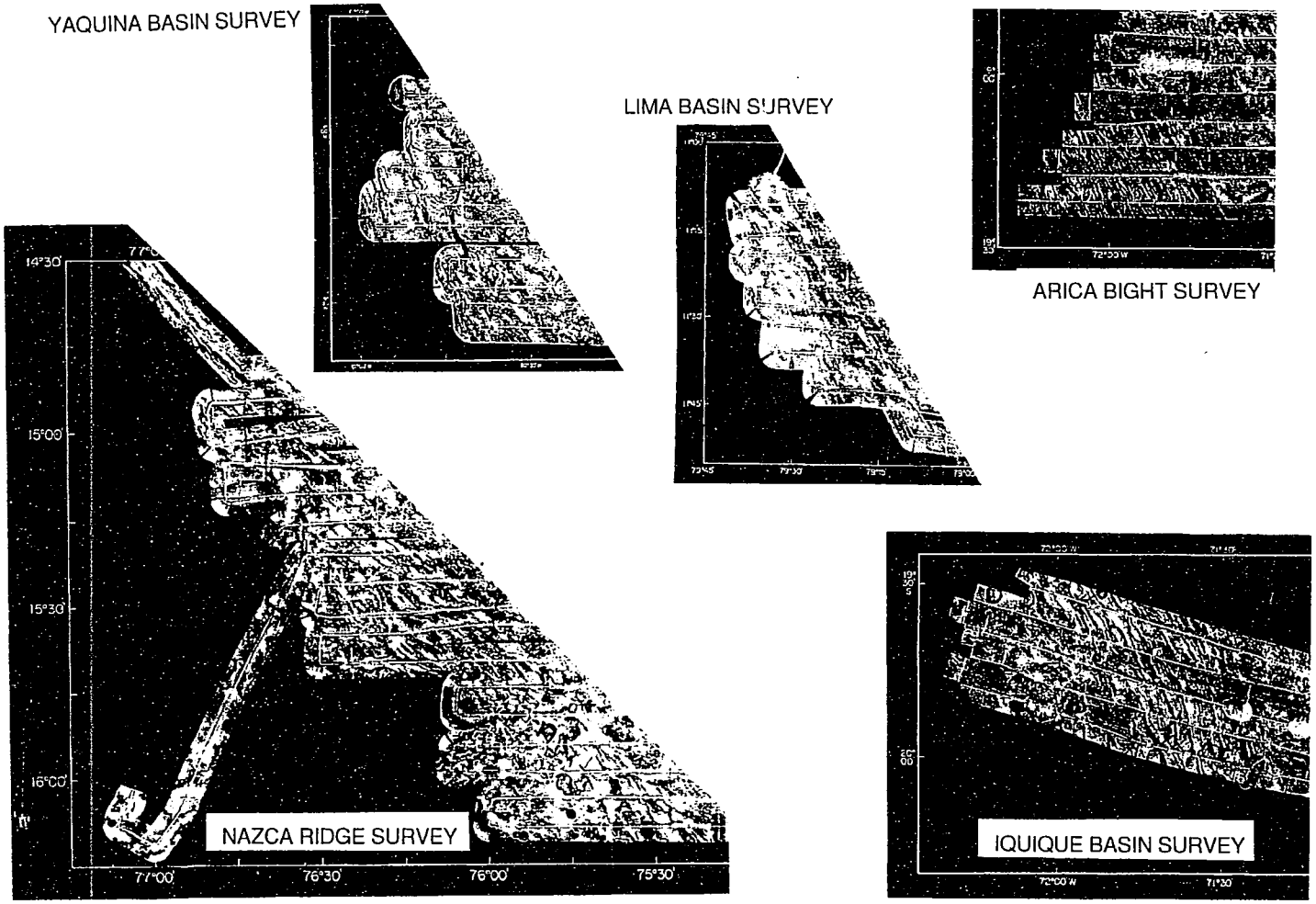
YAQUINA BASIN SURVEY
LIMA BASIN SURVEY
ARICA BIGHT SURVEY
NAZCA RIDGE SURVEY
IQUIQUE BASIN SURVEY
14°30'
15°00'
15°30'
16°00'
77°00'
76°30'
76°00'
75°30'

is generally minor, but becomes a problem in areas with steep slopes. For the surveys presented here, this error is only noticeable within about a kilometer on either side of the shiptrack. Because the east-west oriented shiptracks cross the trench slope at an angle, the fault traces assume a slightly sigmoidal shape where they cross the shiptrack. To minimize the scatter in fault azimuths caused by this distortion, faults were not digitized across the inner portions of the side-scan swaths.

The Yaquina Basin Survey

Approximately 1200 km^2 of the Nazca plate was imaged during the Yaquina Basin survey. The survey extends up to 35 km from the trench axis onto the subducting plate and covers an area that is moderately faulted. The faulting in this area is somewhat varied in azimuth and some faults are noticeably curved (Figure 3.2). The dominant trend of the faults on the subducting plate in the Yaquina Basin survey area is about 339° (Figure 3.3). This trend is clearly different from the trend of either the seafloor spreading magnetic anomalies (332°) or the trench (329°).

The Lima Basin Survey

The Lima Basin survey extends as much as 40 km out onto the subducting Nazca plate and covers an area of about 1500 km^2. Faulting in this area is less pronounced than in the Yaquina Basin area (Figure 3.2). Fault trends also appear to be straighter, of low variability, and trench-parallel. The sector diagram of fault azimuths for this survey confirms these visual observations (Figure 3.4). The faults are confined to a narrow sector around the trends of both the trench and magnetic fabric, which are almost identical in this area.

Figure 3.3 Sector diagram and histogram of fault azimuths for the Yaquina Basin survey area. The sector diagram is weighted by the length of the fault segments. A darker sector plot of the trend of the trench is overlain on the fault sector diagram. T is the trend of the trench in the survey area. M is the trend of magnetic anomalies on the Nazca plate. C is the plate convergence direction.

Yaquina Basin Survey

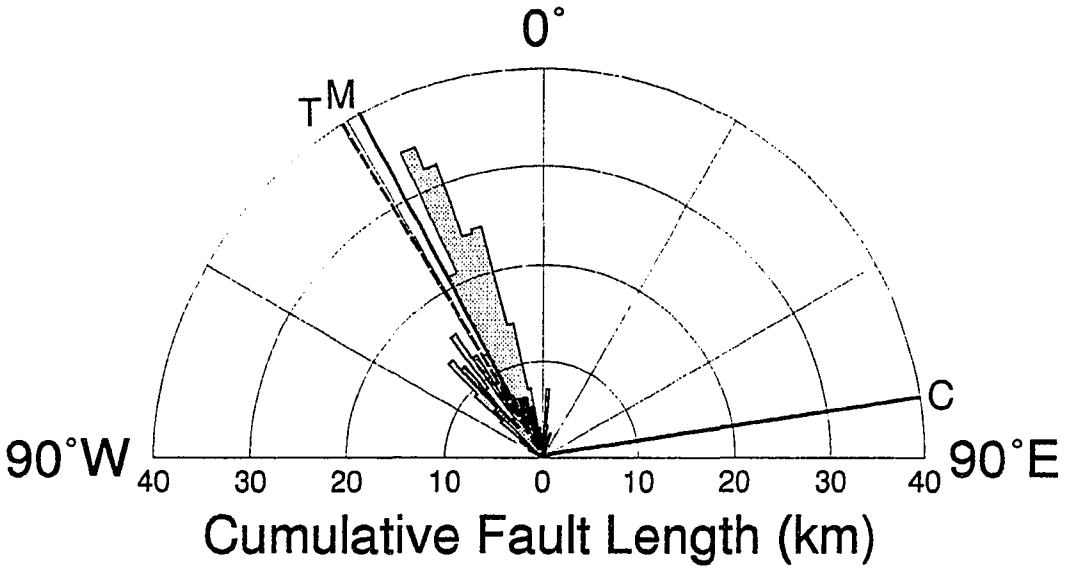

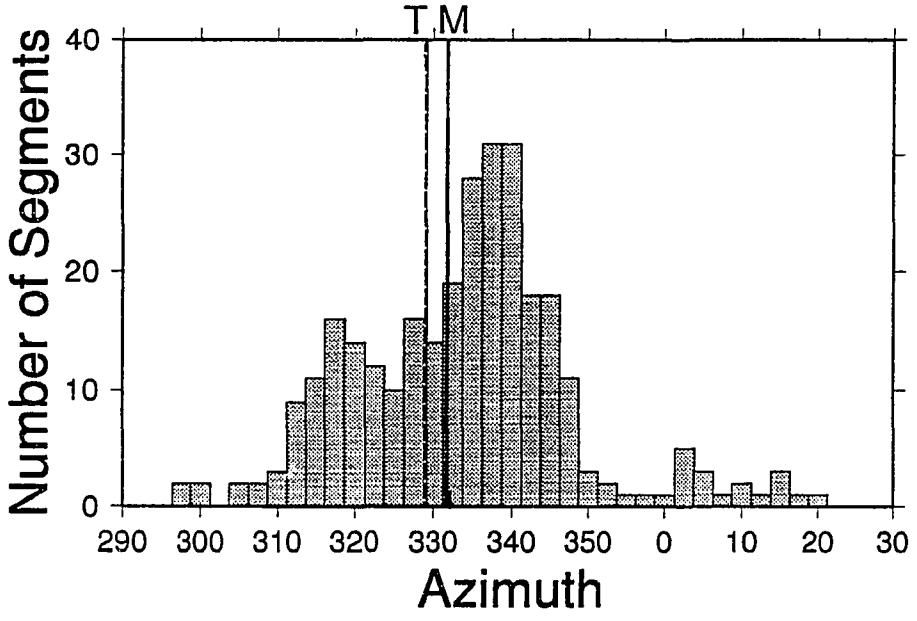

Figure 3.4 Sector diagram and histogram of fault azimuths for the Lima Basin survey area. The sector diagram is weighted by the length of the fault segments. A darker sector plot of the trend of the trench is overlain on the fault sector diagram. T is the trend of the trench in the survey area. M is the trend of magnetic anomalies on the Nazca plate. C is the plate convergence direction.

Lima Basin Survey

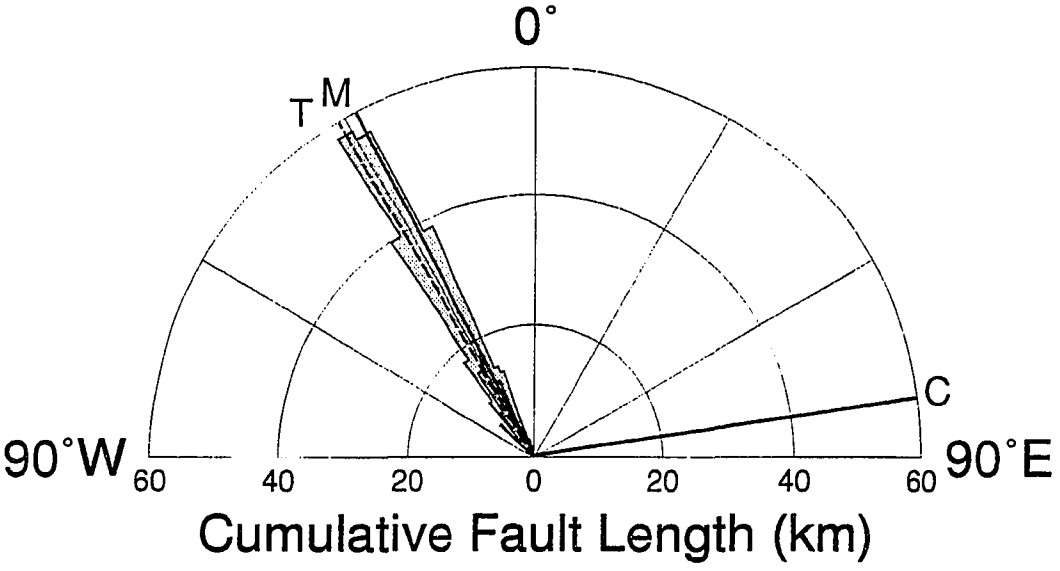

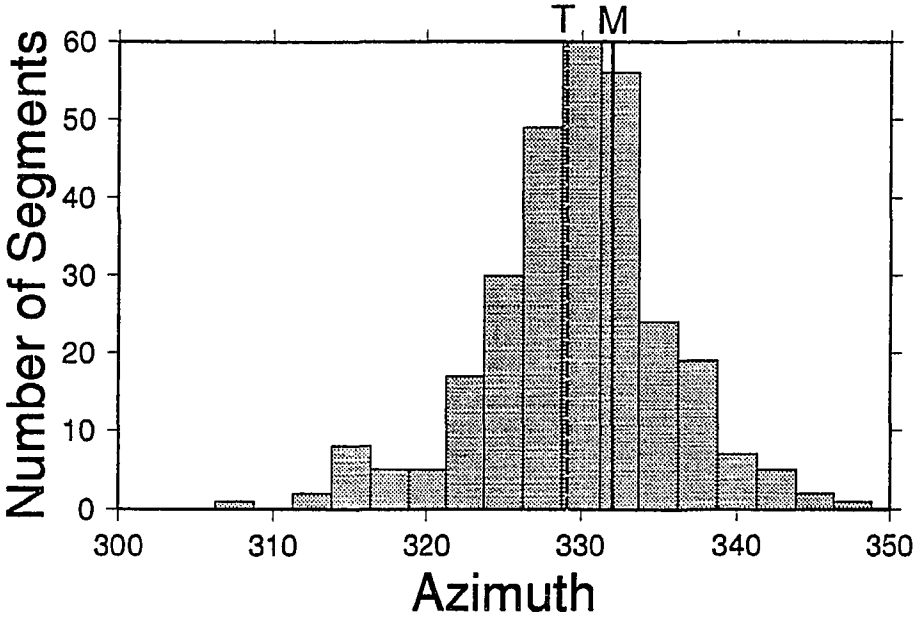

The Nazca Ridge Survey

The Nazca Ridge survey covers an area of about 7500 km^2 of the Nazca plate. Most of this area is within 50 km of the trench axis, although a single swath of data extends out approximately 130 km onto the Nazca plate (Figure 3.2). This survey covers an area where the Nazca Ridge is currently subducting and the seafloor being subducted is therefore not typical Nazca plate crust. The survey area also contains numerous small volcanoes, lava flows, and volcanic areas that may also affect the faulting of the subducting plate.

Fault trends in this area show a wide range of variability (over 30°) (Figure 3.5). The fault trends are centered around the trend of the trench axis (316°) and few of the faults appear to follow the magnetic anomaly trend (332°).

The Arica Bight Survey

Only about 1500 km^2 of the large Arica Bight survey occur on the subducting Nazca plate. The area surveyed, however, is densely faulted by large-offset faults that give the side-scan image a "tiger-stripe" pattern (Figure 3.2). These faults form a well-defined trend that is centered on the magnetic anomaly trend (332°) (Figure 3.6). Very few of the faults share the trend of the trench in this area (322°).

Figure 3.5 Sector diagram and histogram of fault azimuths for the Nazca Ridge survey area. The sector diagram is weighted by the length of the fault segments. A darker sector plot of the trend of the trench is overlain on the fault sector diagram. T is the trend of the trench in the survey area. M is the trend of magnetic anomalies on the Nazca plate. C is the plate convergence direction.

Nazca Ridge Survey

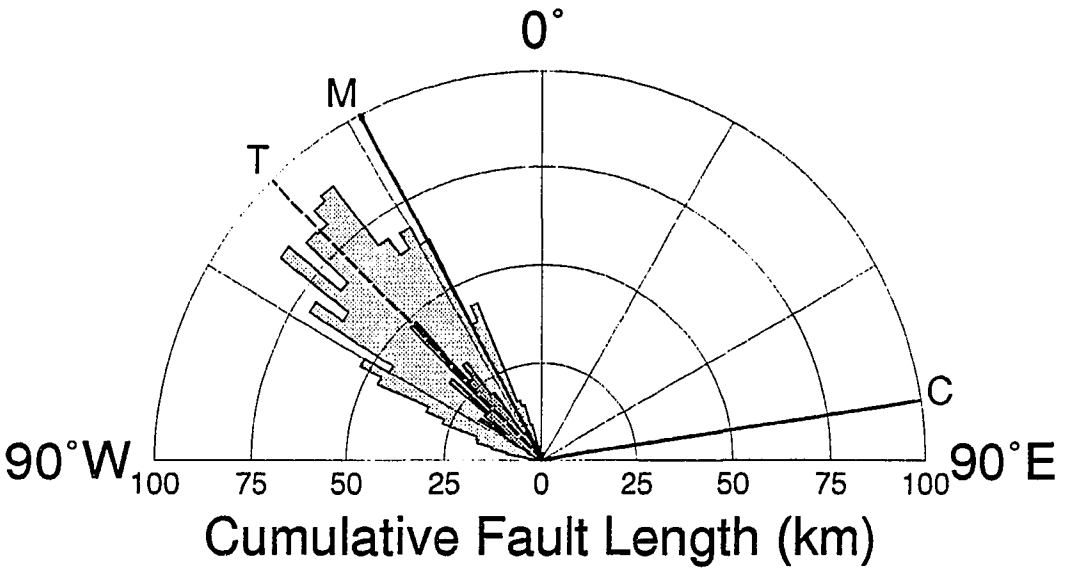

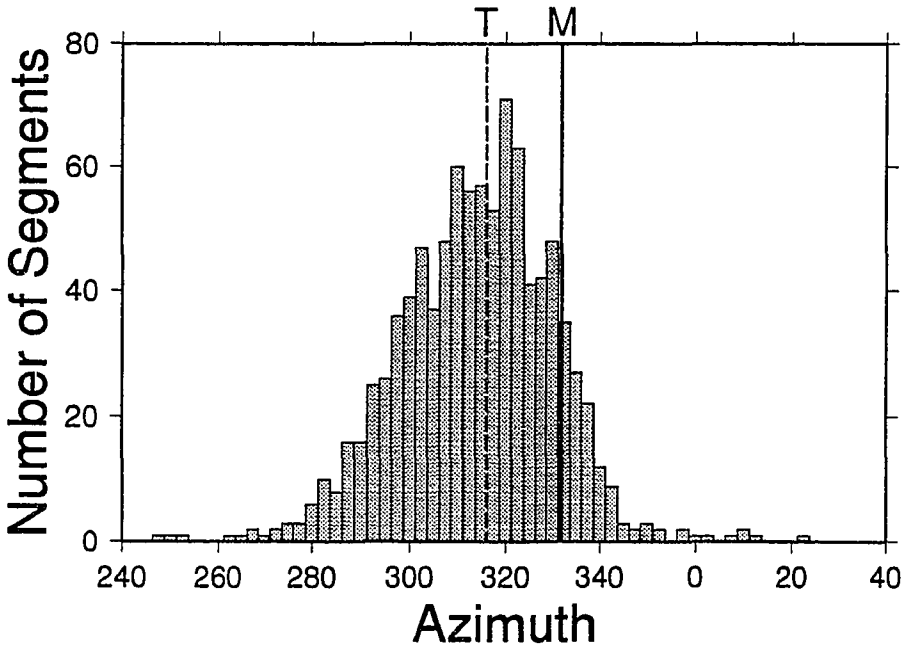

Figure 3.6 Sector diagram and histogram of fault azimuths for the Arica Bight survey area. The sector diagram is weighted by the length of the fault segments. A darker sector plot of the trend of the trench is overlain on the fault sector diagram. T is the trend of the trench in the survey area. M is the trend of magnetic anomalies on the Nazca plate. C is the plate convergence direction.

Arica Bight Survey

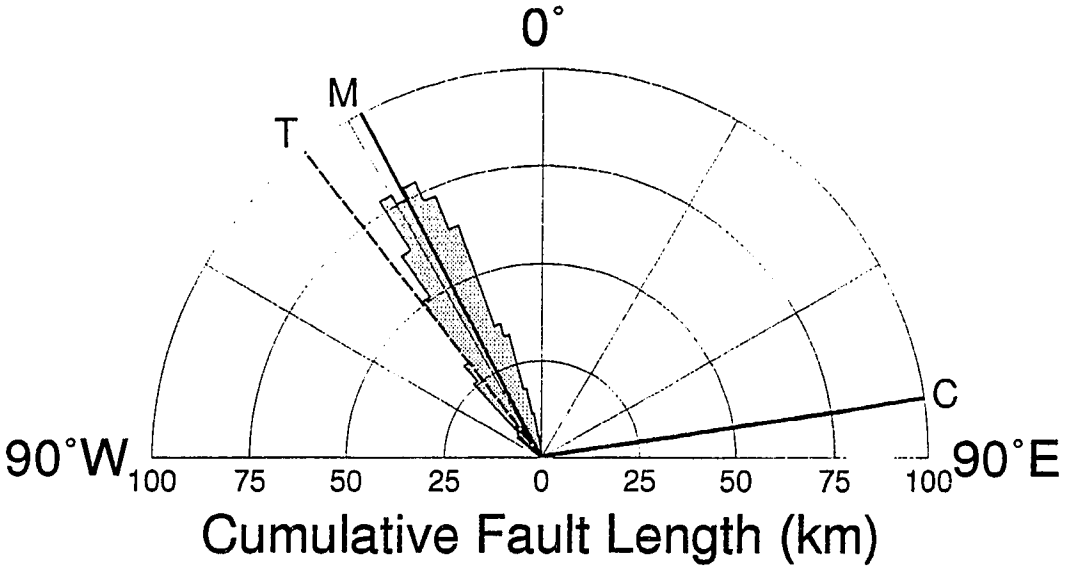

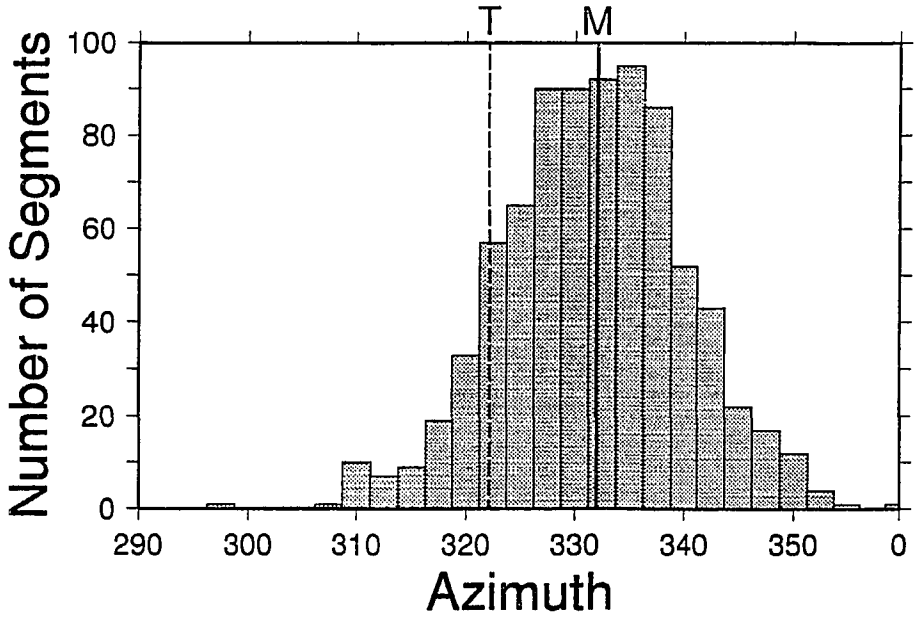

The Iquique Basin Survey

The Iquique Basin survey extends 75 km onto the subducting Nazca plate and covers about 4800 km^2. Like the Arica Bight area just to the north, the seafloor in this area is broken by many high-amplitude faults. The seafloor in this area is dotted with small volcanoes as in the Nazca Ridge survey area. The survey also includes a small seamount that is 25 km in diameter and nearly 2000 m high (Figure 3.2). Fault trends in the Iquique Basin area show a strong preference for the magnetic fabric trend (332°) rather than the trend of the trench (341°) (Figure 3.7).

Discussion

Table 3.1 summarizes various fault and tectonic parameters for the five SeaMARC II surveys discussed above. In four out of the five surveys (Lima Basin, Nazca Ridge, Arica Bight, and Iquique Basin) faulting of the subducting plate is either parallel to the trend of the trench or parallel to the magnetic fabric of the plate. Only in the Yaquina Basin area do the faults appear to prefer neither of these orientations.

Faulting of the Nazca plate in the Yaquina Basin survey area has a dominant trend of about 339°, about 10° more northerly than either the trend of the trench or the trend of the magnetic anomalies. Warsi et al. [*1983*] proposed that the nearby Mendaña fracture zone has been re-activated as a seaward propagating rift. Huchon and Bourgois [*1990*] proposed that the opening associated with the rifting of the Mendaña fracture zone is being accommodated by oblique thrusting and strike-slip motion along the Trujillo trough to the north. It is very likely that this extension in the Nazca plate is affecting the faulting pattern along the nearby trench.

Faulting in the Lima Basin survey area forms a strong trend at about 330°. This

Figure 3.7 Sector diagram and histogram of fault azimuths for the Iquique Basin survey area. The sector diagram is weighted by the length of the fault segments. A darker sector plot of the trend of the trench is overlain on the fault sector diagram. T is the trend of the trench in the survey area. M is the trend of magnetic anomalies on the Nazca plate. C is the plate convergence direction.

Iquique Basin Survey

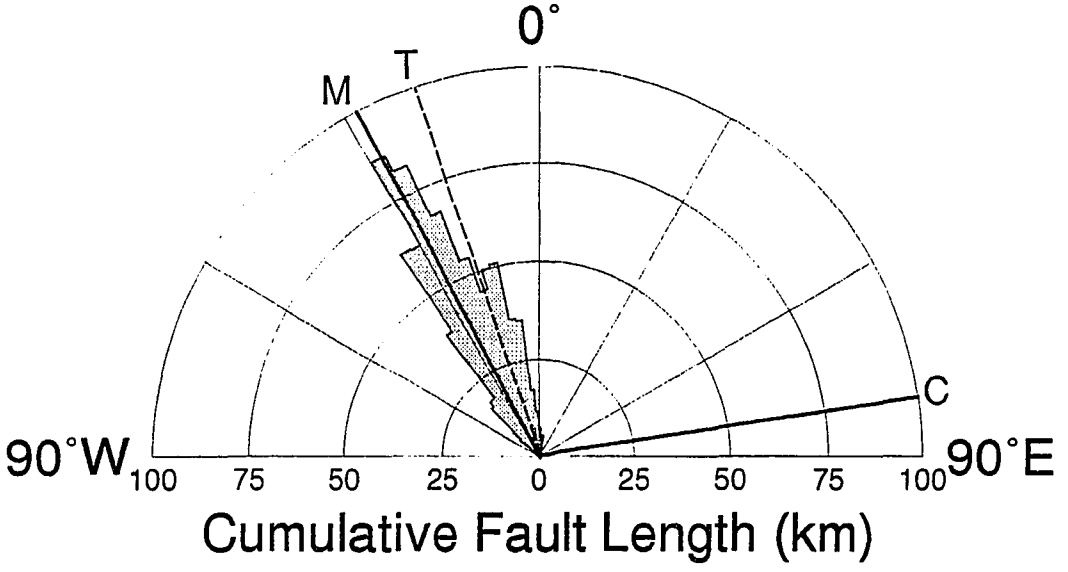

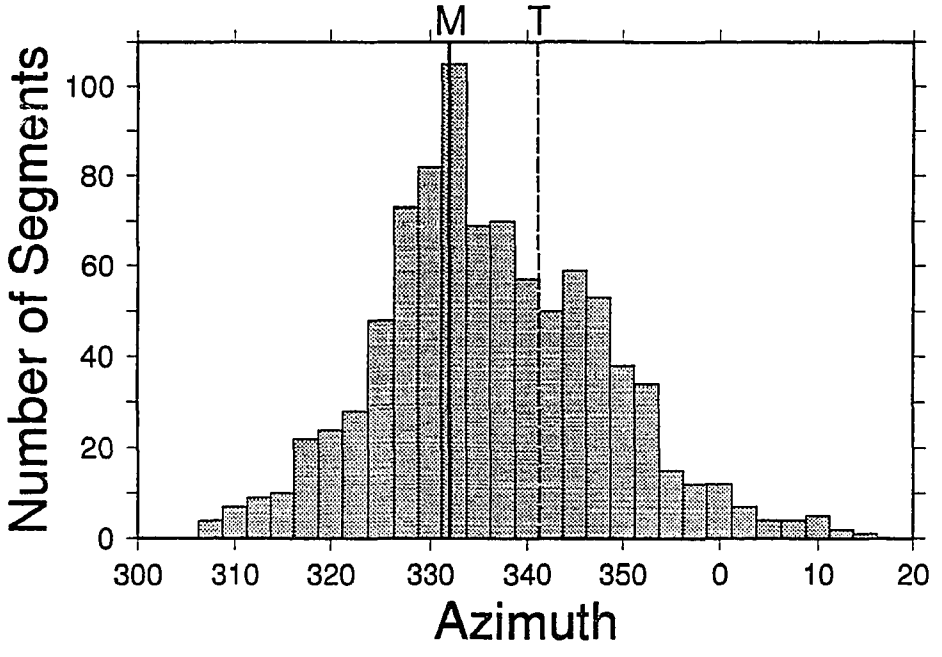

TABLE 3.1. Faulting and subduction related parameters for SeaMARC II surveys along the Peru-Chile trench.

SURVEY	AREA (km^2)	WIDTH OF FAULT ZONE	FAULT SPACING	FAULT THROW	FAULT LENGTHS	MEAN FAULT AZIMUTH	TRENCH AZIMUTH	MAGNETIC TREND	PLATE AGE	PLATE DIP	CONVERGENCE DIRECTION
YAQUINA BASIN	1200	> 35 km	2 - 5 km	50 - 300 m	2 - 26 km	339°	329°	332°	30 Ma	10°	081°
LIMA BASIN	1500	> 40 km	2 - 8 km	50 - 200 m	3 - 24 km	330°	329°	332°	44 Ma	10°	081°
NAZCA RIDGE	7500	50 km	2 - 8 km	50 - 300 m	4 - 50 km	315°	316°	332°	45 Ma	?	081°
ARICA BIGHT	1500	> 50 km	1 - 5 km	50 - 500 m	3 - 24 km	332°	322°	332°	52 Ma	30°	081°
IQUIQUE BASIN	4800	60 km	1 - 5 km	50 - 500 m	3 - 42 km	332°	341°	332°	54 Ma	30°	081°

trend is essentially parallel to both the trend of the trench (329°) and the trend of the magnetic anomalies (332°) in this area. The Lima Basin survey is within the area covered by a larger GLORIA survey along the Peru trench [*Warsi et al.*, 1983]. This GLORIA survey extended well out onto the Nazca plate and revealed seafloor spreading fabric with trends of 325-330° north of the Mendaña fracture zone and 333-338° trends south of the fracture zone. Interestingly, most of the GLORIA survey area shows subduction-induced faulting with a trend of 340-345°, similar to what we see in the Yaquina Basin survey area. In this larger context, the Lima Basin area appears to be anomalous by having faults parallel to the trend of the trench and the spreading fabric.

Faulting trends in the Nazca Ridge survey area are highly varied but are generally grouped around the trend of the trench (316°). Some of this variability may be due to the presence of volcanism on the seafloor in this area. A large east-west trending volcanic ridge in the southern portion of the survey area appears to deflect fault trends adjacent to it. The thickened and presumably inhomogeneous crust of the Nazca Ridge itself may also scatter the fault trends.

The fact that faulting within the Nazca Ridge survey area follows the trend of the trench rather than the spreading fabric trend is not really surprising. The Nazca Ridge is believed to have formed by the interaction of a hotspot with a spreading center [*Pilger and Handschumacher*, 1981]. The ridge probably has no spreading fabric to provide zones of weakness and faulting in the subduction zone therefore occurs on trench-parallel trends.

The Arica Bight and Iquique Basin surveys are along a strongly curving portion of the trench (Figure 3.1). These surveys provide the clearest example of faulting that follows the magnetic fabric trend rather than the trend of the trench. Although the trend of the trench differs by 19° between the two surveys, the faulting maintains a constant trend of 332°, parallel to the magnetic anomaly trend.

Conclusions

In 3 of the 5 survey areas studied (Lima Basin, Arica Bight, Iquique Basin), fault trends on the subducting Nazca plate parallel the trend of magnetic anomalies on the Nazca plate. In the Nazca Ridge survey area faulting parallels the trench trend, probably because of a lack of spreading fabric on the ridge. Only in the Yaquina Basin survey area does faulting follow neither the trench or the spreading fabric trend. This may be due to changes in the stress field of the subducting plate caused by nearby extension along the Mendaña Fracture Zone.

These results generally agree with Masson's [*1991*] study of subduction-related faulting in which he concluded that faulting will follow the trend of the spreading fabric as long as it differs from the strike of the dipping slab by less than 30°. The angle between the trench and the spreading fabric is less than 10° in all 5 of the surveys examined here (Table 1), and the preference for faulting to follow the spreading fabric is clear, particularly in the Arica Bight and Iquique Basin survey areas.

CHAPTER 4

A LARGE MEANDERING SUBMARINE CANYON SYSTEM ON THE PERU-CHILE FOREARC: MORPHOLOGY OF THE UPPER CANYON

Abstract

SeaMARC II side-scan sonar data collected during a survey in the Arica Bight area off southern Peru and northern Chile reveal an extensive submarine canyon system and drainage network in the East Arequipa Basin. The main branch of this canyon system (Tambo submarine canyon) extends for more than 100 km along the axis of the basin in water depths of 400 to 1600 m. This canyon is 350 to 1100 m wide, and has relief of 160 to 230 m through most of this distance. The canyon is highly meandering and has an overall sinuosity of almost 2, comparable to highly meandering subaerial rivers. Morphologic analysis of the canyon shows that the meandering is nearly identical in form to that observed on land.

We believe that Tambo submarine canyon did not develop by mass-wasting and headward erosion, but formed from channelized turbidity flows that filled the basin from the north and began to erode the basin sediments after breaching the structural high bounding the basin. The canyon appears to extend upslope to the mouth of the Rio Tambo in southern Peru and may have been fed by turbidity currents from its delta front. Bordering terraces at several levels above the canyon floor probably formed as meander belts during early stages of canyon formation. Several cutoff meander loops are preserved on these arcuate terraces. Other sedimentary structures observed in the basin and along the canyons include sediment waves, levees, overbank deposits, and crevasse splays.

The terraces observed along the submarine canyon developed as meander belts during periods of canyon stability. Downcutting of the canyon and entrenchment of the meanders may have been caused by breaching of the structural high, faulting of the forearc

seaward of the structural high, or piracy of the lower canyon. An intriguing possibility is that these terraces may correlate with marine terraces observed onshore that formed by uplift of the forearc in the late Pliocene - early Pleistocene.

Introduction

The increasing use of multi-beam bathymetric and swath mapping side-scan sonar systems has shown that submarine canyons are common features on continental margins and island arcs [*Kenyon et al.*, 1978; *Twichell and Roberts*, 1982; *Farre et al.*, 1983; *Scanlon, 1984*; *Taylor and Smoot,* 1984; *Klaus and Taylor*, 1991]. The origin of submarine canyons has been attributed to a variety of mechanisms, including: stream downcutting during low sealevel stands [*Spencer,* 1903; *Shepard*, 1933; *Stetson*, 1936; *Veatch and Smith*, 1939; *Knebel et al.*, 1979], underground water circulation [*Johnson*, 1939], tsunamis [*Bucher*, 1940], faulting [*Gates and Gibson*, 1956; *Belderson and Kenyon*, 1976], turbidity flows [*Daly*, 1936; *Dill*, 1964; *Whitaker*, 1974], or combinations of these [*Shepard and Dill*, 1966]. While some of these ideas have lost favor, others have been incorporated into more comprehensive theories based on data from recent surveys using modern geophysical techniques.

Recently, models for submarine canyon formation have been developed from studies of passive margin canyons, particularly those found along the U.S. Atlantic coast [*Ryan et al.*, 1978; *McGregor et al.*, 1982; *Twichell and Roberts*, 1982; *Farre et al.*, 1983]. Most of the canyons on the U.S. Atlantic continental margin follow direct paths down the slope and do not indent the shelf break. Pinnate drainage patterns characterize the upper reaches of these canyons [*Farre et al.*, 1983]. The larger canyons that indent the shelf break, such as Wilmington Canyon, appear to follow more sinuous paths down the slope

and develop dendritic drainage patterns on the shelf [*McGregor et al.*, 1982; *Stubblefield et al.*, 1982; *Farre et al.*, 1983].

These passive margin submarine canyons are thought to form by mass-wasting and headward erosion on the continental slope. As the canyon develops, episodic sediment suspensions from upslope mass-wasting further modify the channel. Once the canyon head breaches the shelfbreak, transport of shelf sediment and capture of sediment from fluvial drainage systems becomes possible [*Farre et al.*, 1983]. Although this model was developed for canyons on the U.S. Atlantic continental margin, some of the same processes may apply to canyons in active margin settings. It is doubtful, however, if a single model for submarine canyon formation can be applied to active margins which may be subject to tectonic uplift or subsidence, strong seismicity, more varying structural control, and higher rates of sedimentation.

Although submarine canyons are known to be common features on active margins [*Fisher*, 1961; *Barnard*, 1978; *Moore et al.*, 1982; *Gnibidenko and Svarichevskaya*, 1984; *Taylor and Smoot*, 1984; *Thornburg et al.*, 1990], only a few have been studied in detail. In a study of Aoga Shima Canyon on the Izu-Bonin forearc, Klaus and Taylor [*1991*] found that the canyon initiated at a low point in the forearc structural high and developed by headward erosion upslope into the forearc basin. The canyon apparently did not form until the forearc basin had been filled by arc sediments to the spillpoint through the saddle in the structural high. Although the canyon apparently formed by headward erosion in much the same fashion as the U.S. Atlantic margin canyons, its location is controlled by basement structure and the time of its development was controlled by sedimentation.

More than 27,000 km^2 of SeaMARC II side-scan sonar data were collected during a 9.5 day survey of the Arica Bight region off southern Peru and northern Chile in 1987 (Figure 4.1). The entire Arica Bight survey extends from 500 m water depths on the shelf, across the trench axis at more than 7000 m, and onto the subducting Nazca Plate. Survey

Figure 4.1 Tectonic, structural, and morphologic features in the Arica Bight and Iquique Basin survey areas. The outlined areas show the extent of SeaMARC II side-scan sonar coverage. Canyons and channels are shown by the dotted-dashed lines. Tambo submarine canyon flows from north to south across the East Arequipa Basin. Thin solid lines show faults based on the seismic reflection profiles, side-scan images, and swath bathymetry.

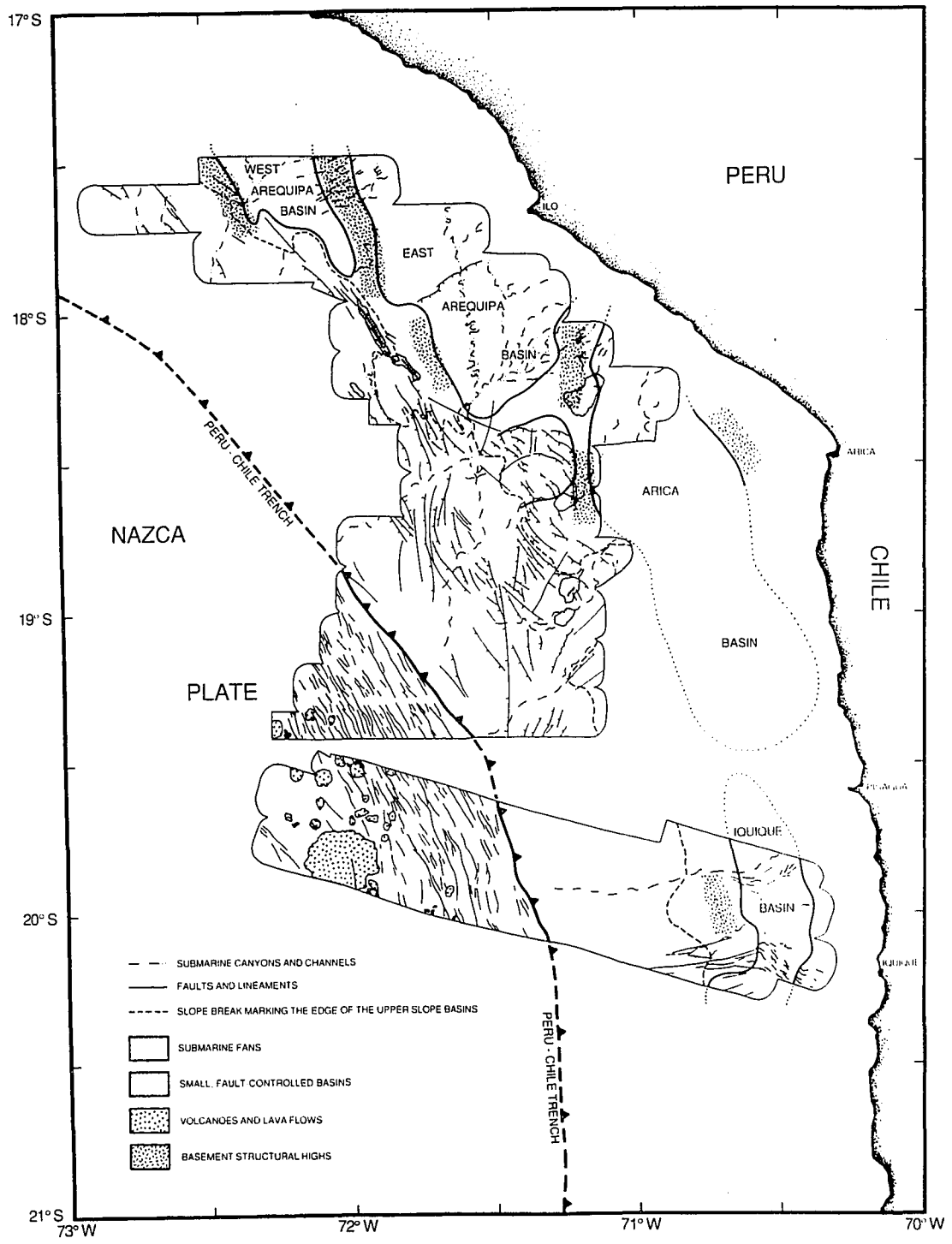
17° S
18° S
19° S
20° S
21° S
73° W
72° W
71° W
70° W
PERU
CHILE
NAZCA
PLATE
WEST
AREQUIPA
BASIN
EAST
AREQUIPA
BASIN
ILO
ARICA
ARICA
BASIN
IQUIQUE
BASIN
PERU - CHILE TRENCH
PERU - CHILE TRENCH
SUBMARINE CANYONS AND CHANNELS
FAULTS AND LINEAMENTS
SLOPE BREAK MARKING THE EDGE OF THE UPPER SLOPE BASINS
SUBMARINE FANS
SMALL, FAULT CONTROLLED BASINS
VOLCANOES AND LAVA FLOWS
BASEMENT STRUCTURAL HIGHS

lines were arranged in a parallel, east-west pattern resulting in nearly 100% side-scan coverage within the survey area. Swath bathymetric coverage is dependent on water depth and ranges from 100% in depths greater than 3000 m to less than 35% in the shallowest parts of the basin. The locations of single-channel seismic reflection profiles collected during this survey are shown in Figure 4.2. This chapter will discuss the portion of the Arica Bight survey across the East Arequipa Basin.

This survey revealed a large, highly meandering submarine canyon system on the Peru-Chile forearc, which appears to have formed as the submarine extension of subaerial drainage systems. The main canyon apparently heads near the mouth of the Rio Tambo in southern Peru and flows for more than 100 km along the axis of the East Arequipa Basin before breaching the forearc structural high and continuing down to the trench axis. Swath bathymetry and nearly complete side-scan sonar coverage of the forearc basin reveal a highly meandering canyon (overall sinuosity nearly 2) with a striking similarity to meandering rivers on land.

Morphology of the East Arequipa Basin and Tambo Submarine Canyon

The Arequipa Basin

The East Arequipa Basin is separated by north-south-trending structural highs from the West Arequipa Basin and the Arica Basin to the east (Figure 4.1). The East and West Arequipa basins are elongated in a north-south direction and form sediment-filled troughs that are truncated at their southern ends by the steep middle forearc slope. The West Arequipa Basin is about 45 km wide and 60 km long within the study area. The East Arequipa Basin is about 60 km wide and about 100 km long (Figure 4.1). The north-south-

Figure 4.2 Contoured SeaMARC II bathymetry of the Arica Bight and Iquique Basin survey areas. Contours in 100's of meters, contour interval is 500 m. Heavy solid lines are the locations of single-channel seismic reflection profiles. Dashed lines are Chilean multi-channel seismic reflection profiles (not discussed in this chapter).

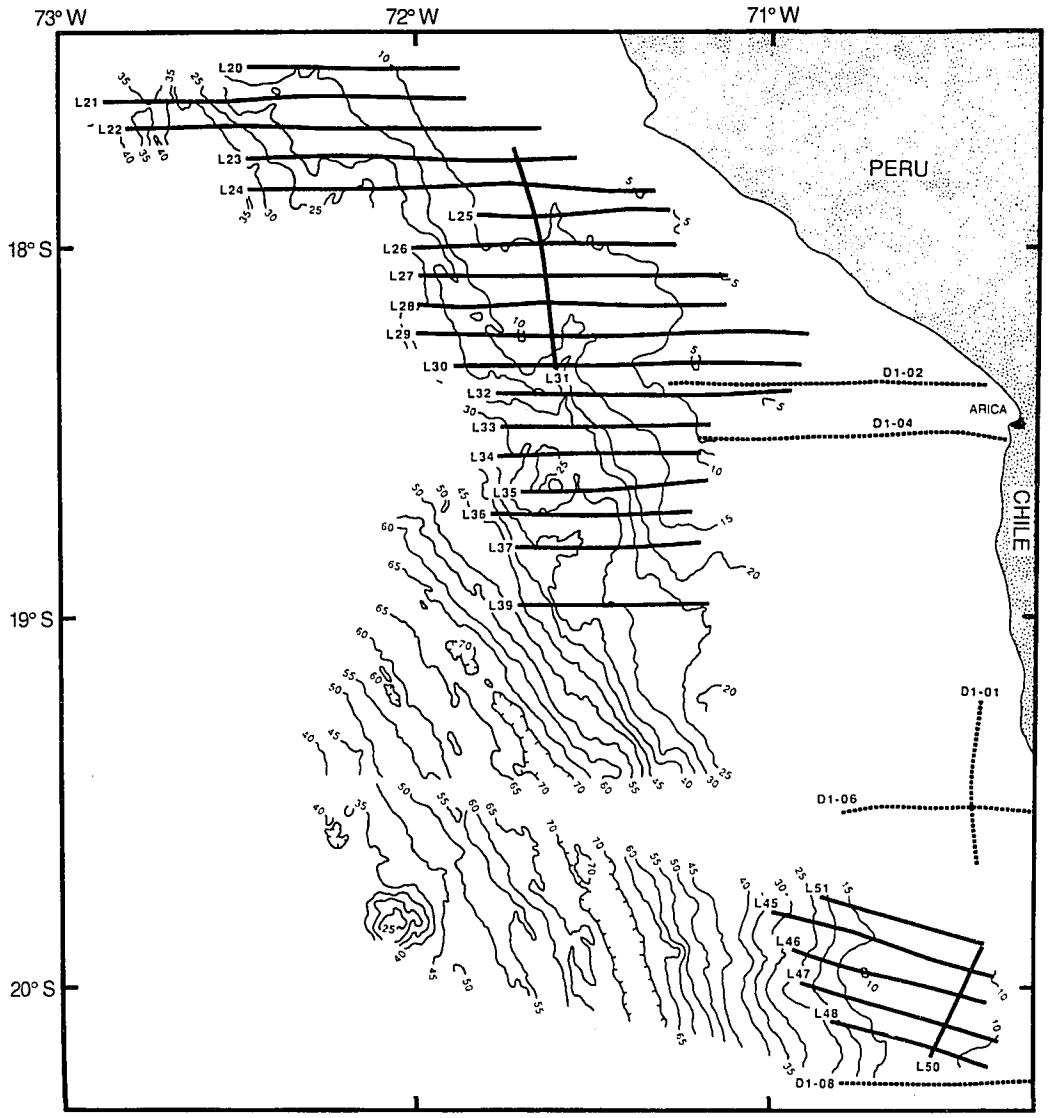
73° W
72° W
71° W
18° S
19° S
20° S
PERU
CHILE
ARICA
L20
L21
L22
L23
L24
L25
L26
L27
L28
L29
L30
L31
L32
L33
L34
L35
L36
L37
L39
L45
L46
L47
L48
L50
L51
D1-01
D1-02
D1-04
D1-06
D1-08

trending structural high separating the two basins is generally covered by sediment but is exposed at the surface near the southern end of the West Arequipa Basin.

The East Arequipa Basin contains as much as 1.6 s of stratified sediment. The maximum thickness of sediment is confined to a narrow north-south trending zone in the west-central part of the basin. Acoustic basement beneath the basin is poorly imaged by our single-channel seismic reflection profiles, but when visible it is highly irregular. The acoustic basement reflection appears to form a series of large blocks that step down toward the trench (Figure 4.3). Movement along these faults does not seem to be recent, since the basin sediments above these blocks appear to be unfaulted. However, the lack of strong reflectors within the basin and the poor quality of our seismic data may limit our ability to observe fault offsets. A single large normal fault with a surface offset of as much as 0.2 s cuts across the basin from northeast to southwest, forming a low-relief scarp visible in the side-scan images. This trend is perpendicular to the trend of the trench and may contribute to the along-strike segmentation of the forearc in this area observed by Coulbourn and Moberly [*1977*].

Tambo submarine canyon and several smaller tributaries form a submarine drainage system within the East Arequipa Basin. The basin forms a shallow north-south oriented bathymetric trough that lies at depths ranging from less than 400 m, to 1600 m where the canyon exits the basin in the south (Figure 4.4). Tambo submarine canyon flows from north to south along the west-central portion of the basin. In the eastern part of the basin several less sinuous tributary canyons coalesce into a larger canyon that joins the Tambo submarine canyon at the southern margin of the basin (Figure 4.5). The resulting canyon is briefly deflected to the southeast along a northwest-trending fault before continuing down the lower forearc slope to the trench axis [*Bergersen*, 1989].

The surface of the basin between and surrounding the canyons appears to be almost completely covered by sediment waves (Figure 4.5). These waves vary in orientation and

Figure 4.3 Single-channel seismic reflection profile across the East and West Arequipa Basins showing the rough basement topography formed by faulting. The large fault blocks appear to step down toward the trench axis along normal faults. M = multiple reflection. Profile location is shown on figure 2 (L24). Vertical exaggeration approximately 9 x.

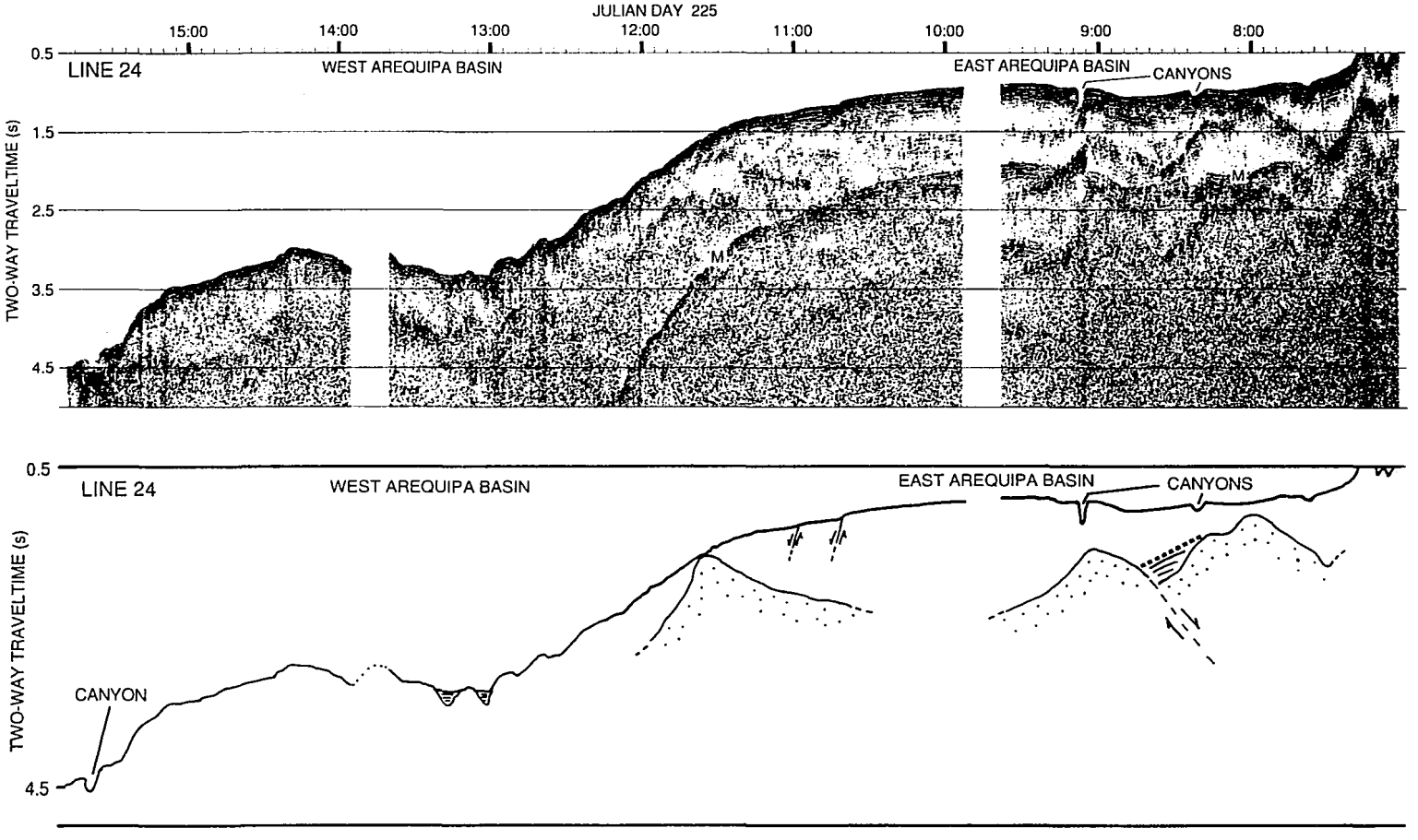
JULIAN DAY 225
15:00
14:00
13:00
12:00
11:00
10:00
9:00
8:00
0.5
LINE 24
WEST AREQUIPA BASIN
EAST AREQUIPA BASIN
CANYONS
TWO-WAY TRAVELTIME (s)
1.5
2.5
3.5
4.5
M
0.5
LINE 24
WEST AREQUIPA BASIN
EAST AREQUIPA BASIN
CANYONS
TWO-WAY TRAVELTIME (s)
CANYON
4.5

Figure 4.4 Contoured SeaMARC II bathymetry of the East Arequipa Basin. Canyon thalwegs are shown by the dashed lines. Contour interval is 100 m.

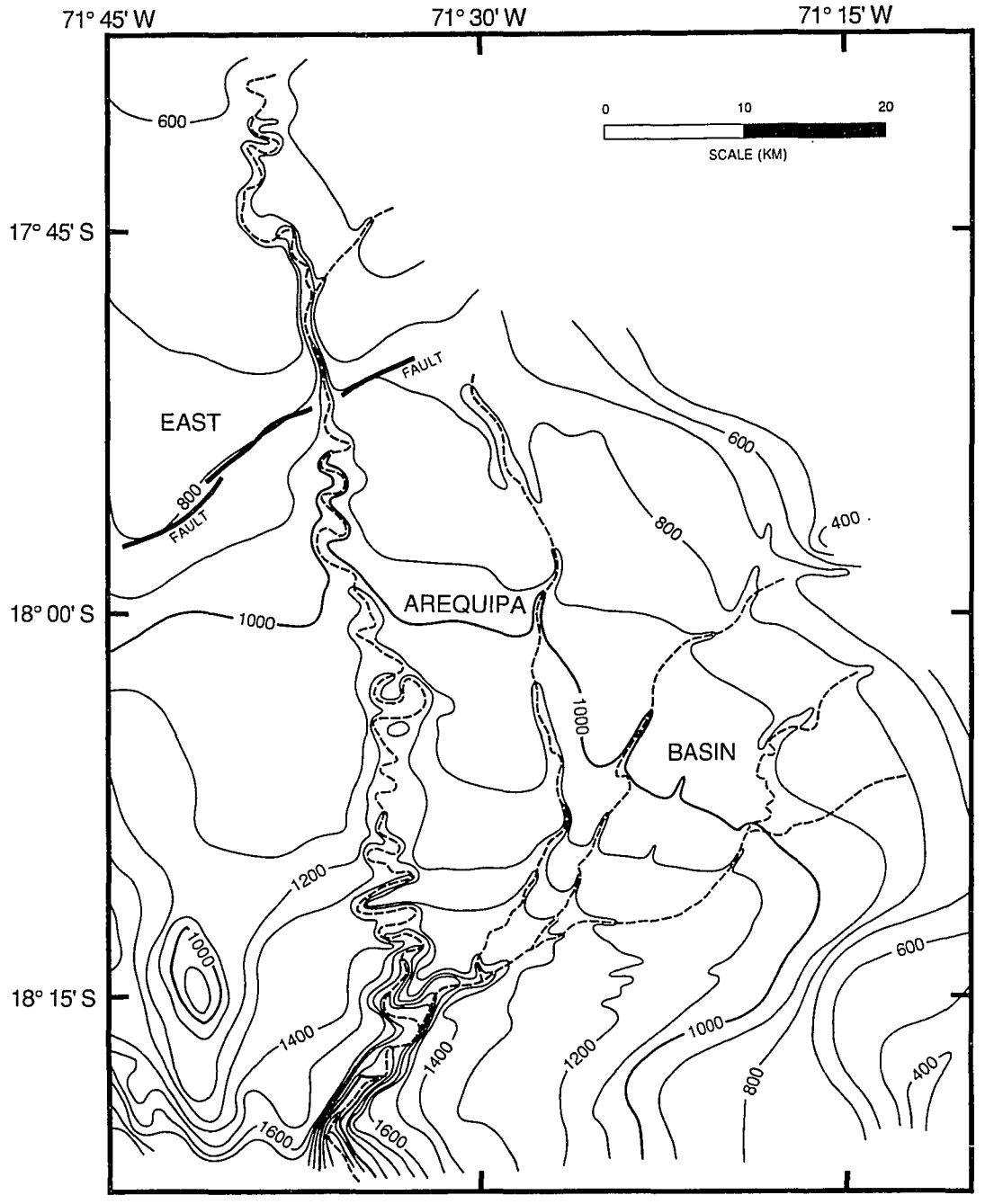
71° 45' W
71° 30' W
71° 15' W
17° 45' S
18° 00' S
18° 15' S
0
10
20
SCALE (KM)
EAST
FAULT
FAULT
FAULT
AREQUIPA
BASIN
600
800
1000
1200
1400
1600
400

Figure 4.5 SeaMARC II side-scan sonar data from the East Arequipa Basin. The highly meandering Tambo submarine canyon and its less sinuous tributaries are clearly visible in this image. Arcuate terraces form a meander belt bordering Tambo submarine canyon. Sediment waves cover the surface of the basin between the canyons. High backscatter areas such as rough-surfaced outcrops and slopes facing the tow vehicle appear dark gray to black. Low backscatter areas appear light gray to white. Steep slopes facing away from the tow vehicle appear as white shadow zones. The image is a mosaic of 10 km wide swaths. The gray stripe down the center of each swath is the shiptrack. Area shown is the same as in Figure 4.4.

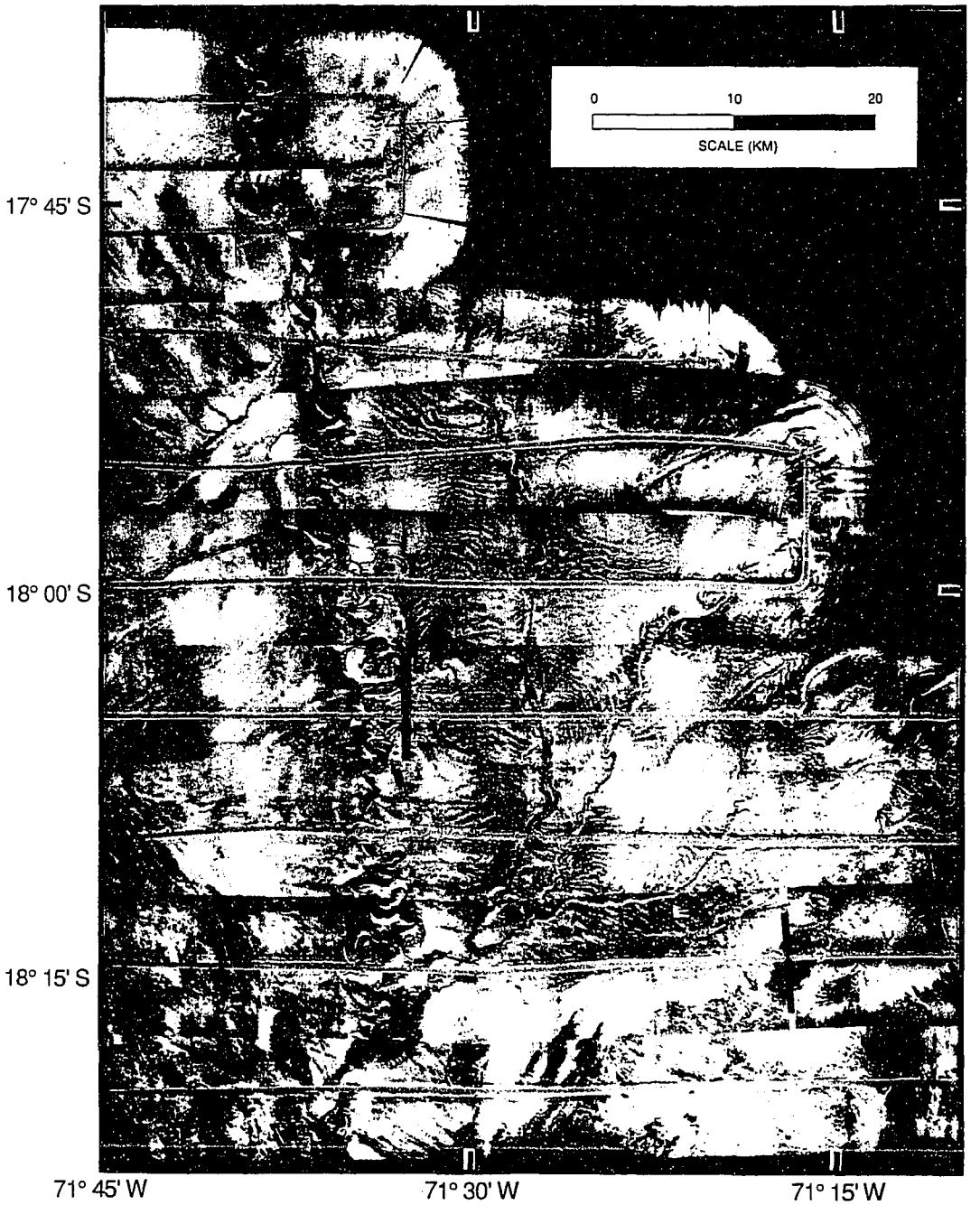
0
10
20
SCALE (KM)
17° 45' S
18° 00' S
18° 15' S
71° 45' W
71° 30' W
71° 15' W

have wavelengths of 400 to 800 m. The sediment waves are of very low amplitude (less than 5 m) and are recognizable on 3.5 kHz echograms only when they are crossed perpendicularly by the shiptrack. Individual wave crests can be traced for up to 6 km on the side-scan image (Figure 4.5). They appear to form several distinct wave fields within which the waves have a common orientation and wavelength. These fields appear to be associated with convex downslope curves in the canyons, suggesting that the sediment waves form by turbidity current overflow from the canyons. Absence of these waves from the west side of Tambo submarine canyon suggests that the canyon is so deeply incised that no turbidity current overflow occurs there.

Tambo Submarine Canyon

Within the East Arequipa Basin, meandering is confined to a 3 to 6 km wide band along Tambo submarine canyon as it follows a generally straight course along the axis of the basin (Figures 4.5 and 4.6). The canyon is 350 to 1100 m wide and exhibits relief of from 160 to 230 m through most of the basin (Figure 4.7). At the southern margin of the basin, however, it becomes much more deeply incised, forming a gorge 2.5 km wide and more than 600 m deep. On the middle forearc slope the canyon is 2 to 4 km wide and its relief decreases to about 200 m before increasing again to nearly 400 m as it approaches the trench axis [*Bergersen*, 1989].

Tambo submarine canyon is bordered by arcuate, canyon-facing scarps within the central part of the East Arequipa Basin. These features were initially interpreted to be large slumps caused by undercutting of the canyon walls by turbidity currents [*Bergersen et al.*, 1987; *Coulbourn*, 1988]. Such slumps are common features along many submarine canyons [*Farre et al.*, 1983; *McHargue and Webb*, 1986; *Carlson and Karl*, 1988; *Klaus*

Figure 4.6 Interpretation of the side-scan data of Figure 4.5 showing the outline of the East Arequipa Basin and the paths of the canyons and channels within the basin. Canyon banks and thalwegs are shown as well as the cutoff meanders and the edges of the meander belt along Tambo submarine canyon. The numbers along Tambo submarine canyon show the 74 meanders examined in this study. The labeled dashed lines show the locations of 3.5 kHz echosounder profiles shown in figure 4.7. The dashed boxes show the locations of side-scan closeups in figures 4.8 - 4.11.

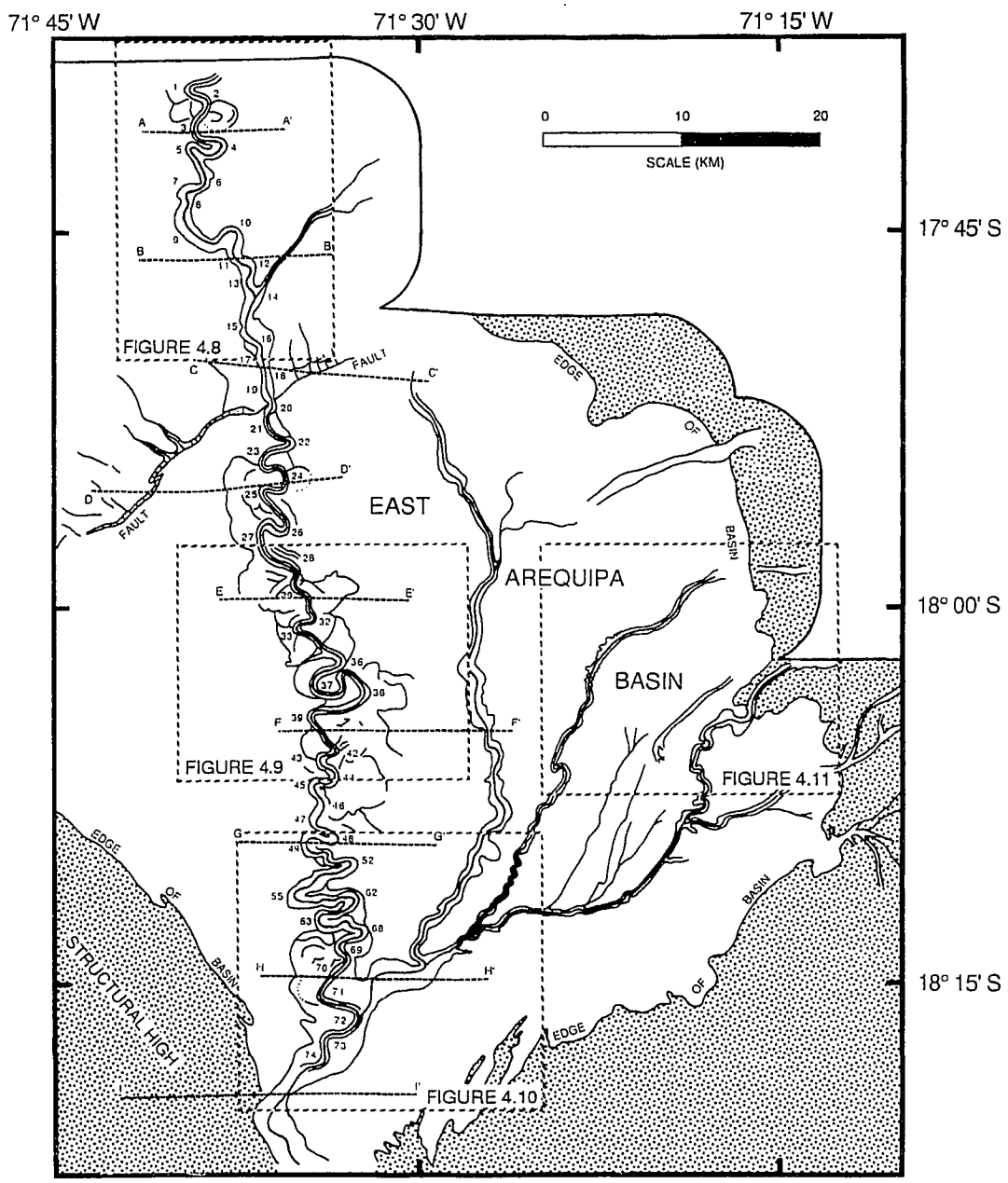
71° 45' W
71° 30' W
71° 15' W
17° 45' S
18° 00' S
18° 15' S
0
10
20
SCALE (KM)
FIGURE 4.8
FIGURE 4.9
FIGURE 4.10
FIGURE 4.11
FAULT
FAULT
EAST
AREQUIPA
BASIN
EDGE OF BASIN
EDGE OF STRUCTURAL HIGH
EDGE OF BASIN

Figure 4.7 3.5 kHz echosounder profiles of canyon crossings. Profile locations are shown on figure 4.6. Each profile shown represents an area about 15 km wide. Vertical exaggeration is approximately 18 x.

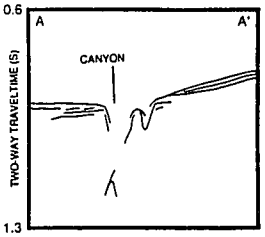
0.6
A
A'
CANYON
TWO-WAY TRAVELTIME (S)
1.3

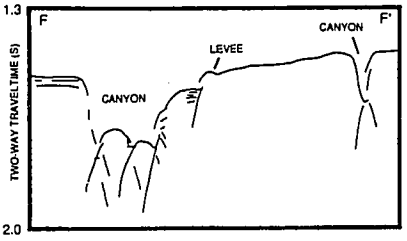
1.3
F
F'
CANYON
LEVEE
CANYON
TWO-WAY TRAVELTIME (S)
2.0

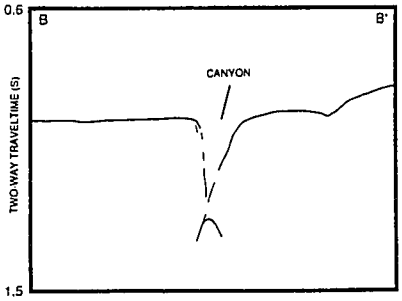
0.6
B
B'
CANYON
TWO-WAY TRAVELTIME (S)
1.5

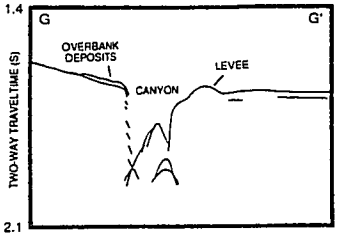
1.4
G
G'
OVERBANK DEPOSITS
LEVEE
CANYON
TWO-WAY TRAVELTIME (S)
2.1

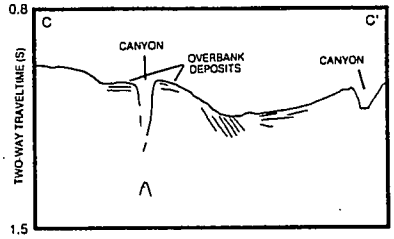
0.8
C
C'
CANYON
OVERBANK DEPOSITS
CANYON
TWO-WAY TRAVELTIME (S)
1.5

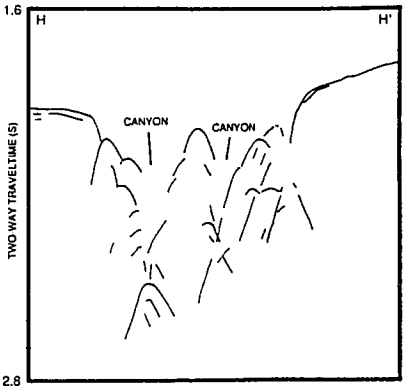
1.6
H
H'
CANYON
CANYON
TWO WAY TRAVELTIME (S)
2.8

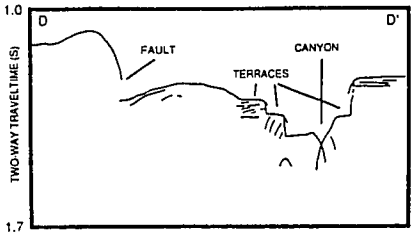
1.0
D
D'
FAULT
CANYON
TERRACES
TWO-WAY TRAVELTIME (S)
1.7

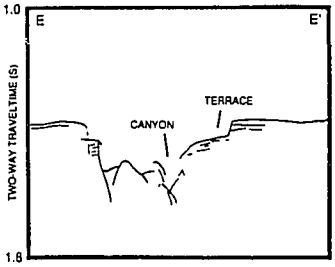
1.0
E
E'
TERRACE
CANYON
TWO-WAY TRAVELTIME (S)
1.8

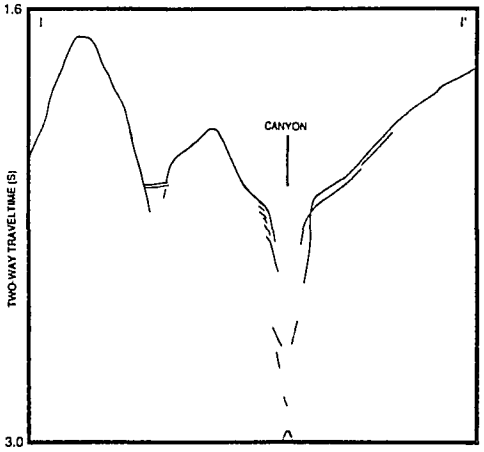
1.6
I
I'
CANYON
TWO WAY TRAVELTIME (S)
3.0

and Taylor, 1991]. Greene et al. [*1989*] proposed that sidewall slumping is responsible for the meandering in the upper Monterey Submarine Canyon.

Recent improvements in SeaMARC II side-scan processing techniques [*Sender et al.*, 1989; *Shor*, 1990] allow new details to be seen in the images of Tambo submarine canyon that lead us to re-interpret these arcuate scarps as the borders of terraces formed by the meandering canyon. One important observation that supports this interpretation is the presence of abandoned channel segments or cutoff meander loops on some of these terraces (Figures 4.8, 4.9, and 4.10). The directional "illumination" of the side-scan sonar acoustic energy reflects strongly from canyon walls that face the towfish and leaves shadows as it looks over the edges of the near walls. Cutoff meanders on the terraces surrounding the canyon are clearly recognized by the sharp-edged reflections and shadows from the former channel walls, and the high areas in the center of the meander loops (Figures 4.8, 4.9, and 4.10). The terraces generally extend perpendicular to or even downslope from the canyon, unlike the upslope-oriented slumps along Aoga Shima Canyon in the Bonin forearc that often lead to canyon branching [*Klaus and Taylor*, 1991]. The terraces also appear to occur at common levels on either side of the canyon, which would be unlikely if they formed by slumping. Terrace width is not symmetric about the canyon but generally alternates between the east and west side of the present canyon (Figure 4.6). Near profile D-D' terraces are best developed on the west side of the canyon. To the south, near profile F-F', the terraces are most prominent on the east. At the southern edge of the basin, near profile H-H', the terraces are once again best developed on the west side of the canyon. This suggests that the canyon meanders at long wavelengths (about 36 km) within the basin as well as in the readily observed meander loops.

Slumping on a smaller scale does occur along the canyon and occasionally on the terrace walls. These slumps probably result from bank undercutting by turbidity currents.

Figure 4.8 Closeup of side-scan sonar data across the northern portion of Tambo submarine canyon. The canyon has a sinuosity of nearly 2 along this stretch, which lies above the northeast-trending fault that divides the basin. The cutoff meander in the upper portion of this figure has a steep-sided central high that casts a strong acoustic shadow on the side away from the shiptrack. Location of this figure is shown on Figure 4.6.

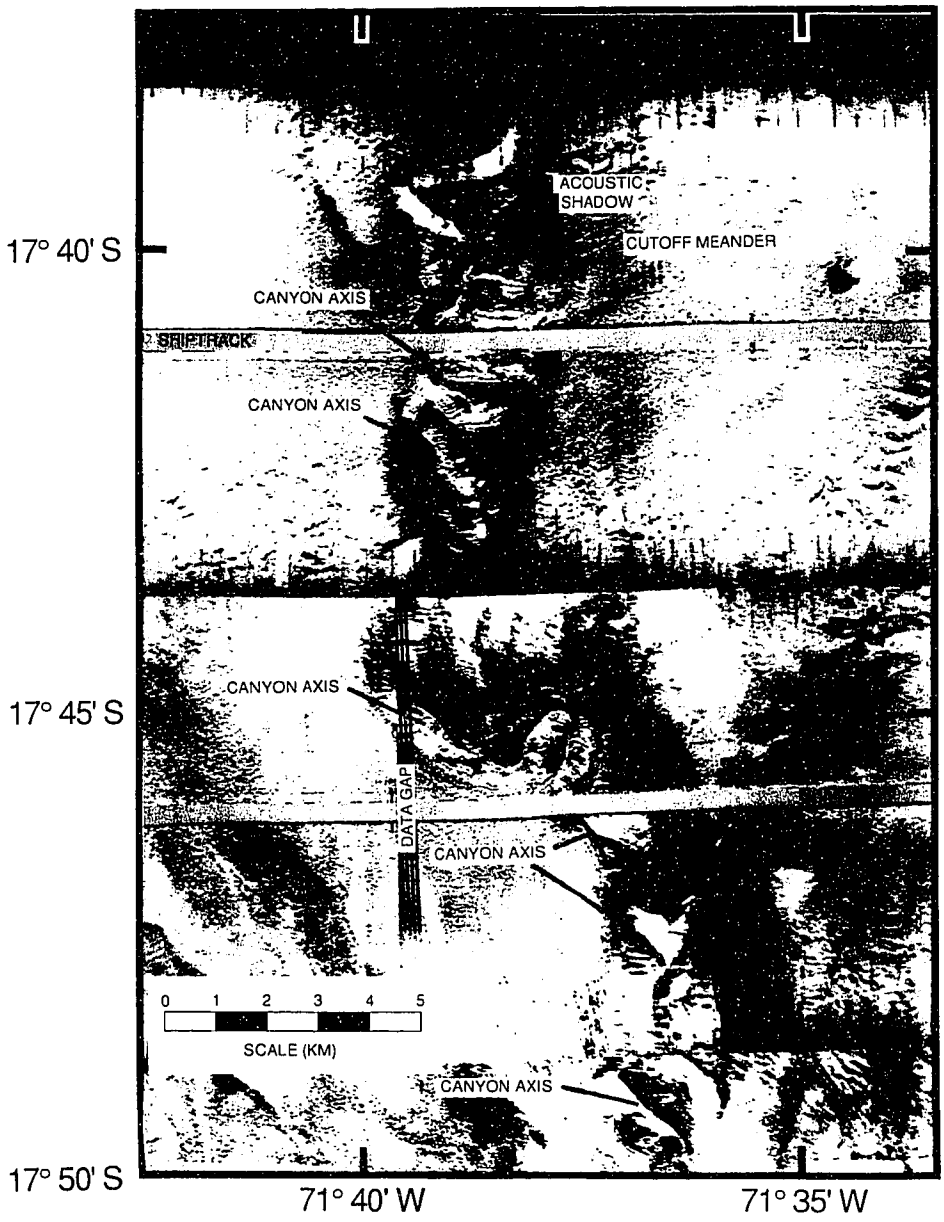
17° 40' S
17° 45' S
17° 50' S
71° 40' W
71° 35' W
ACOUSTIC SHADOW
CUTOFF MEANDER
CANYON AXIS
SHIPTRACK
CANYON AXIS
CANYON AXIS
DATA GAP
CANYON AXIS
0 1 2 3 4 5
SCALE (KM)
CANYON AXIS

Figure 4.9 Closeup of side-scan sonar data across the central portion of Tambo submarine canyon, just south of the northeast-trending fault. Canyon sinuosity in this stretch is over 3. Several arcuate terraces are visible in this image. A cutoff meander is clearly shown in the upper portion of the figure. Sediment waves are prominent on the basin floor to the east of the canyon but are noticeably absent on the western side. Location of this figure is shown on Figure 4.6.

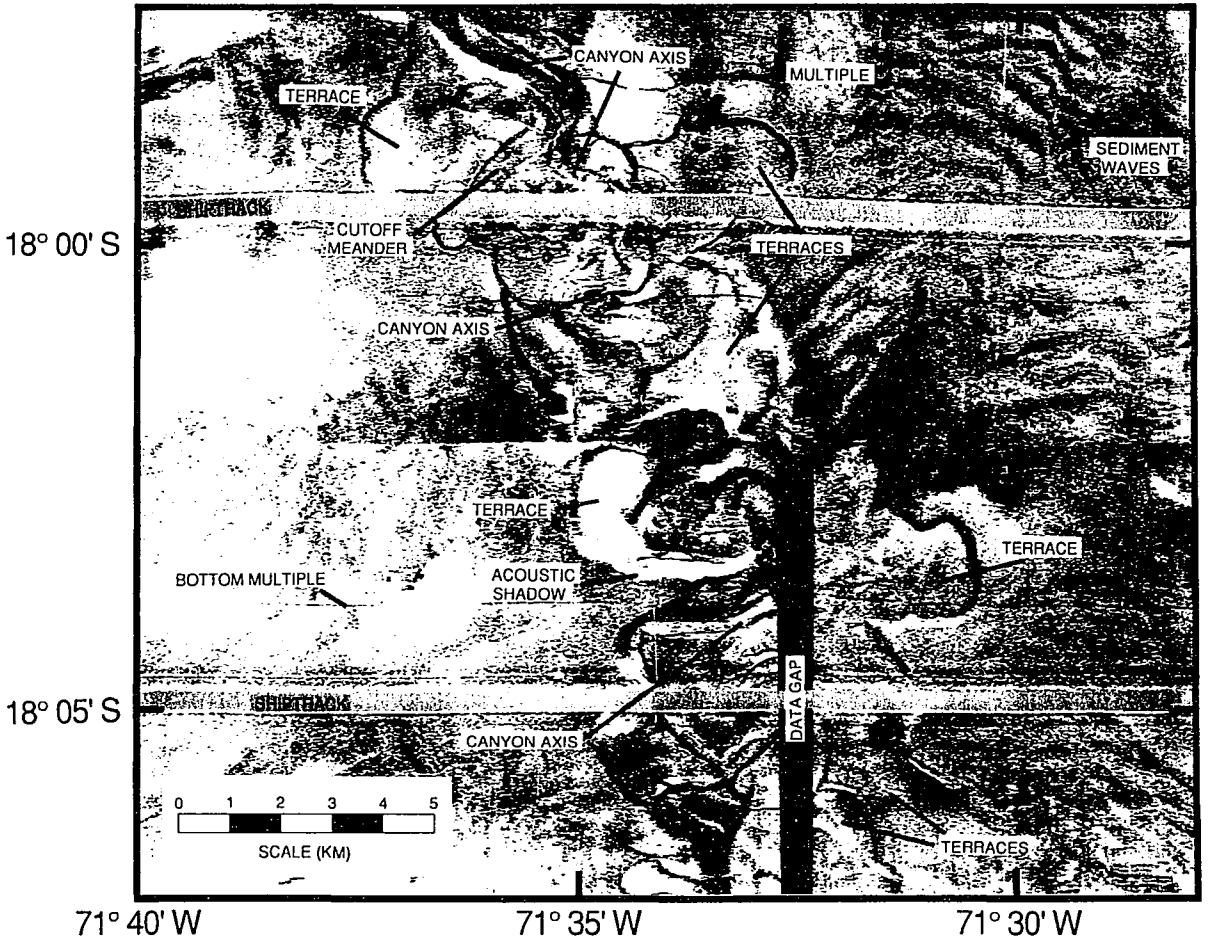
CANYON AXIS
MULTIPLE
TERRACE
SEDIMENT WAVES
GRIDTRACK
CUTOFF MEANDER
TERRACES
18° 00' S
CANYON AXIS
TERRACE
TERRACE
BOTTOM MULTIPLE
ACOUSTIC SHADOW
DATA GAP
GRIDTRACK
18° 05' S
CANYON AXIS
0 1 2 3 4 5
SCALE (KM)
TERRACES
71° 40' W
71° 35' W
71° 30' W

Figure 4.10 Closeup of side-scan sonar data across the southern portion of Tambo submarine canyon and the three smaller tributary canyons to the east. Tambo submarine canyon has a sinuosity of more than 3 in this area whereas the smaller canyons have sinuosities of only 1.2 to 1.5. The relief of Tambo submarine canyon increases rapidly in this area, from 210 m at the top of the figure to about 550 m in the south as the canyon approaches the breach in the forearc structural high. Location of this figure is shown on Figure 4.6.

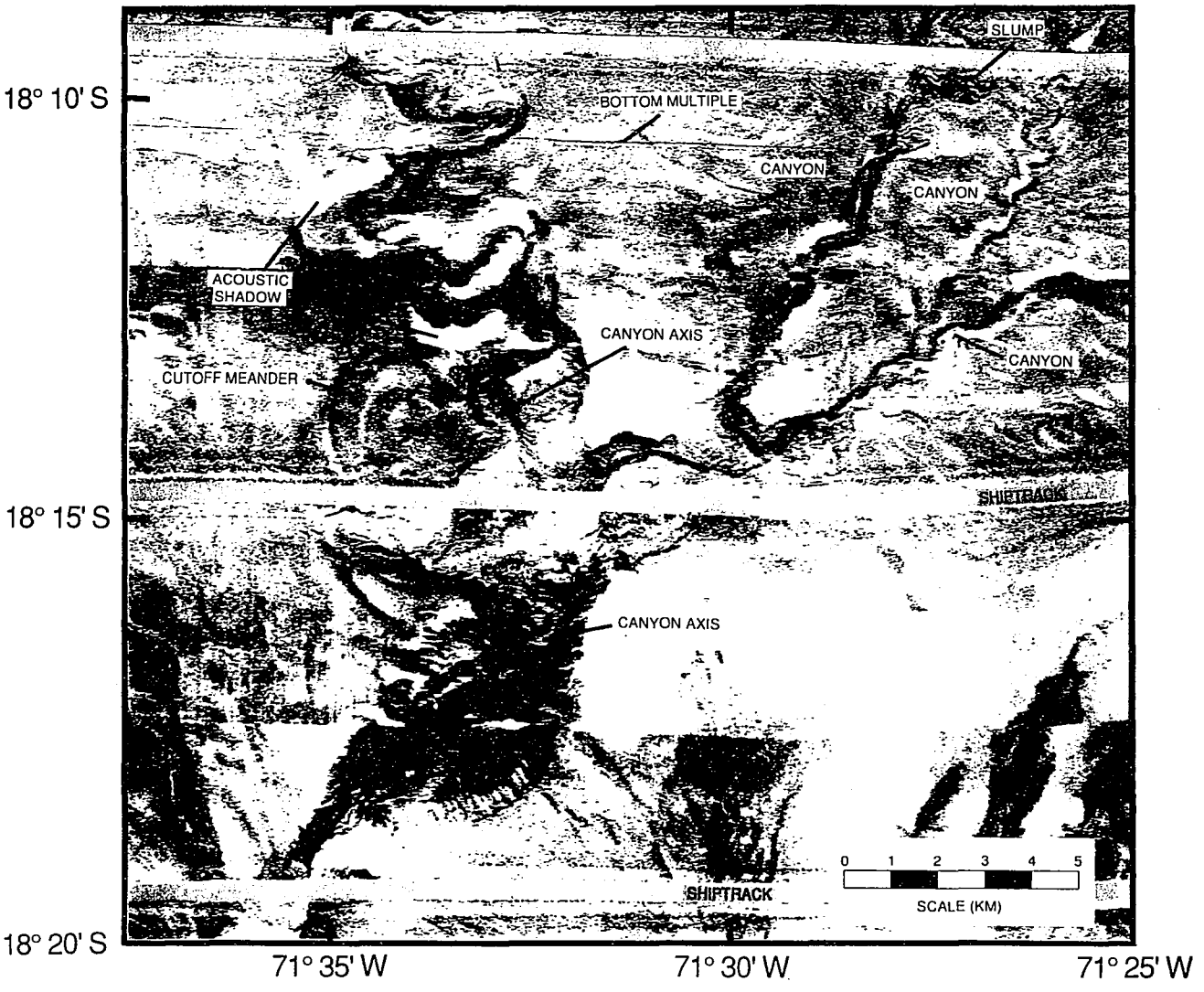
SLUMP
BOTTOM MULTIPLE
CANYON
CANYON
ACOUSTIC SHADOW
CANYON AXIS
CANYON
CUTOFF MEANDER
SHIPTRACK
CANYON AXIS
SHIPTRACK
0 1 2 3 4 5
SCALE (KM)
18° 10' S
18° 15' S
18° 20' S
71° 35' W
71° 30' W
71° 25' W

They generally occur on the outside banks of canyon meander loops and provide a mechanism for meander growth and migration similar to meandering subaerial rivers.

Other characteristic features of meandering subaerial rivers that also appear along the East Arequipa Basin submarine canyons are levees, overbank deposits, and crevasse splays. Levees and overbank deposits occur along all of the canyons, forming low sediment ridges along the banks of the canyons that are 500 to 1500 m wide and 10 to 20 m high (Figure 4.7). Along the unterraced and less incised canyons east of Tambo submarine canyon, these levees are often cut by crevasse splays where canyon overflow became focused (Figure 4.11).

Morphologic Analysis of Tambo Submarine Canyon

Tambo submarine canyon is divided into two reaches within the East Arequipa Basin by the northeast-trending fault that crosses the basin (Figure 4.6). Although the morphology of the canyon is generally uniform, slope changes caused by this fault reduce the sinuosity of the canyon as it cuts through the uplifted block. As a result, the 24.1 km of the canyon north of the fault has a channel length of 37.5 km yielding a sinuosity of 1.55, while the 43.8 km of the canyon between the fault and the tributary intersection has a channel length of 95.1 km and a resulting sinuosity of 2.17. The sinuosity of the entire canyon above the forearc structural high is 1.95. River channels with sinuosity greater than 1.5 are termed meandering [*Leopold and Wolman*, 1957] (the highly meandering 100 km of the Mississippi River below the Arkansas River has a sinuosity of 2.3 [*Schumm et al.*, 1972]).

Although sinuous submarine canyons have been noted along other margins [*McGregor et al.*, 1982; *Stubblefield et al.*, 1982; *Farre et al.*, 1983; *Greene et al.*, 1989; *Klaus and Taylor*, 1991], none matches the degree of meandering exhibited by this canyon.

Figure 4.11 Closeup of side-scan sonar data across the eastern portion of the study area showing sediment waves, small dendritic debris channels, and crevasse splays along one of the small canyons. Location of this figure is shown on Figure 4.6.

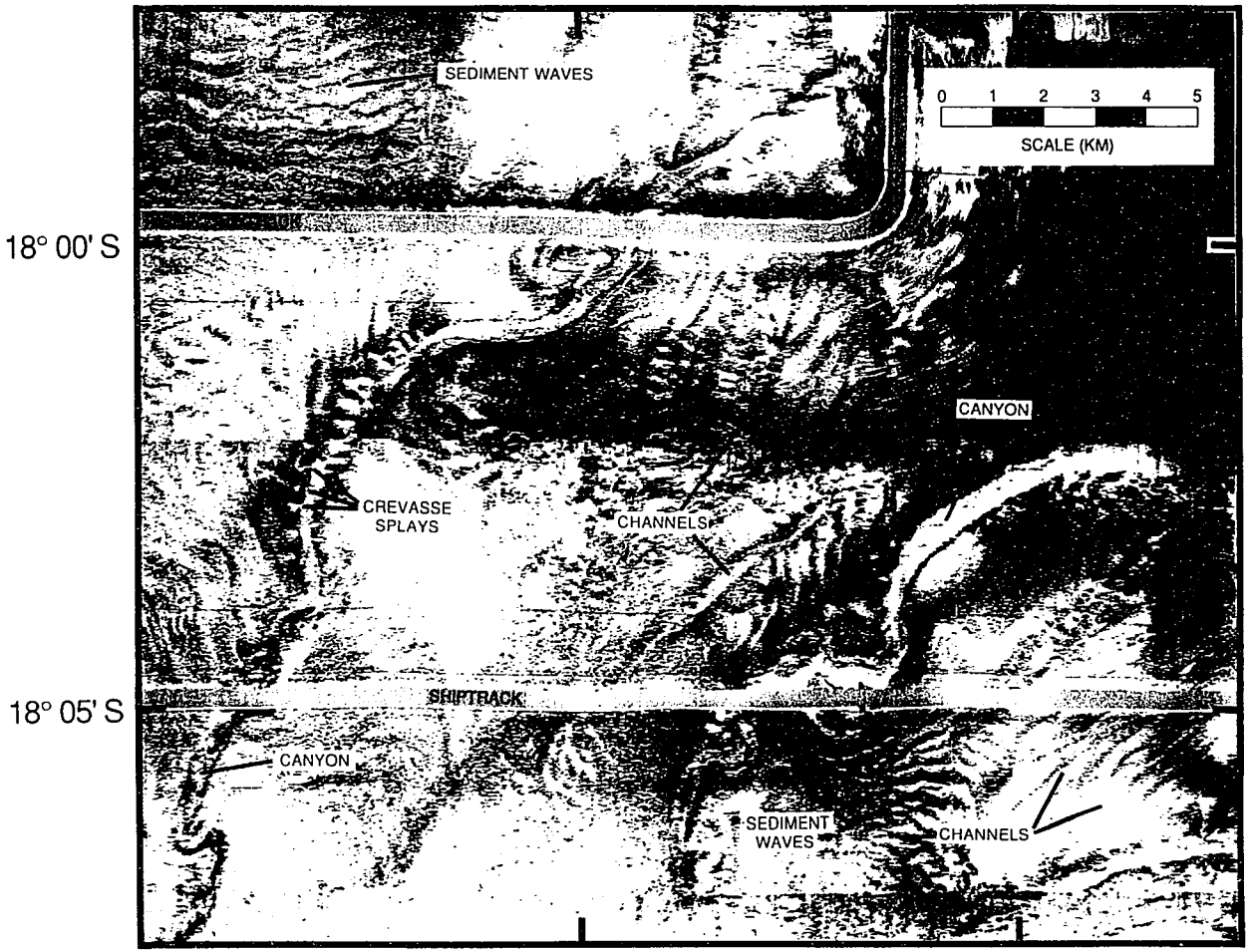
SEDIMENT WAVES
0 1 2 3 4 5
SCALE (KM)
CANYON
CREVASSE SPLAYS
CHANNELS
SHIPTRACK
CANYON
SEDIMENT WAVES
CHANNELS
18° 00' S
18° 05' S
71° 25' W
71°20' W
71° 15' W

The highly meandering form of the Tambo submarine canyon is difficult to explain with turbidity current models for canyon flow involving infrequent, large, high-velocity flows. Frequent or continuous low-velocity turbidity flows would seem to be required to develop and maintain the intricate meanders of Tambo submarine canyon. This same conclusion was also reached by Flood and Damuth [*1987*] and Damuth et al. [*1988*] to explain intricately meandering distributary channels they observed on the Amazon Fan.

In an effort to understand the processes involved in creating this canyon, we studied variations in several canyon parameters. Measurements of basin depth and channel depth from 3.5 kHz echosounder records were made at the nine crossings of the canyon (at spacings ranging from 8.2 to 10 km). Measurements of channel length and channel width were made directly from the side-scan mosaic, as were measurements of meander wavelength, amplitude, and radius of curvature for 74 meanders along Tambo submarine canyon (Figure 4.6) and the smaller canyons to the east. Meander length was measured between inflection points in the curving channel. Meander wavelength was taken as twice this distance and meander amplitude as the lateral offset of the canyon from the straight line connecting the inflection points. The radius of curvature was determined as the best visual fit to the sometimes asymmetrical meanders.

Laboratory experiments and observations of meandering in rivers have shown that sinuosity is related to valley slope and sediment load[*Schumm and Khan*, 1972; *Schumm et all.*, 1972]. Meanders are believed to develop as a stream attempts to maintain the optimal channel slope for its sediment load on varying valley slopes. Sinuosity in rivers is seen to increase with increasing valley slope until a threshold is reached, at which point a relatively straight braided channel develops [*Schumm*, 1977]. In large rivers such as the Mississippi this threshold value for maximum valley slope is at about 0.14 m/km [*Schumm*, 1977]. Sinuosity in submarine fan channels has been observed on slopes of more than 10 m/km [*Flood and Damuth*, 1987]. These steeper submarine gradients may be due to the smaller

density difference of turbidity current vs. water compared to water vs. air [*Flood and Damuth*, 1987].

In the case of the Tambo submarine canyon, sinuosity mimics basin slope and increases with increasing basin slope up to slope values of about 15 m/km (Figure 4.12). The sudden drop in sinuosity (from 3.7 to 1.7) that occurs with the rise in basin slope (from 12 to 21 m/km) between -18 and 0 km down basin may result from crossing a maximum slope threshold for submarine meandering. Figure 4.12 also shows that while basin slope and sinuosity vary widely along the canyon, channel slope varies only slightly, remaining near 7 m/km through most of the basin. Only when the basin slope exceeds 15 m/km does the channel slope increase, reaching values greater than the basin slope as the downcutting canyon exits the basin.

Basin slope is not the only control on meandering. An intriguing aspect of the Arequipa Basin canyons is the difference in sinuosity between Tambo submarine canyon and the smaller tributary canyons, even though they are all flowing across essentially the same basin slopes (Figure 4.13). The smaller canyons east of Tambo submarine canyon may have formed later than Tambo submarine canyon and thus may represent earlier stages in canyon development along this margin. Their relative youth cannot, however, fully explain their low-sinuosity channels.

Canyon B (immediately east of Tambo submarine canyon) is incised up to 100 m into the basin, an amount comparable to the depth of the present channel of Tambo submarine canyon below the deepest terrace. Assuming that this depth of incision represents an equal period of time, why is the sinuosity of Canyon B so much less than that of Tambo submarine canyon? Figure 4.14 shows a plot of canyon channel slope vs. basin distance for Tambo submarine canyon, Canyon B, and Canyon C. This plot shows that the preferred gradient for Tambo submarine canyon is about 7 m/km while Canyon B and Canyon C prefer a gradient of about 12 m/km across the same basin slopes. All of the

Figure 4.12 Plot of basin slope, canyon slope, and sinuosity along Tambo submarine canyon. Canyon channel length was measured every 2 km and sinuosity was computed every 4 km along the canyon. Basin and canyon slopes were measured between 3.5 kHz echosounder crossings of the canyon. Sinuosity has no units, but is multiplied by 10 and plotted on the same scale as the slope values. Sinuosity varies with basin slope while canyon slope remains near 7 m/km along most of the canyon. Basin distance 0 is the intersection of Tambo submarine canyon with the smaller canyons to the east. Up canyon distances are given in negative kilometers from this point. The northeast-trending fault that crosses the basin is shown by the vertical line at -43 km.

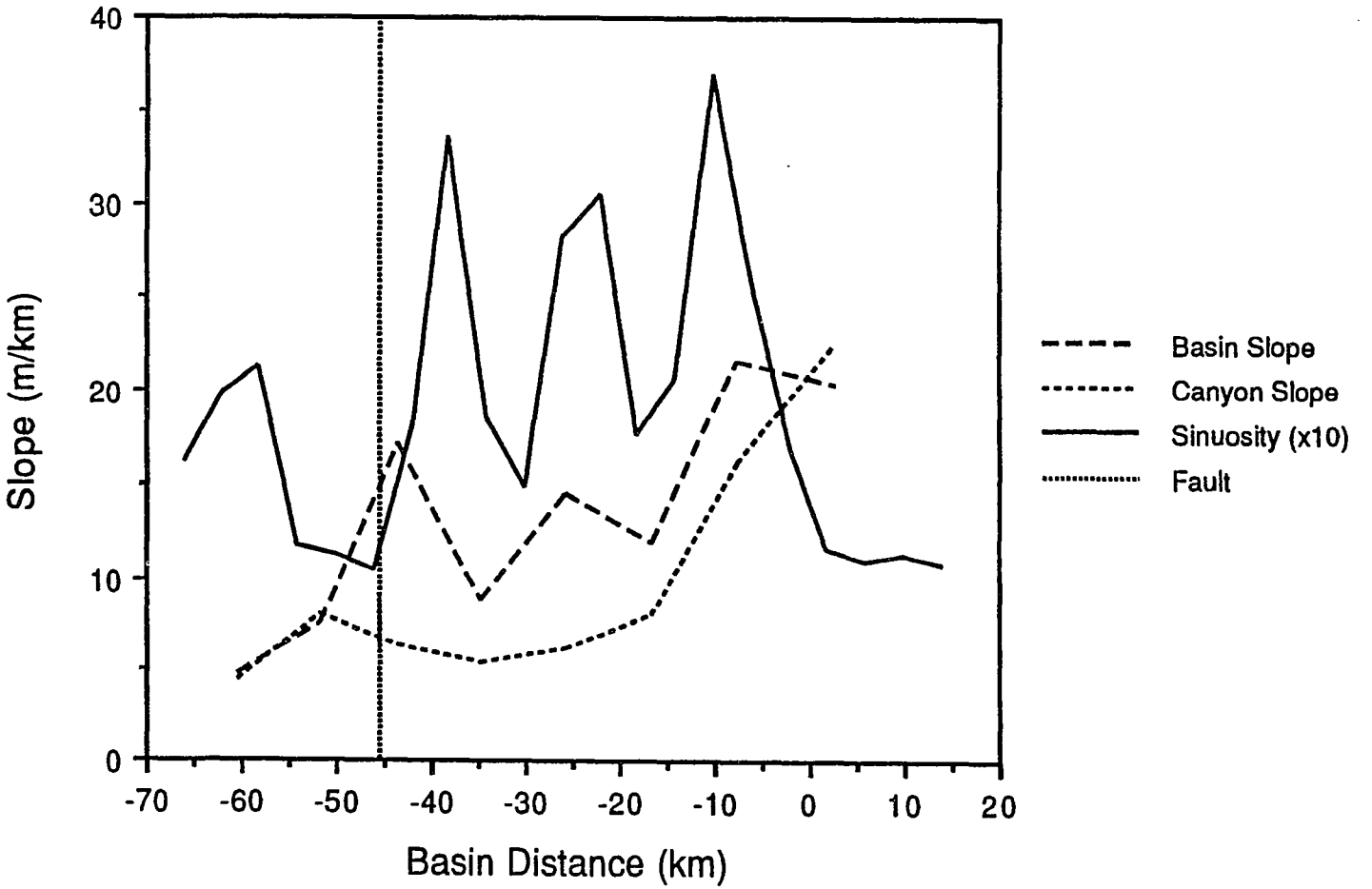
40
30
20
10
0
Slope (m/km)
-70
-60
-50
-40
-30
-20
-10
0
10
20
Basin Distance (km)
Basin Slope
Canyon Slope
Sinuosity (x10)
Fault

Figure 4.13 Plot of sinuosity vs. basin distance for all of the East Arequipa Basin canyons. Basin distance 0 is the intersection of Tambo submarine canyon with the smaller canyons to the east. Up canyon distances are given in negative kilometers from this point. Canyon channel lengths were measured every 2 km and sinuosity was computed every 4 km along the canyons. Canyon B is the canyon immediately east of Tambo submarine canyon, Canyon C is next to the east, while Canyon D is farthest east of Tambo submarine canyon.

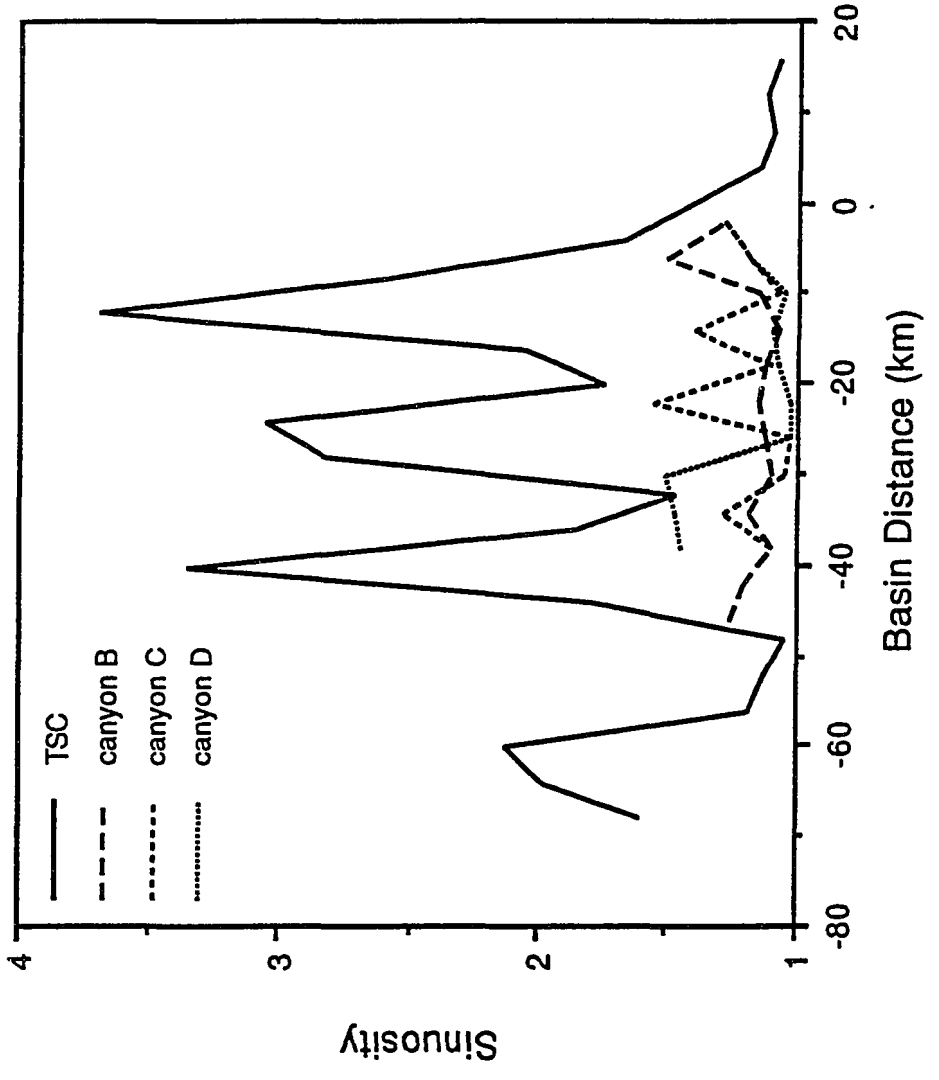
TSC
canyon B
canyon C
canyon D
Sinuosity
4
3
2
1
-80
-60
-40
-20
0
20
Basin Distance (km)

Figure 4.14 Plot of canyon slope vs. basin distance for Tambo submarine canyon and the two smaller canyons immediately to the east. Basin distance 0 is the intersection of Tambo submarine canyon with the smaller canyons to the east. Up canyon distances are given in negative kilometers from this point. Canyon slopes were measured between 3.5 kHz echosounder profiles.

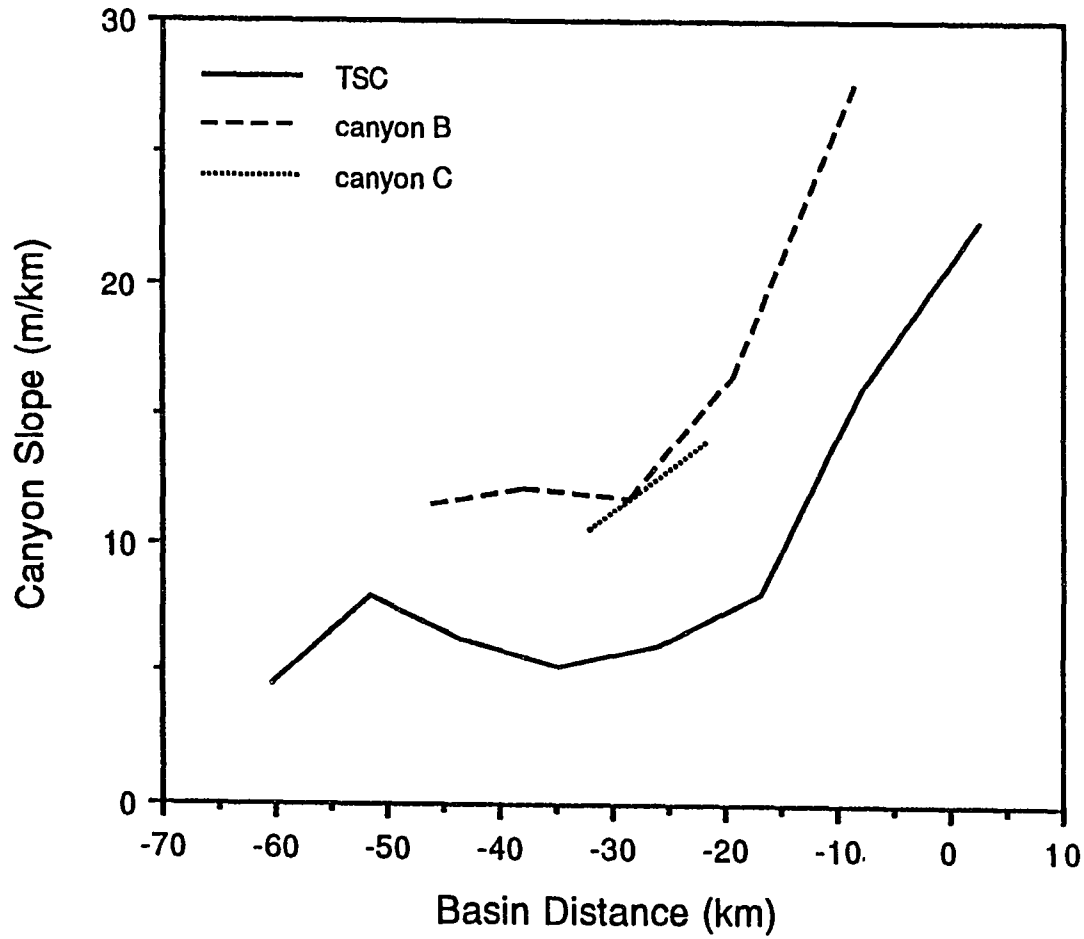
TSC
canyon B
canyon C
Canyon Slope (m/km)
30
20
10
0
-70
-60
-50
-40
-30
-20
-10
0
10
Basin Distance (km)

canyons show a sharp increase in channel slope as they approach the southern end of the basin. By analogy with subaerial rivers, we infer that Tambo submarine canyon carries more sediment than the smaller canyons to the east. This may be accomplished through larger, more frequent, or denser turbidity currents. Tambo submarine canyon therefore needs to meander more than the smaller canyons to the east in order to maintain its ideal channel gradient.

Figure 4.15 shows plots of meander wavelength, meander amplitude, meander radius of curvature, and channel width vs. distance for the 74 measured meanders along Tambo submarine canyon. Meander wavelength, amplitude, and radius of curvature show no systematic change downslope along the canyon. Channel width begins at about 500 m, increases to around 900 m (maintaining that width for about 15 km), and then decreases rapidly to about 450 m before slowly increasing again. The sudden decrease in channel width near -43 km occurs at the intersection of the canyon with the northeast-trending fault that crosses the basin. Erosion of the upraised material north of this fault results in a wider and straighter channel. We suggest that the fault occurred before or during canyon formation, since no entrenched or abandoned meanders are observed immediately on the upthrown side of the fault.

Studies of meandering river systems have shown that parameters such as meander wavelength and channel width, meander wavelength and meander radius of curvature, and channel width and meander radius of curvature are strongly correlated, indicating that channel meandering is a fundamental property of flow systems [*Leopold and Wolman*, 1960; *Leopold and Longbein*, 1966]. Flood and Damuth [*1987*] found that similar relationships exist for meandering distributary channels on the Amazon Fan. These relationships also exist for Tambo submarine canyon.

Figure 4.16a shows a log-log plot of meander wavelength vs. meander radius of curvature for all of the Arequipa Basin submarine canyons and river meanders from

Figure 4.15 Plot of measured canyon parameters vs. basin distance for Tambo submarine canyon. Basin distance 0 is the intersection of Tambo submarine canyon with the smaller canyons to the east. Up canyon distances are given in negative kilometers from this point. No systematic change or pattern is observed in meander wavelength, meander amplitude, or meander radius of curvature along the canyon. Channel width shows a sharp discontinuity as the canyon crosses the fault at -43 km.

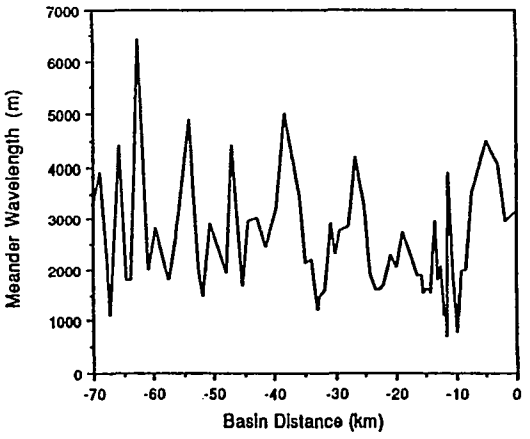
Meander Wavelength (m)
7000
6000
5000
4000
3000
2000
1000
0
-70 -60 -50 -40 -30 -20 -10 0
Basin Distance (km)

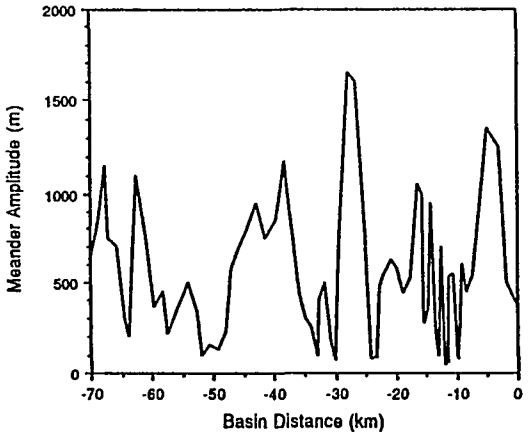
Meander Amplitude (m)
2000
1500
1000
500
0
-70 -60 -50 -40 -30 -20 -10 0
Basin Distance (km)

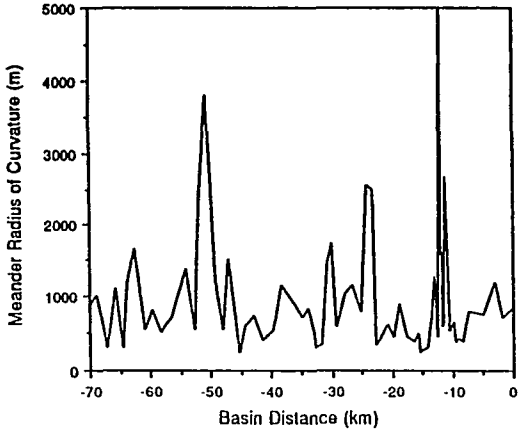
Meander Radius of Curvature (m)
5000
4000
3000
2000
1000
0
-70 -60 -50 -40 -30 -20 -10 0
Basin Distance (km)

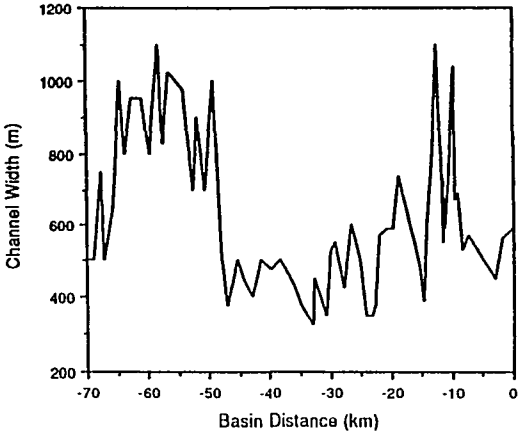
Channel Width (m)
1200
1000
800
600
400
200
-70 -60 -50 -40 -30 -20 -10 0
Basin Distance (km)

Figure 4.16 Log-log plots of meander parameters for meanders along all of the East Arequipa Basin submarine canyons compared to river data from Leopold and Wolman [*1960*].

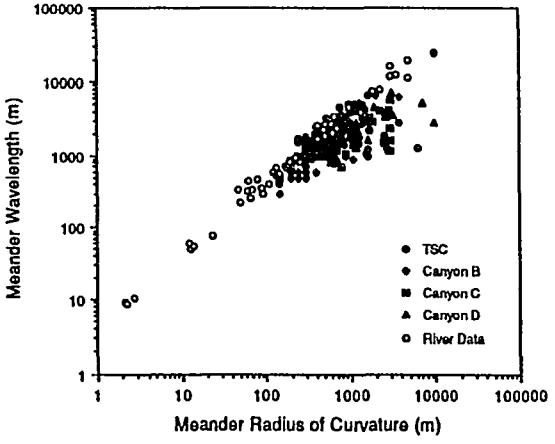
Meander Wavelength (m)
100000
10000
1000
100
10
1
1
10
100
1000
10000
100000
Meander Radius of Curvature (m)
TSC
Canyon B
Canyon C
Canyon D
River Data

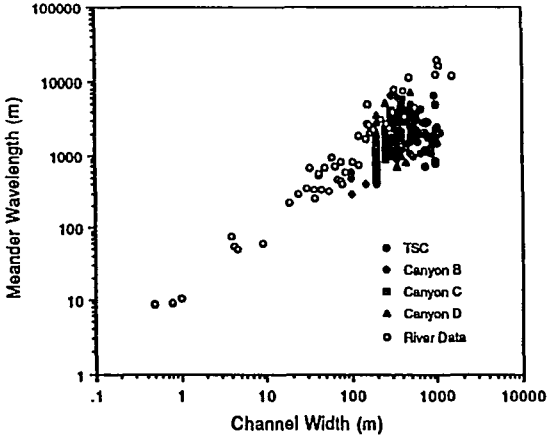
Meander Wavelength (m)
100000
10000
1000
100
10
1
.1
1
10
100
1000
10000
Channel Width (m)
TSC
Canyon B
Canyon C
Canyon D
River Data

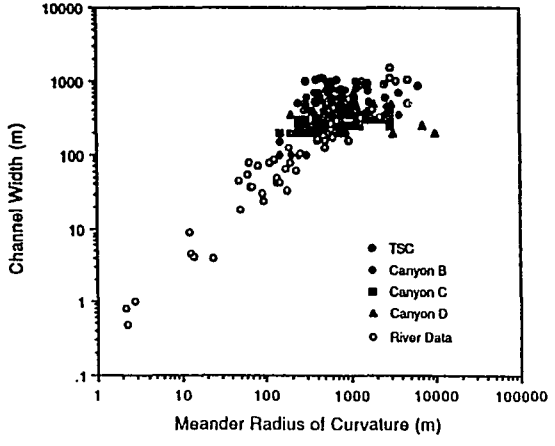
Channel Width (m)
10000
1000
100
10
1
.1
1
10
100
1000
10000
100000
Meander Radius of Curvature (m)
TSC
Canyon B
Canyon C
Canyon D
River Data

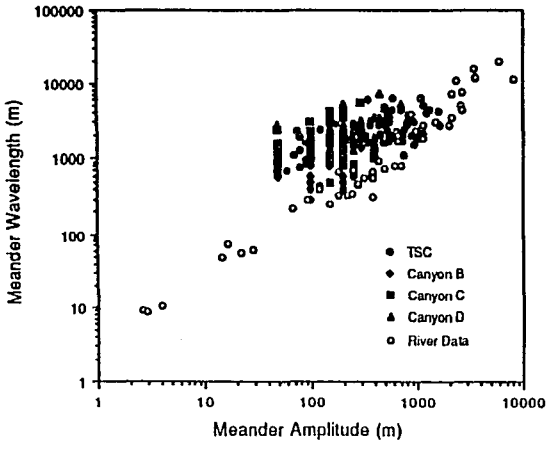
Meander Wavelength (m)
100000
10000
1000
100
10
1
1
10
100
1000
10000
Meander Amplitude (m)
TSC
Canyon B
Canyon C
Canyon D
River Data

Leopold and Wolman [*1960*] (They carefully selected their data to contain meanders that were nearly sinusoidal, resulting in very well-defined trends in the following plots). Most of the submarine canyon meanders fall along the trend defined by the river data, indicating that meander radius of curvature increases steadily with increasing meander wavelength. The scatter in the submarine canyon data probably results from asymmetric meanders (difficult to choose a single appropriate radius) and low-amplitude long-wavelength bends in the channel (probably not true meanders).

Similar plots of meander wavelength vs. channel width (Figure 4.16b) and channel width vs. meander radius of curvature (Figure 4.16c) show little or no correlation with the river data. The limited range of canyon wavelengths and channel widths makes it difficult to determine if the ratios of meander wavelength to channel width and channel width to meander radius of curvature are inherently different in submarine canyon channels. Some of the scatter in the canyon data likely results from the difficulty in accurately measuring the channel width on the side-scan mosaic, distortions in the image, and the problem of determining channel boundaries within the eroded slopes of the canyon. Also, non-flow processes such as slumping of the canyon walls may contribute to increasing the channel width in the canyon.

One case where there may be a difference between subaerial and submarine meanders is shown by a plot of meander wavelength vs. meander amplitude (Figure 4.16d). Since both meander wavelength and amplitude are easily measured on the side-scan mosaic, the effect of measurement errors should be minor in this plot. While the amplitude of Tambo submarine canyon meanders is generally lower than that of the rivers (for a given wavelength), the amplitude apparently increases much more rapidly with increasing wavelength. This may indicate that submarine meanders tend to grow outward at a greater rate than their subaerial counterparts. Further study of this and other

meandering submarine canyons will be necessary, however, before definite conclusions regarding the nature of submarine meandering will be possible.

Discussion

The preceding analysis of meander parameters shows that the meandering Tambo submarine canyon has a form that is similar to meandering subaerial rivers. We believe that the East Arequipa Basin submarine canyons did not develop by headward erosion and mass-wasting, but formed from channelized turbidity flows that filled the basin. The East Arequipa Basin submarine canyons currently lie at depths of from 400 to 2200 m and it is unlikely that the canyons were ever exposed subaerially during low sealevel stands. Meander formation would therefore seem to require a frequent supply of small, low-velocity channelized turbidity currents to create the observed intricate meanders. Large, rapidly moving turbidity currents would probably have difficulty negotiating the tight canyon meanders and would expend their energy against the canyon walls (occasional flows of this type probably do occur and contribute to the formation of meander cutoffs).

Low-velocity turbidity currents have been reported from several submarine canyons [*Shepard et al.*, 1979]. They observed currents with velocities of 30 to 100 cm/s that apparently occur many times each year - especially where large amounts of sediment are introduced into the canyon heads. They proposed that tidal currents or storm surges may cause slope failure in unconsolidated sediments, initiating turbidity flows.

Another potential source of low-velocity turbidity currents is through density underflows formed when sediment-laden rivers or streams enter a larger body of water. Such flows have been observed in lakes such as Lake Mead [*Gould*, 1960] where turbid water from the Colorado River has been observed to plunge beneath the lake surface and travel downlake along the submerged channel of the river. At least 12 of these flows

(between 1935 and 1941) were observed to travel the length of the lake (110 to 190 km) in periods of from 1 to 4.5 days. The density contrast between the turbidity flows and the lake water was estimated to be about 0.05 g/cm^3. Similar currents in the Walensee (Lake of Walenstadt, Switzerland) were determined to have velocities of up to 30 cm/s and density contrasts of about 0.04 g/cm^3 [*Lambert et al.*, 1976].

Zeng et al. [*1991*] studied turbidity currents that originate on delta fronts at the head of Bute Inlet (British Columbia, Canada) and flow downslope along a sinuous channel 30 km long and 100 to 400 m wide. During the low river discharge season flows with velocities of 5 to 10 cm/s and thicknesses of less than 7 m were measured in the middle section of the channel, 20 km from the delta front. Turbidity flows with velocities from 75 to 330 cm/s and thicknesses of 7 to 32 m were recorded during the river flood season. The density contrast between these flows and the seawater was calculated as 0.005 to 0.026 g/cm^3. The above examples suggest a possible model in which density underflows and/or delta front collapse may cause the frequent, low-velocity turbidity currents that seem to be required for the formation of the Arequipa Basin submarine canyons.

Several rivers empty into the Pacific Ocean along the coast of southern Peru. These rivers drain the high Andes and may introduce large quantities of sediment onto the shelf. The submarine canyons of the East Arequipa Basin appear to extend upslope to the mouths of some of these rivers (Figure 4.17). Tambo submarine canyon appears to extend north to the mouth of the Rio Tambo. Deposits from this river have built out the shoreline at the river's mouth and presumably form a delta on the seafloor. This river delta may have fed Tambo submarine canyon as well as another canyon system in the West Arequipa Basin. The northeast-trending branch of Tambo submarine canyon north of 17° 45' S shown in Figure 4.8 appears to project towards the mouth of the Rio Moquegua. The smaller tributary canyons to the east seem to head near the mouths of the Rio Locumba and the Rio

Figure 4.17 Relationship of the Arequipa Basin submarine canyons to subaerial drainage systems. Small triangles are volcanoes in the high Andes. The coast of southern Peru and northern Chile consists of a pediment covered by alluvial fans (seaward of diagonal dashed line). Several rivers and erosional ravines form deep canyons as they cut across this wide, gently sloping surface. Tambo submarine canyon and several canyons in the West Arequipa Basin appear to extend toward the mouth of the Rio Tambo. The smaller canyons in the East Arequipa Basin may extend to the Rio Moquegua, the Rio Locumba, and the Rio Sama although the connections are not clear. Longshore currents may move sediment along the coast and affect the development of the submarine canyons.

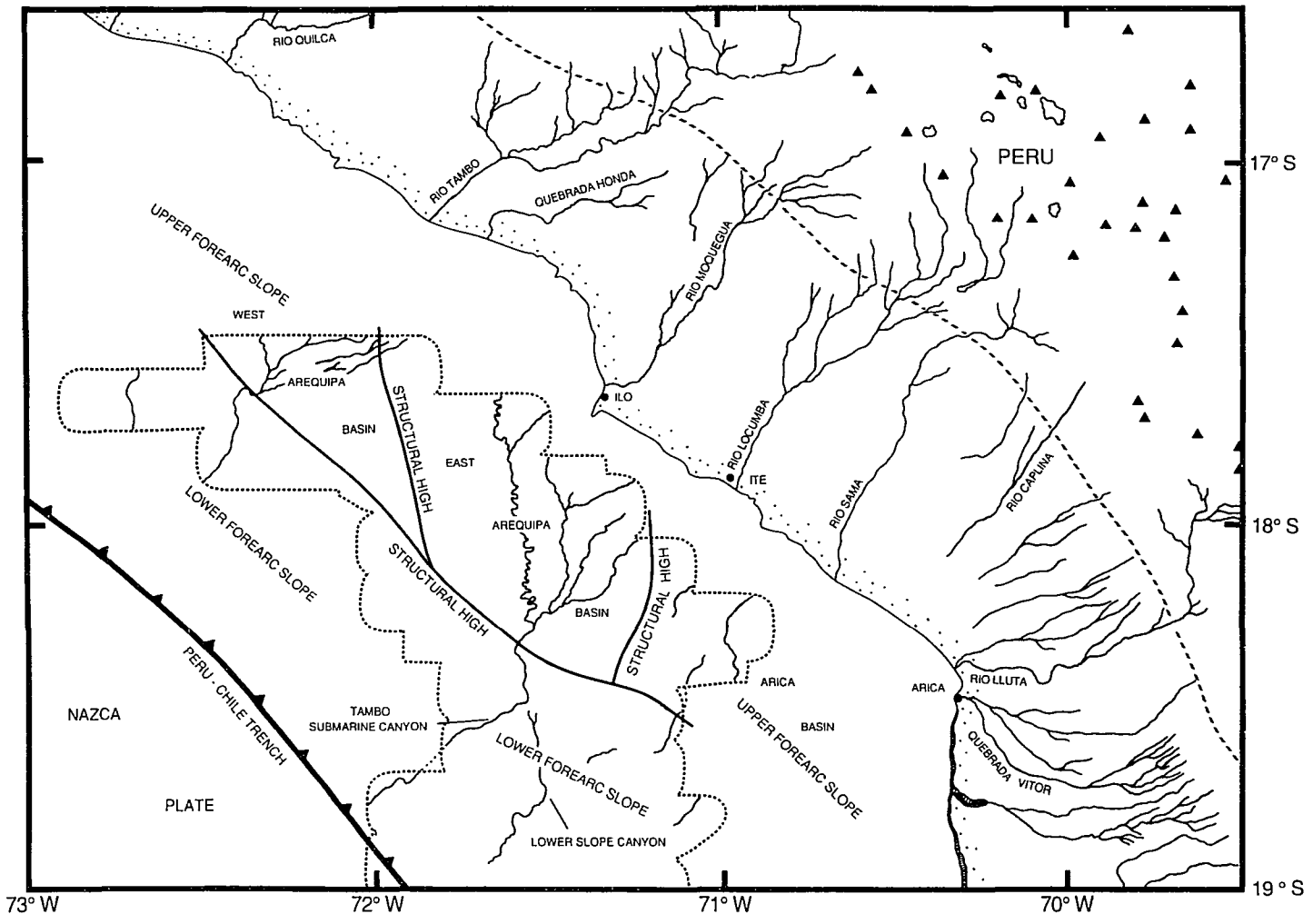
RIO QUILCA
RIO TAMBO
QUEBRADA HONDA
RIO MOQUEGUA
PERU
17° S
UPPER FOREARC SLOPE
WEST
AREQUIPA
BASIN
STRUCTURAL HIGH
EAST
AREQUIPA
ILO
RIO LOCUMBA
ITE
RIO SAMA
RIO CAPLINA
18° S
LOWER FOREARC SLOPE
STRUCTURAL HIGH
BASIN
STRUCTURAL HIGH
ARICA
ARICA
RIO LLUTA
PERU - CHILE TRENCH
NAZCA
TAMBO
SUBMARINE CANYON
UPPER FOREARC SLOPE
BASIN
QUEBRADA VITOR
LOWER FOREARC SLOPE
PLATE
LOWER SLOPE CANYON
19 ° S
73° W
72° W
71° W
70° W

Sama. Unfortunately, the SeaMARC II survey of the Arequipa Basin only extends into water as shallow as 500 m and thus no nearer than 12 km to the coast. We are therefore unable to prove conclusively that the submarine canyons are extensions of these subaerial drainage systems.

Landforms in the coastal regions of southern Peru and northern Chile reflect episodic uplift of the central Andes since the early Miocene [*Tosdal et al.*, 1984]. Successive periods of uplift in the middle and late Miocene produced several regional pediment surfaces. A late Miocene - early Pliocene relative drop in sealevel led to the incision of deep canyons into the Cordillera de la Costa. During the late Pliocene and early Pleistocene the Cordillera de la Costa underwent several cycles of marine transgression and regression that formed coastal terraces.

It is possible that the Arequipa Basin submarine canyons began to develop during the late Miocene - early Pliocene uplift that incised the deep river valleys of the coast. The erosion of the river valleys would have supplied large amounts of sediment to the shelf. Channelized turbidity currents from these point sources may have helped fill the basin and initiated formation of the submarine canyons. The available data provide no direct indication of whether or not the canyon is currently active. The active tectonics of the forearc, however, make it unlikely that the canyon would exhibit the observed continuous, clear channel if the flushing action of turbidity currents has not been recently active.

The terraces along Tambo submarine canyon indicate a history of vertical tectonics for the forearc in this area. Seismic reflection profiles and SeaMARC II swath bathymetry across the lower trench slope in this area show extensive faulting and collapse of the forearc seaward of the structural high [*Bergersen*, 1989]. These sudden modifications of the lower and middle forearc slope may have led to pulses of canyon downcutting at the edge of the upper slope that would have then propagated upslope into the basin, leading to canyon entrenchment and terrace formation. Piracy of the canyon on the lower trench slope

by a headward eroding canyon as proposed by Bergersen [*1989*] may also have led to a downcutting episode.

It is interesting to speculate that the terraces along Tambo submarine canyon may be related to terraces observed along the nearby coast of southern Peru. Tosdal et al. [*1984*] described and correlated two major terraces along the coast of southern Peru adjacent to our study area. Distinct differences in the elevations of these two terraces along the coast suggest that these cycles were caused by tectonism rather than sealevel changes.

Terrace heights above the submarine canyon floor were measured on 3.5 kHz echosounder profiles (Figure 4.7) and the differences in terrace heights between the two main terraces were determined. Terrace height differences of 87 m (profile D-D'), 79 m (profile E-E'), and 135 m (profile F-F') were observed. These terrace height differences along Tambo submarine canyon are comparable to that observed along the coast near Ito (115 m) but less than the difference seen further north at Ilo (175 m). Obviously the canyon and its terraces need to be surveyed in greater detail and the tectonics of the area better understood to determine if there is any merit of these correlations. The submarine canyon terrace data do, however, apparently support the coastal data showing that the uplift of the forearc increases to the north in this area.

Conclusions

Side-scan sonar coverage of the East Arequipa Basin offshore southern Peru and northern Chile reveals an extensive submarine canyon system. The largest branch of the canyon system, the Tambo submarine canyon, extends for over 100 km along the axis of the basin, is 350 to 1100 m wide, and has relief of 160 to 230 m through most of this distance. This canyon is highly meandering and has an overall sinuosity of almost 2, comparable to highly meandering subaerial streams. The present canyon channel is

bordered by terraces at various levels above the canyon floor. Cutoff meander loops are preserved on some of these arcuate terraces. Other sediment structures observed in the basin and along the canyons include sediment waves, levees, overbank deposits, and crevasse splays.

Morphologic analysis of the Arequipa Basin submarine canyons shows that the meandering is nearly identical in form to that observed on land. The upper threshold of basin slope for submarine meandering appears to occur at around 15 m/km, a value about 10 times greater than that observed for subaerial rivers. Although all of the canyons flow across the same basin slopes, only Tambo submarine canyon is strongly meandering. This indicates that in addition to a dependence on basin slope, meandering is also dependent on the size, frequency, and density of the turbidity currents that formed the canyons.

Tambo submarine canyon appears to extend to the mouth of the Rio Tambo in southern Peru and may have been fed by turbidity currents from its delta front. The smaller canyons to the east may head near the mouths of the Rio Locumba and the Rio Sama. The late Miocene - early Pliocene period of uplift that incised the deep river valleys along the coast of southern Peru may have supplied much of the sediment that fills the basin..

Tambo submarine canyon probably developed from channelized turbidity flows that flowed down the axis of the basin from the north. After the basin filled, the main distributary channel within the basin became a conduit to bypass sediment onto the middle and lower forearc slope. The canyon initially existed within a wide valley formed by the meandering channel (a meander belt). Subsidence of the forearc seaward of the structural high may have resulted in downcutting and entrenchment of the canyon, leaving the meander belt as a level of terraces. Following this period of downcutting, the canyon would have developed a new, deeper meander belt until another period of vertical tectonics repeated the cycle. The smaller tributary canyons to the east of Tambo submarine canyon have lower sinuosity, are generally not as deeply incised, and have no terraces. This

probably indicates that they developed more recently than Tambo submarine canyon and that they are fed by smaller rivers with less sediment load.

Seismic reflection profiles across the lower trench slope in this area show extensive faulting and collapse of the forearc seaward of the structural high. These sudden modifications of the lower trench slope may have led to pulses of canyon downcutting at the edge of the upper forearc slope that would have then propagated upslope into the basin, leading to canyon entrenchment and terrace formation.

CHAPTER 5

MORPHOLOGY AND STRUCTURAL FRAMEWORK OF THE OFFSHORE FOREARC OF SOUTHERN PERU AND NORTHERN CHILE

Abstract

Extension of the offshore portion of the forearc of southern Peru and northern Chile has produced a left-stepping series of en-echelon forearc slope basins. The basins form north-south oriented sediment-filled troughs that are oblique to the curving subduction zone in the Arica Bight area. The northernmost of these rift basins, the West Arequipa Basin, contains up to 1 s of sediment in a west-facing half graben, faulted down toward the trench axis by synthetic faults. The East Arequipa Basin and the Arica Basin contain up to 1.6 s and 2.5 s of sediment respectively in east-facing, synthetically faulted half grabens. The north-south trending faults that define the forearc slope basins break the middle forearc slope into large blocks that are visible in SeaMARC II side-scan and bathymetry data. These north-south trending structures interact with northwest-southeast trending trench-parallel faults and northeast-southwest trending faults to create embayments visible in the forearc bathymetry. Growth of these embayments continues through surface erosion and slumping.

The surface of the West Arequipa Basin and the Iquique Basin show downslope oriented channels and sediment flow features. The surface of the East Arequipa Basin is covered by low amplitude sediment waves. Both the East and West Arequipa basins contain major submarine canyon systems that flow from north to south along the axes of the basins. Remnants of old north-south trending canyons are visible on side-scan images in several areas. Some of these abandoned canyons overlie basement highs, suggesting that basin depocenters have migrated over time.

A single prominent angular unconformity is visible in seismic reflection profiles across both the East and West Arequipa basins. Both the unconformity and the sediments beneath it dip to the west, indicating subsidence of the leading edge of the forearc. I propose a model in which initial extension of the forearc produced block-faulted depressions in which sediment was deposited. As extension continued, faulting became concentrated along the margins of these basins and created the observed half-grabens. Following this rotational motion, deposition of a second sequence of sediment was concentrated in the deep portions of the basins next to the large-offset boundary faults. Sediment loading and possible uplift of the bounding structural highs cause the basin sediments to dip toward the center of the basin.

The extension observed in the offshore portion of the forearc in the Arica Bight area is consistent with structures observed on land, and fits into a pattern of tectonic erosion of the forearc that has been observed at other places along the Peru-Chile Trench. It is also possible that the extension that formed the upper forearc slope basins resulted from strike-slip motion of lower forearc slivers. Lateral motion of portions of the lower forearc may have removed support at the base of the forearc slope, causing extension and collapse of the upslope areas.

Introduction

The Pacific margin of South America is known as the type locality for the Andean style of convergent margin. The Andean style margin is traditionally associated with sediment accretion, uplift, folding, mountain-building, and volcanism [*Dewey and Bird*, 1970; *Uyeda*, 1982; *Suarez et al.*, 1983]. Since the mid-1970s, geophysical surveys and drilling in the offshore regions of Peru have painted a quite different picture: one of tectonic erosion of the forearc rather than accretion, and crustal extension and subsidence at the

edge of the South American continent rather than compression and uplift [*von Huene et al.*, 1988; *von Huene et al.*, 1989; *von Huene and Lallemand*, 1990].

The Nazca plate is currently subducting beneath the South American plate along the Peru-Chile trench. In the Arica Bight area the motion of the Nazca plate relative to the South American plate is 9.2 cm/yr toward 081° [*Cande*, 1986]. The subducting slab is believed to be segmented along strike into alternating shallow (about 10°) and steeper (about 30°) subducting segments [*Barazangi and Isacks*, 1976, 1979]. The Arica Bight region overlies one of the 30° dipping segments of the subducting Nazca plate. These segments appear to correlate to geologic and tectonic boundaries in the overlying South American plate [*Megard and Philip*, 1976; *Jordan et al.*, 1983; *Megard*, 1989].

The major onshore geologic and tectonic elements of northern Chile are oriented generally parallel to the trend of the coast and the subduction zone (Figure 5.1). Exposed along the coast of northern Chile and forming the Coastal Range, or Cordillera de la Costa, are rocks of the Jurassic magmatic arc, consisting of marine sediments interbedded with andesitic lava flows [*Mordojovich*, 1981; *Coira et al.*, 1982] (Figure 5.2). The planated Coastal Range reaches heights of more than 2 km and is truncated along the ocean by the Coastal Scarp, a sea cliff that extends for more than 700 km with an average height of over 1000 m [*Armijo and Thiele*, 1990]. To the east, the Coastal Range slopes gently into the Longitudinal Valley. During the Neogene the Coastal Range acted as a dam to westward drainage from the Andes. Only relatively recently has sediment accumulation overtopped the Coastal Range in a few places, allowing rivers to incise deep gorges across the Coastal Range [*Mortimer and Saric*, 1975; *Armijo and Thiele*, 1990].

The Longitudinal Valley, also called the Pampa del Taramugal, forms a low-lying basin situated between the Coastal Range and the west flank of the Andes between about 18° to 28° S (Figure 5.1). Up to a kilometer of non-marine sediments and ignimbrite flows are deposited in the valley [*Mortimer and Saric*, 1975; *Armijo and Thiele*, 1990]. About

Figure 5.1. Morphotectonic map of southern Peru, northern Chile, and the eastern Nazca plate.

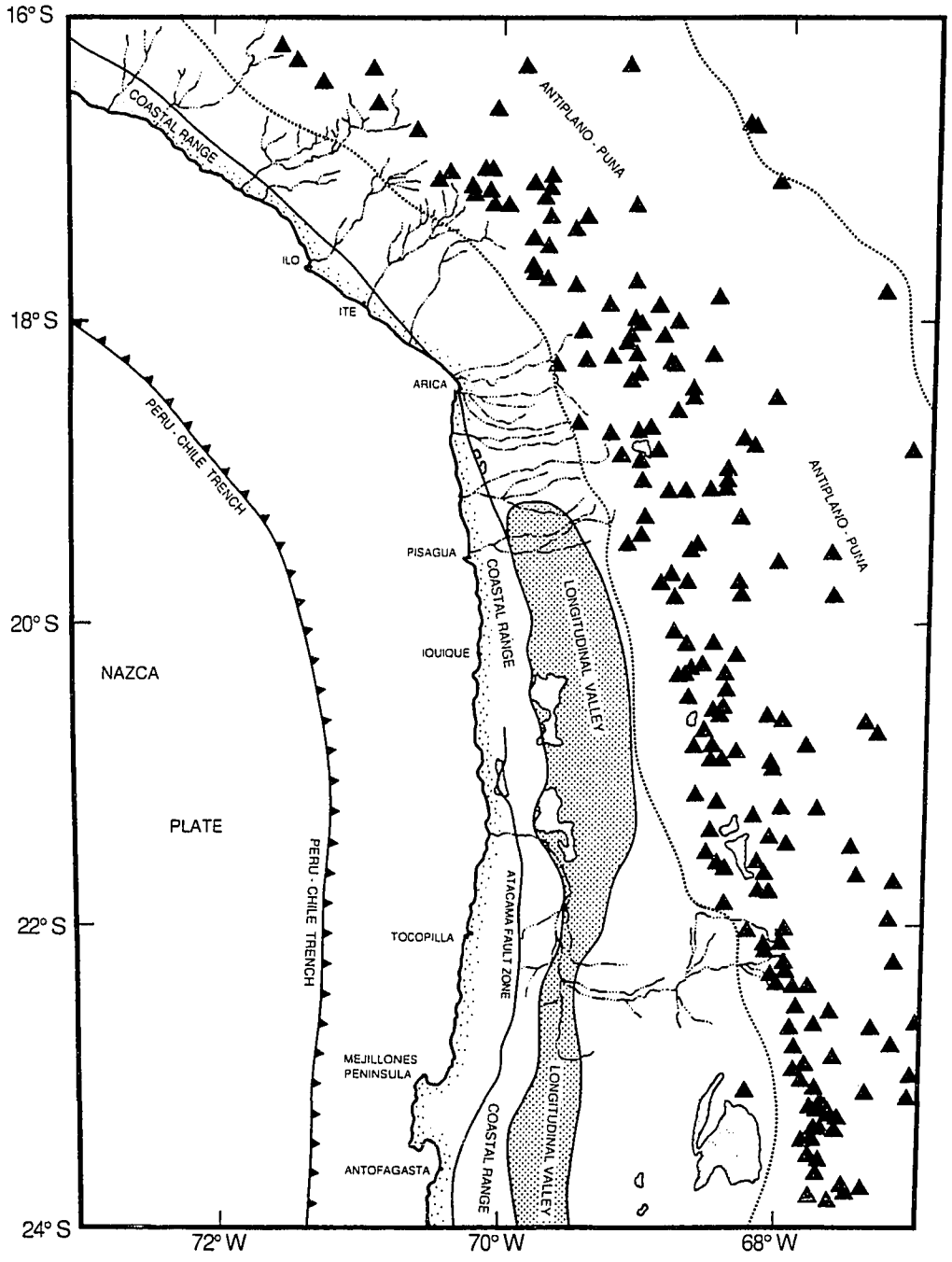
16° S
18° S
20° S
22° S
24° S
72° W
70° W
68° W
COASTAL RANGE
ANTIPLANO - PUNA
ILO
ITE
ARICA
PERU - CHILE TRENCH
PISAGUA
COASTAL RANGE
LONGITUDINAL VALLEY
ANTIPLANO - PUNA
IQUIQUE
NAZCA
PLATE
PERU - CHILE TRENCH
ATACAMA FAULT ZONE
TOCOPILLA
MEJILLONES PENINSULA
COASTAL RANGE
LONGITUDINAL VALLEY
ANTOFAGASTA

Figure 5.2. Geologic map of southern Peru and northern Chile. Modified from Ziel [*1979*].

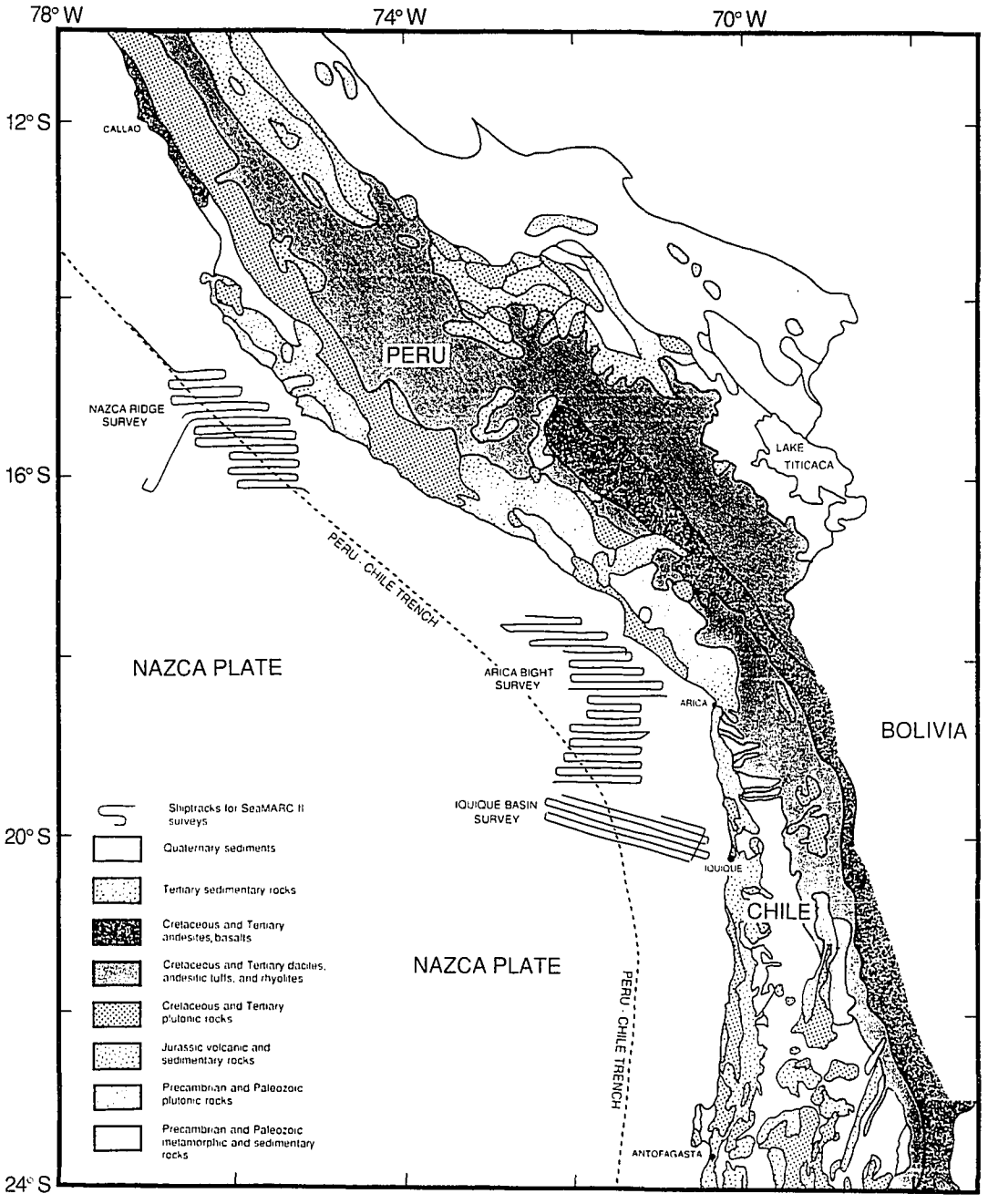
78° W
74° W
70° W
12° S
16° S
20° S
24° S
CALLAO
PERU
NAZCA RIDGE SURVEY
LAKE TITICACA
PERU - CHILE TRENCH
NAZCA PLATE
ARICA BIGHT SURVEY
ARICA
BOLIVIA
IQUIQUE BASIN SURVEY
IQUIQUE
CHILE
NAZCA PLATE
PERU - CHILE TRENCH
ANTOFAGASTA
Shiptracks for SeaMARC II surveys
Quaternary sediments
Tertiary sedimentary rocks
Cretaceous and Tertiary andesites, basalts
Cretaceous and Tertiary dacites, andesitic tuffs, and rhyolites
Cretaceous and Tertiary plutonic rocks
Jurassic volcanic and sedimentary rocks
Precambrian and Paleozoic plutonic rocks
Precambrian and Paleozoic metamorphic and sedimentary rocks

75 km east of the coast (200 km east of the trench) the Western Cordillera of the Andes begins as a gradual monocline that rises to a crest in the currently active volcanic arc along the eastern border of Chile. Volcanic activity in the Western Cordillera began in the late Oligocene (about 26 Ma) and continues to the present [*Jordan and Gardeweg*, 1989]. Near the borders of Peru, Bolivia, and Chile, uplift, crustal shortening, and horizontal rotation have created a high plateau, the Antiplano-Puna, at an average height of almost 4 km [*Isacks*, 1988]. To the east of the Antiplano-Puna lies the Miocene thrust belt of the Eastern Cordillera and the actively deforming foreland fold and thrust ranges of the sub-Andean belt [*Jordan and Alonso*, 1987] (Figure 5.1).

Whereas the high Andes and the Antiplano-Puna continue into southern Peru, the geology exposed along the coast of southern Peru is quite different from that seen in northern Chile. The Jurassic arc rocks of the Coastal Range of northern Chile narrow rapidly north of Iquique and disappear at Arica (Figure 5.2). Rocks exposed along the coast of southern Peru are: Tertiary continental deposits, Cretaceous and Tertiary plutonic rocks, and Precambrian and Paleozoic plutonic rocks [*Ziel*, 1979]. The Longitudinal Valley also disappears near the Peru-Chile border where it is filled by ignimbrites.

Several paleomagnetic studies have found that Peru north of 19° S has rotated counterclockwise relative to the stable shield area of South America [*Heki et al.*, 1984; *Turner et al.*, 1984; *Kono et al.*, 1985; *Beck et al.*, 1986]. Similar studies in northern Chile show a clockwise rotation of the forearc relative to the shield [*Hartley et al.*, 1988]. Isacks [*1988*] notes from seismic data that the strike of the subducted Nazca plate at depths of more than 150 km is much straighter and less embayed than the trace of the present trench axis. He uses this seismicity pattern in conjunction with the paleomagnetic data as evidence that the westward concavity of the forearc has increased during the past 12 m.y. and proposes that seaward concavity in the Arica Bight area was enhanced (but not produced) by along strike variations in the amount of late Cenozoic crustal shortening above a

shallow subducting slab. Hartley et al. [*1988*] proposed that rotation of the forearc may result from differential movement of thrust sheets relative to a buttress in the Arica area, or by extension of the forearc at an oblique angle to the present direction of motion of the South American plate.

The trench in the northern Chile region is more than 7500 m deep and is essentially free of terrigenous sediment [*Schweller et al.*, 1981], reflecting the arid climate of the coast in this area. Few permanent streams reach the coast in this region and most of the sediment eroded from the Andes is trapped inland [*Galli-Olivier*, 1969; *Armijo and Thiele*, 1990; *Flint et al.*, 1991].

The submarine portion of the Peru forearc, just north of the Arica Bight, is only about 100 km wide and consists of a narrow shelf and a steep forearc slope leading down more than 7000 m to the deep trench. Off Arica the shelf becomes broader and the submarine portion of the forearc widens to more than 170 km. To the south, offshore of northern Chile, the submarine portion of the forearc once again narrows to about 100 km in width (Figure 5.1).

Sediment reaching the ocean in the Arica Bight region is trapped in forearc slope basins behind structural highs. An undetermined amount of sediment bypasses the forearc slope basins through several submarine canyons and is deposited in the trench axis [*Coulbourn*, 1977; *Bergersen*, 1989]. The Arequipa Basin extends south into the Arica area from about 16° S. This basin has also been called the Mollendo Basin [*Couch and Whitsett*, 1981], and the southern portion of the basin has also been referred to as the Tarapaca Basin [*Mordojovich*, 1981]. Coulbourn and Moberly [*1977*] named and described the Arica and Iquique Basins, which are situated off those Chilean cities. To the south of the Iquique Basin no large forearc basins are observed until about 33° S, where the Valparaiso Basin is encountered. Throughout the intervening area the steep, narrow

forearc is broken only by small sediment ponds and sediment-covered ledges at various depths [*Coulbourn*, 1981].

The Nazca Plate Project, a multidisciplinary study by scientists from the Hawaii Institute of Geophysics (HIG) and Oregon State University (OSU) in the 1970s, collected thousands of kilometers of geophysical data over nearly the whole length of the trench and forearc. These data sets were used by several authors [*Coulbourn and Moberly*, 1977; *Schweller et al.*, 1981; *Johnson and Ness*, 1981; *Couch and Whitsett*, 1981; and *Coulbourn*, 1981] to examine the tectonics, structure, and sedimentary framework of the forearc of southern Peru and northern Chile.

Several multi-channel seismic reflection lines were collected offshore of northern Chile in 1977 by Empresa Nacional del Petróleo (ENAP) with the cooperation of the United Nations [*Mordojovich*, 1981]. These seismic profiles reveal much about the structure of the forearc basins and are presented here with the permission of ENAP.

In August 1987 SeaMARC II side-scan sonar and swath bathymetric, single-channel seismic reflection, and standard underway geophysical data were collected in the Arica Bight region during a cruise of the R/V Moana Wave (Figure 5.1). East-west oriented survey lines between 17° 30' S and 20° 20' S extend from the forearc shelf, across the trench axis, and onto the subducting Nazca plate. More than 3400 km of gravity, seismic, and 3.5 kHz echosounder data were collected and over 27,000 km^2 of seafloor were imaged by the side-scan sonar system. These surveys were conducted to determine the sources, supply, and pathways of sediment transport, the role of tectonics in basin development, and the relationship between sedimentation and basin evolution.

Basin Geometry and Basement Structure

North-south-trending basement structural highs divide the upper forearc of the Arica Bight area into a series of forearc slope basins (Figure 5.3). The East and West Arequipa basins are elongate in a north-south direction and form sediment-filled troughs that are truncated at their southern ends by the steep middle forearc slope. Neither the East nor West Arequipa Basins are bounded by structural highs at their southern ends. The trough-shaped basins thin as they approach the steeper slopes at the edge of the upper slope, where they are truncated by creep and gravitational collapse of sediment down the slope toward the trench axis. The West Arequipa Basin is about 40 km wide and 60 km long within the study area. The East Arequipa Basin is about 60 km wide and about 100 km long.

The surveyed portion of the West Arequipa Basin lies in water depths of 1200 to 2500 m. The basin contains up to 1 s of stratified sediments overlying acoustic basement. A single unconformity is visible on most of the seismic reflection profiles across this basin and divides the basin sediment into two major sequences. Acoustic basement beneath all of the basins is poorly imaged in our single-channel seismic reflection profiles, but where visible it is highly irregular.

The East Arequipa Basin forms a north-south oriented bathymetric trough that lies at depths of from 400 to 1600 m and contains as much as 1.6 s of stratified sediment. The maximum thickness of sediment is confined to a narrow north-south trending zone in the west-central part of the basin. Like the West Arequipa Basin, a single angular unconformity is visible on the seismic reflection profiles across this basin, defining two major basin fill sequences. The unconformity and the underlying sediment dip gently to the west. Sediment overlying the unconformity is generally flat-lying and is thickest on the west side of the basin. A large normal fault with a surface offset of as much as 0.2 s trends

Figure 5.3 Tectonic, structural, and morphologic features in the Arica Bight and Iquique Basin survey areas. The outlined areas show the extent of SeaMARC II side-scan sonar coverage. Canyons and channels are shown by the dotted-dashed lines. Tambo submarine canyon flows from north to south across the East Arequipa Basin. Thin solid lines show faults based on the seismic reflection profiles, side-scan images, and swath bathymetry.

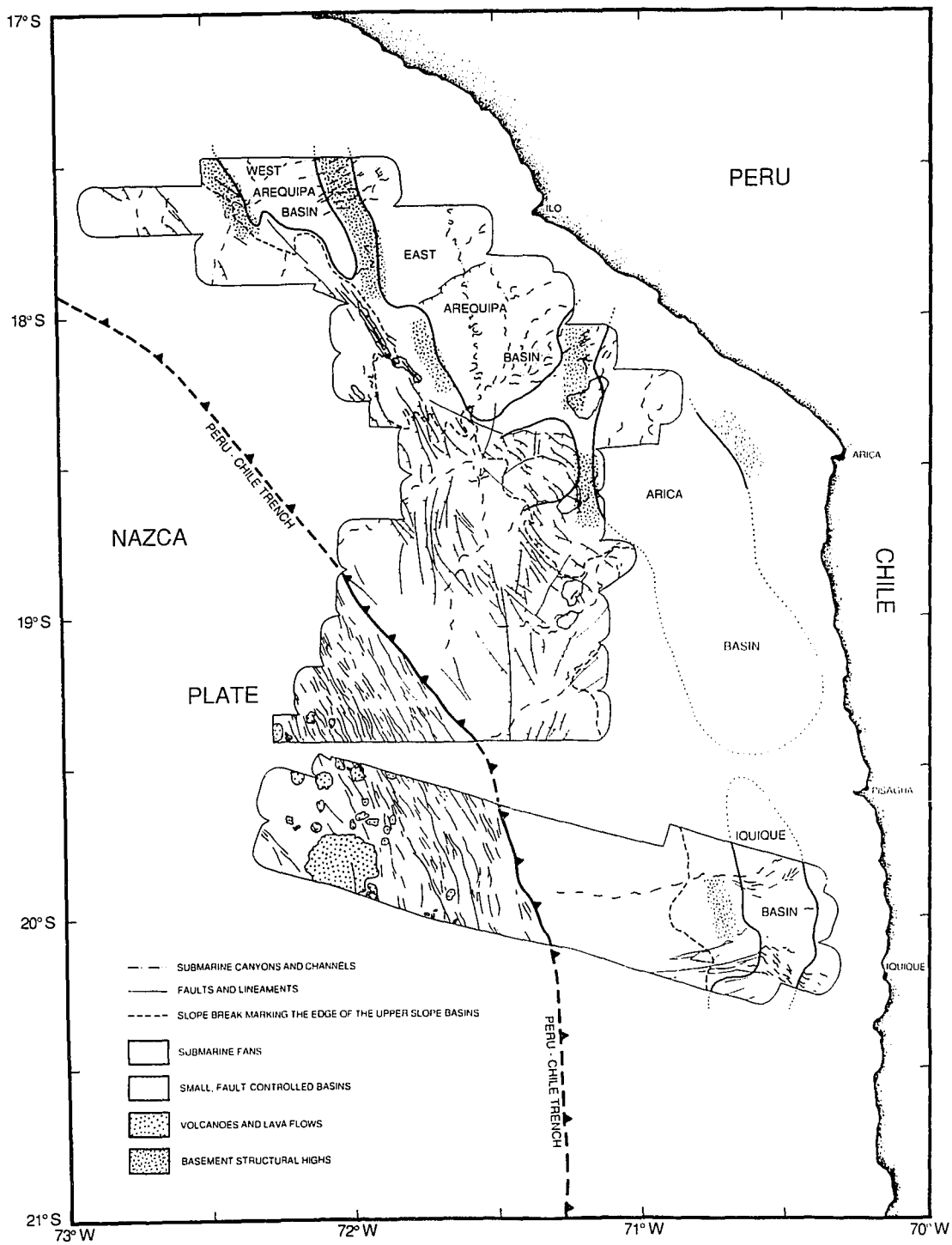
17° S
18° S
19° S
20° S
21° S
73° W
72° W
71° W
70° W
PERU
CHILE
NAZCA
PLATE
WEST
AREQUIPA
BASIN
EAST
AREQUIPA
BASIN
ILO
ARICA
ARICA
BASIN
IQUIQUE
BASIN
IQUIQUE
PERU - CHILE TRENCH
PERU - CHILE TRENCH
SUBMARINE CANYONS AND CHANNELS
FAULTS AND LINEAMENTS
SLOPE BREAK MARKING THE EDGE OF THE UPPER SLOPE BASINS
SUBMARINE FANS
SMALL, FAULT CONTROLLED BASINS
VOLCANOES AND LAVA FLOWS
BASEMENT STRUCTURAL HIGHS

obliquely across the basin from northeast to southwest, forming a low-relief scarp (north side high) visible in the side-scan images. This trend is perpendicular to the trend of the trench and may contribute to the along-strike segmentation of the forearc in this area reported by Coulbourn and Moberly [*1977*].

The Arica Basin is the thickest basin in the area, containing more than 2.5 s of stratified sediment. Like the East and West Arequipa Basins, The Arica Basin is elongate in a north-south direction (Figure 5.3). The areal extent of the basin is poorly known, but it may be up to 50 km wide and 120 km long. The Arica Basin occupies the outer part of the forearc shelf and the upper forearc slope in water depths of 700 to 1200 m.

Figure 5.4 shows a series of interpretations of single-channel seismic reflection profiles in the Arica Bight area. These profiles are aligned along a north-south line to show the along strike relationships of the basins. The profiles clearly show the basement structural highs that separate the basins and the irregular basement topography. In some cases, faulting of the forearc basins is clearly seen as offsets of the seafloor, the basin strata, and the acoustic basement (Figure 5.5). In other instances the sense of offset and dip directions of faults are inferred from the dip of sediments immediately overlying the basement blocks. Figure 5.6 shows an example of this situation, in which rotation of blocks along east-dipping faults is inferred from the westward dip of sediments immediately overlying the irregular acoustic basement.

The block-faulted acoustic basement of the forearc in the Arica Bight area appears to define a series of half grabens. Faulting within the West Arequipa Basin forms a west-facing half graben with boundary faults along the west side of the structural high that separates the West Arequipa Basin from the East Arequipa Basin (Figure 5.4). Secondary faulting within this basin is dominantly synthetic. The structural high bounding the west side of the basin appears to be a locally high fault block among the down-dropped blocks. Faulting within the East Arequipa Basin defines an east-facing half graben. Faulting within

Figure 5.4 Interpretations of single-channel seismic reflection profiles in the Arica Bight area. The profiles are aligned along a north-south line to show the overlap of the basins along strike. Profile locations and 500 m contoured SeaMARC II bathymetry are shown on the inset map. Vertical exaggeration is approximately 9 x.

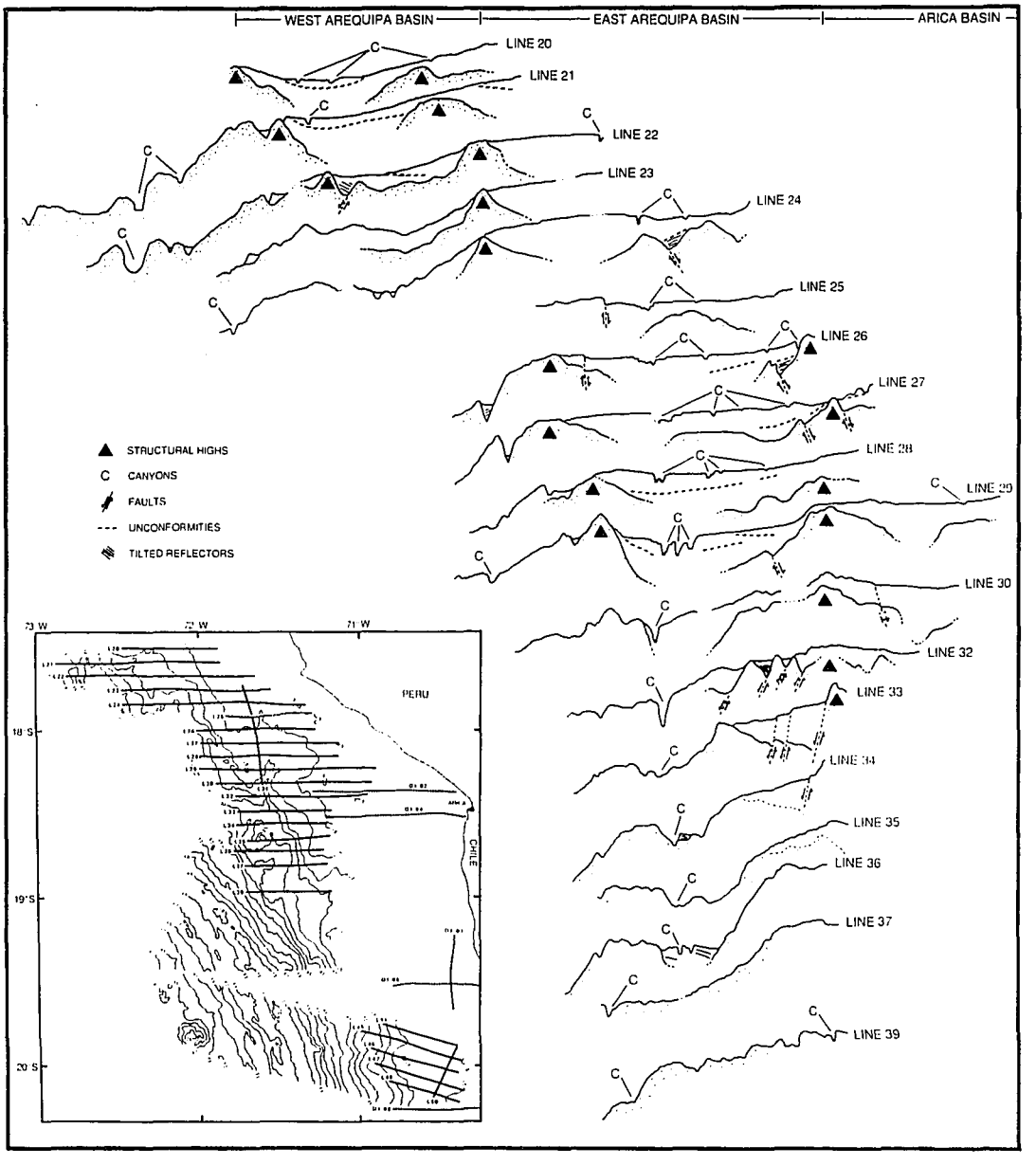
WEST AREQUIPA BASIN
EAST AREQUIPA BASIN
ARICA BASIN
LINE 20
LINE 21
LINE 22
LINE 23
LINE 24
LINE 25
LINE 26
LINE 27
LINE 28
LINE 29
LINE 30
LINE 32
LINE 33
LINE 34
LINE 35
LINE 36
LINE 37
LINE 39
STRUCTURAL HIGHS
CANYONS
FAULTS
UNCONFORMITIES
TILTED REFLECTORS
PERU
CHILE
18°S
19°S
20°S

Figure 5.5 Single-channel seismic reflection Line 33. This profile crosses a small unnamed basin perched on the edge of the upper forearc slope. Faults within the basin can be seen offsetting the acoustic basement, the basin strata, and the seafloor. See Figure 5.4 for profile location.

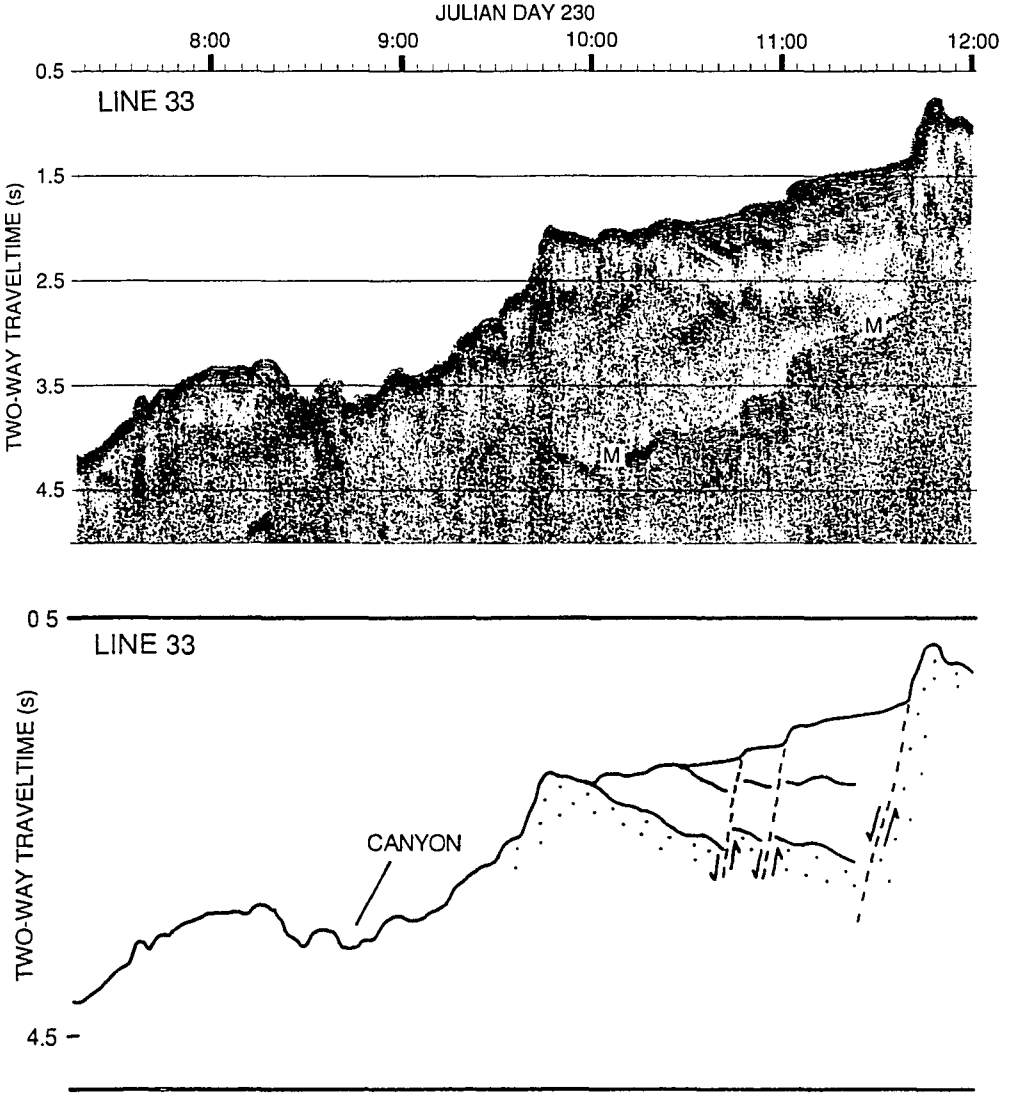
JULIAN DAY 230
8:00
9:00
10:00
11:00
12:00
0.5
LINE 33
TWO-WAY TRAVELTIME (s)
1.5
2.5
3.5
4.5
M
M
0 5
LINE 33
TWO-WAY TRAVELTIME (s)
CANYON
4.5

Figure 5.6 Single-channel seismic reflection Line 24. In this profile several large basement blocks can be seen beneath the East Arequipa Basin. Westward dipping reflectors in the notch between two of the blocks suggests rotation of the blocks along east-dipping faults. See Figure 5.4 for profile location.

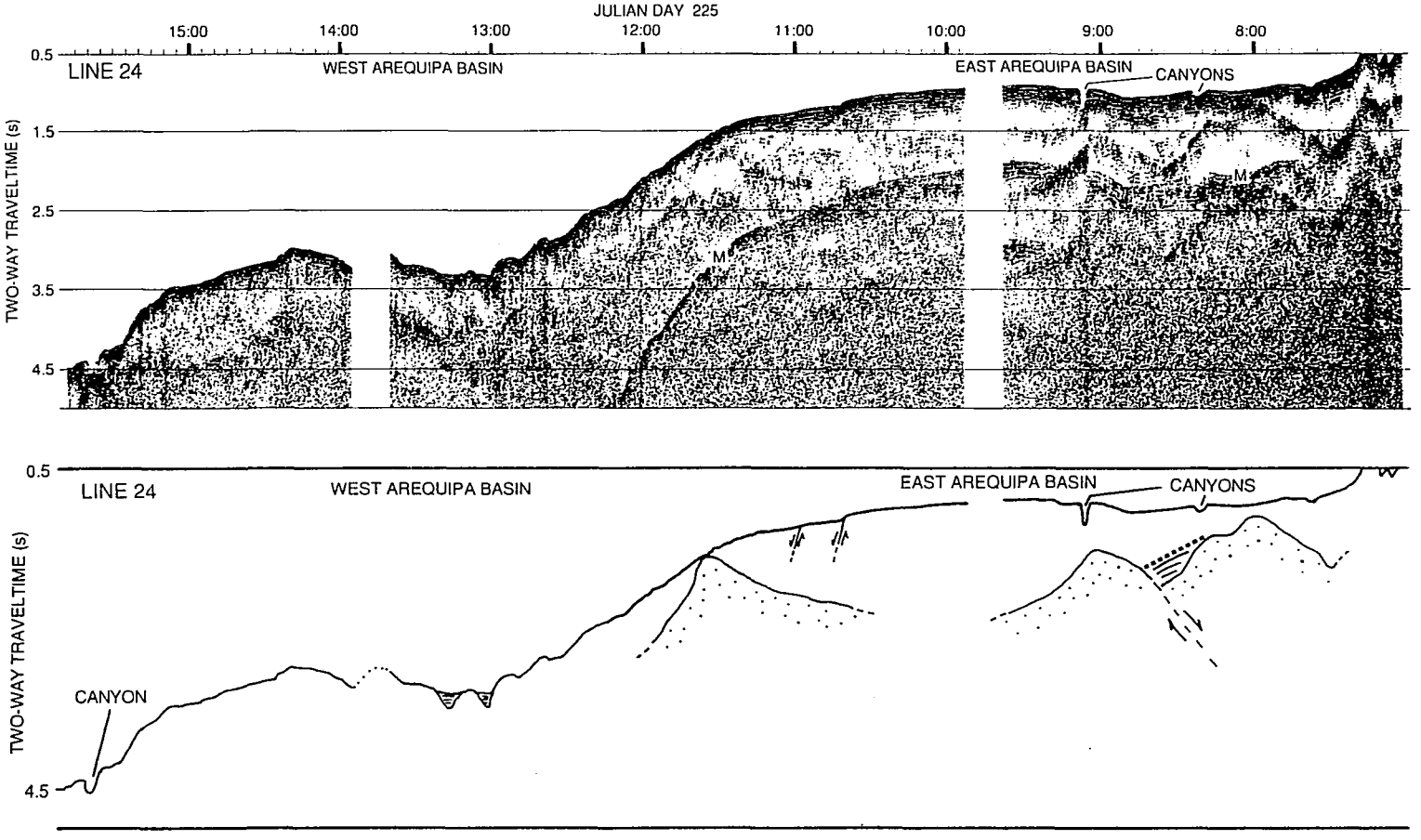
JULIAN DAY 225
15:00
14:00
13:00
12:00
11:00
10:00
9:00
8:00
0.5
LINE 24
WEST AREQUIPA BASIN
EAST AREQUIPA BASIN
CANYONS
TWO-WAY TRAVELTIME (s)
1.5
2.5
3.5
4.5
M
0.5
LINE 24
WEST AREQUIPA BASIN
EAST AREQUIPA BASIN
CANYONS
TWO-WAY TRAVELTIME (s)
CANYON
4.5

this basin is also predominantly synthetic. The sediment of the basin is asymmetrically distributed, with the thickest sediment accumulations near the structural high separating the East Arequipa Basin from the West Arequipa Basin. The boundary fault for the East Arequipa Basin probably lies along the east edge of this structural high, which forms a horst between the two basins (Figure 5.4).

Multi-channel seismic reflection profiles across the Arica Basin clearly show that the basin is formed in an east-facing half graben that thickens rapidly to the south (Figure 5.7). As in the East Arequipa Basin, sediment thickness within the Arica Basin is greatest along the western edge of the basin near the boundary fault of the graben. Secondary faulting within the basin is dominantly synthetic and recent motion along these faults is clearly seen near the center of profile D1-02, where fanning reflectors over the fault block and seafloor depressions (filled by fan deposits) are indicators of on-going growth and rotation of these faults (Figure 5.8).

The Iquique Basin is about 25 km wide and 50 km long (Figure 5.3). The basin contains up to 1 s of sediment that is ponded behind a pronounced structural high in the survey area (Figure 5.9). The basin occupies a slight bathymetric depression landward of the structural high and is bounded on the south by a series of faults that are oriented perpendicular to the forearc. Like the basins to the north, a single unconformity divides the basin fill into two major sequences. The basement structure of the Iquique Basin is poorly imaged, but the landward asymmetry of sediment accumulation and fanning of reflectors suggests that the basin is formed in a west-facing half graben.

Surface Morphology of the Forearc Basins

SeaMARC II side-scan sonar imagery and swath bathymetry reveal details of the surface morphology of the forearc basins in the Arica Bight area. The most prominent

Figure 5.7 Multi-channel seismic reflection profiles d1-02 and d1-04 across the Arica Basin. Basement depth and sediment thickness increases rapidly to the south in this basin. The basement blocks, separated by east-dipping faults, are particularly well developed in profile d1-02. Profile locations are shown in Figure 5.4.

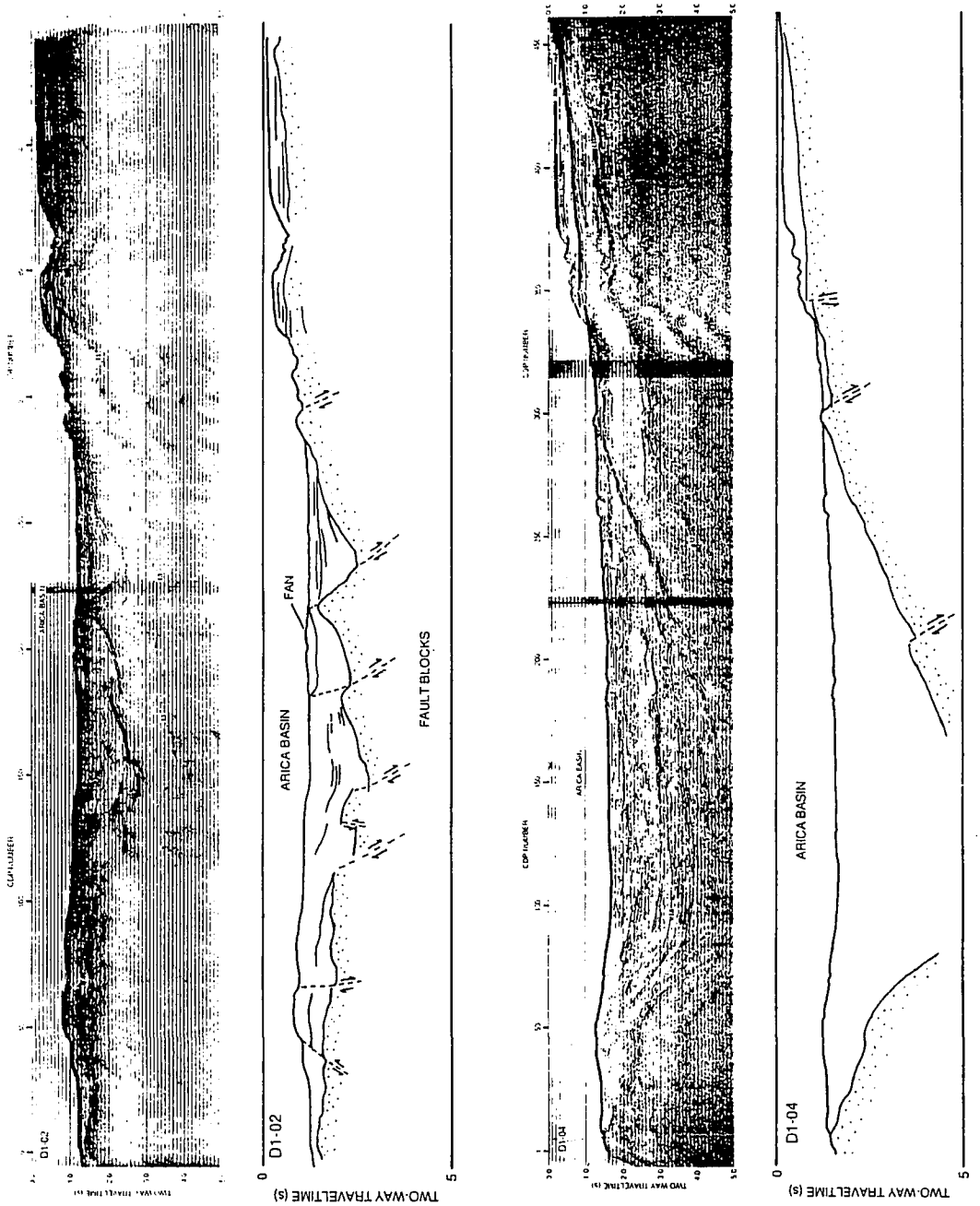
D1-02
ARICA BASIN
FAN
FAULT BLOCKS
TWO-WAY TRAVELTIME (s)
0
5
D1-04
ARICA BASIN
TWO-WAY TRAVELTIME (s)
0
5

Figure 5.8 Close-up of multi-channel seismic reflection profile D1-02 across the Arica Basin. Fanning of reflectors within the grabens indicates that movement of these fault blocks occured during the filling of the basin. A recent pulse of movement created a depression above the reflector labeled "A" that has subsequently been filled by sediment, including a fan deposit above the western graben.

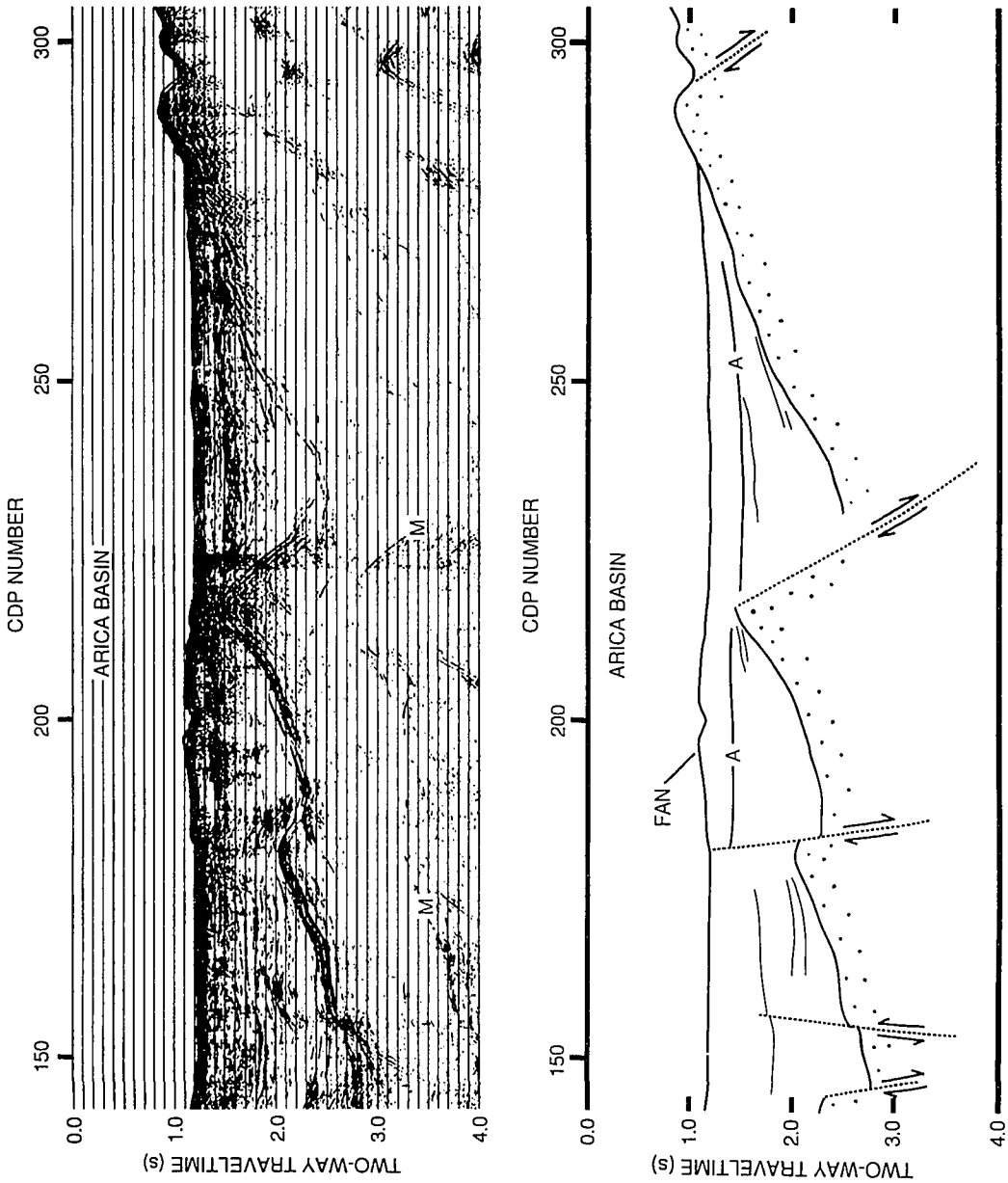
CDP NUMBER
150
200
250
300
ARICA BASIN
M
M
TWO-WAY TRAVELTIME (s)
0.0
1.0
2.0
3.0
4.0
CDP NUMBER
150
200
250
300
ARICA BASIN
FAN
A
A
TWO-WAY TRAVELTIME (s)
1.0
2.0
3.0
4.0

Figure 5.9 Single-channel seismic reflection Line 47 across the Iquique Basin. Profile location is shown on Figure 5.4.

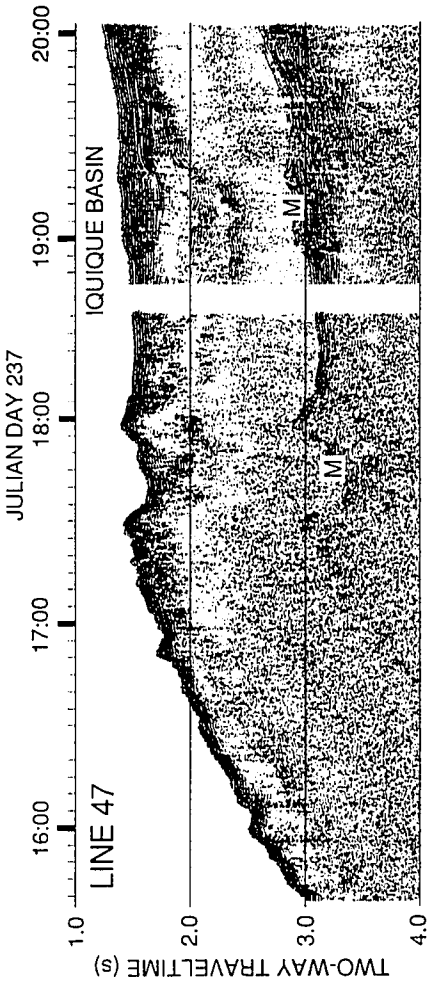
LINE 47
IQUIQUE BASIN
JULIAN DAY 237
16:00
17:00
18:00
19:00
20:00
1.0
2.0
3.0
4.0
TWO-WAY TRAVELTIME (s)
M
M

surficial features of the basins are those caused the movement and deposition of sediment: gravity flows, slumps, sediment waves, fans, channels, and submarine canyons.

Tambo submarine canyon and several smaller tributaries form a submarine drainage system within the East Arequipa Basin (Figure 5.10) that was discussed in Chapter 4. The surface of the East Arequipa Basin between and surrounding the canyons is almost completely covered by sediment waves (Figure 5.10). These waves vary in orientation and have wavelengths of 400 to 800 m. The sediment waves are of very low amplitude (less than 5 m). They appear to form distinct wave fields within which the waves have a common orientation and wavelength. These fields appear to be most pronounced near convex downslope curves in the canyons, suggesting that the sediment waves form by turbidity current overflow from the canyons.

Another large and apparently separate submarine canyon system occurs in the West Arequipa Basin (Figure 5.11). Only the southernmost portion of the basin was imaged, but the canyon system shows a pattern similar to the Tambo submarine canyon system. Three canyons coalesce at the southern end of the basin, a meandering canyon flowing from the north along the axis of the basin, and two less sinuous canyons flowing from the northeast. Where the canyon exits the basin it is deflected to the northwest along the trend of a trench-parallel fault.

The surface of the southern West Arequipa Basin is characterized by downslope-oriented channels and sediment-flow features (Figure 5.11), unlike the fields of generally slope-parallel sediment waves observed in the East Arequipa Basin.

The surface of the Iquique Basin is also covered by channels and sediment-flow features (Figure 5.12). The channels and sediment flow diverge to pass to the north and south of the prominent structural high bounding a portion of the basin. Transported material flows into a small canyon to the north and into a group of faults to the south that carry the sediment down to the trench axis.

Figure 5.10 SeaMARC II side-scan sonar backscatter data from the East Arequipa Basin. The centerpiece of this image is the highly meandering Tambo submarine canyon and its tributaries that form a drainage network within the basin. low-amplitude sediment waves cover the basin floor between the canyons.

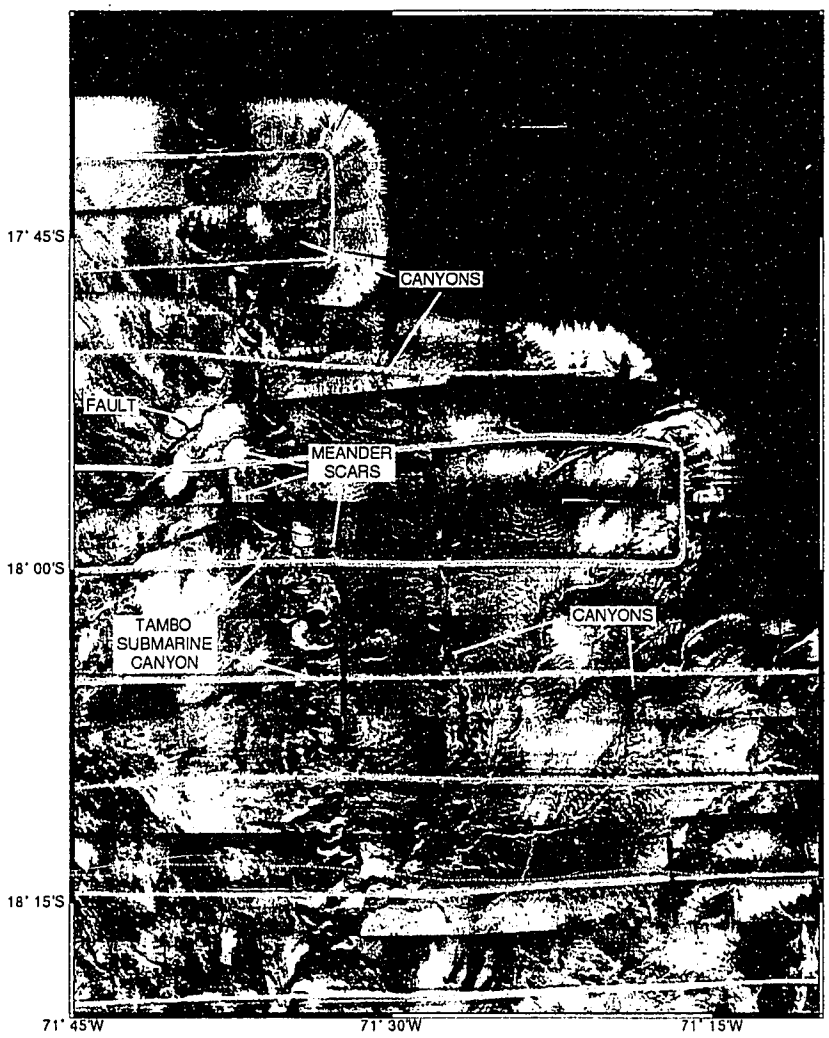
17° 45'S
18° 00'S
18° 15'S
71° 45'W
71° 30'W
71° 15'W
CANYONS
FAULT
MEANDER SCARS
TAMBO SUBMARINE CANYON
CANYONS

Figure 5.11 SeaMARC II side-scan sonar backscatter data from the West Arequipa Basin. A submarine canyon system, much like the one seen in the East Arequipa Basin, flows through this basin. The canyon is offset right-laterally by a fault as it exits the basin. The surface of the basin is characterized by sediment flow features and small channels.

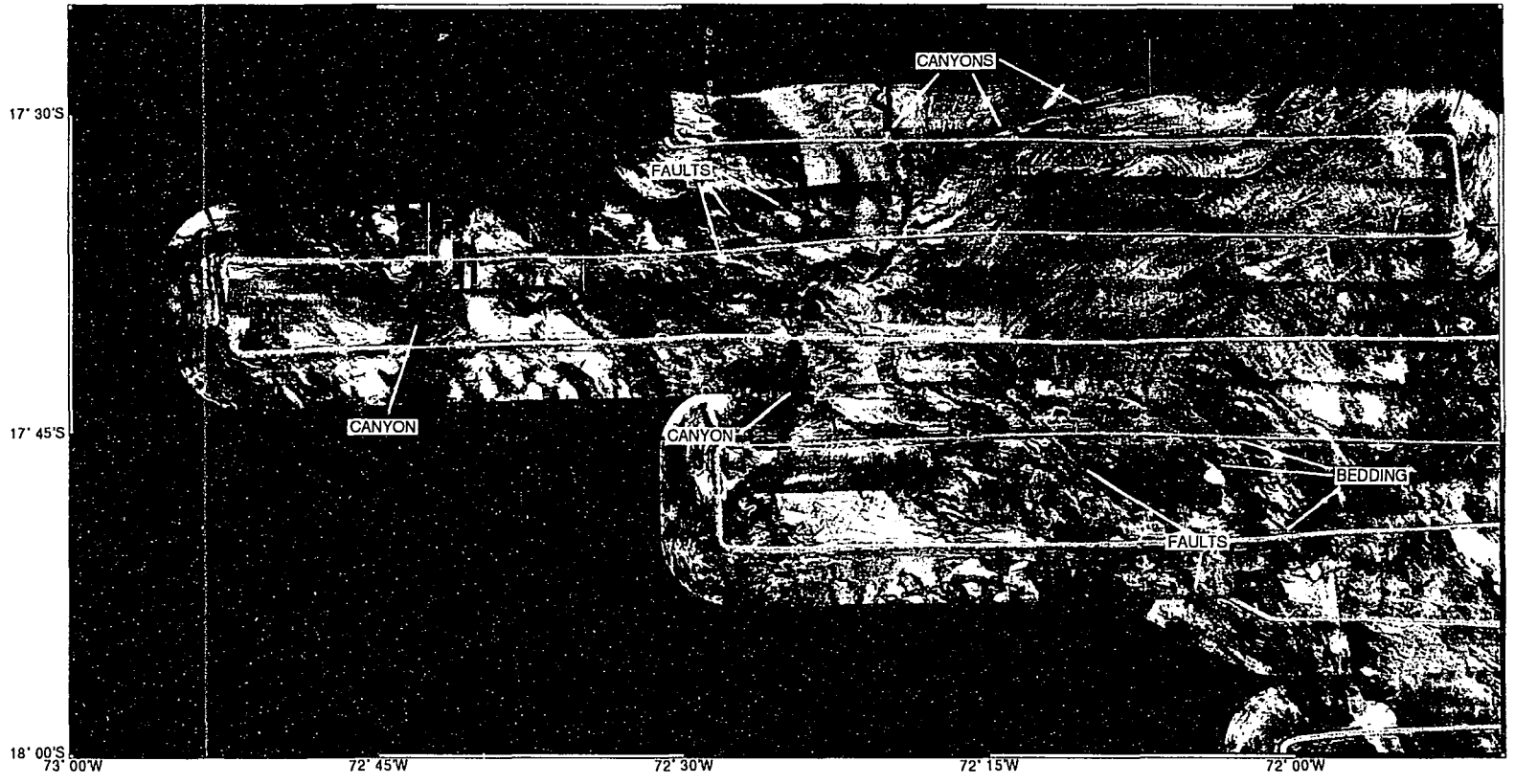
CANYONS
FAULTS
CANYON
CANYON
BEDDING
FAULTS
17° 30'S
17° 45'S
18° 00'S
73° 00'W
72° 45'W
72° 30'W
72° 15'W
72° 00'W

Figure 5.12 SeaMARC II side-scan sonar backscatter data from the Iquique Basin. Sediment flow across the surface of this basin is diverted to the north and south around a prominent structural high in the survey area. To the north the sediment enters a small canyon that carries it down to the trench axis. On the south, sediment is channeled into ENE-trending faults and fractures.

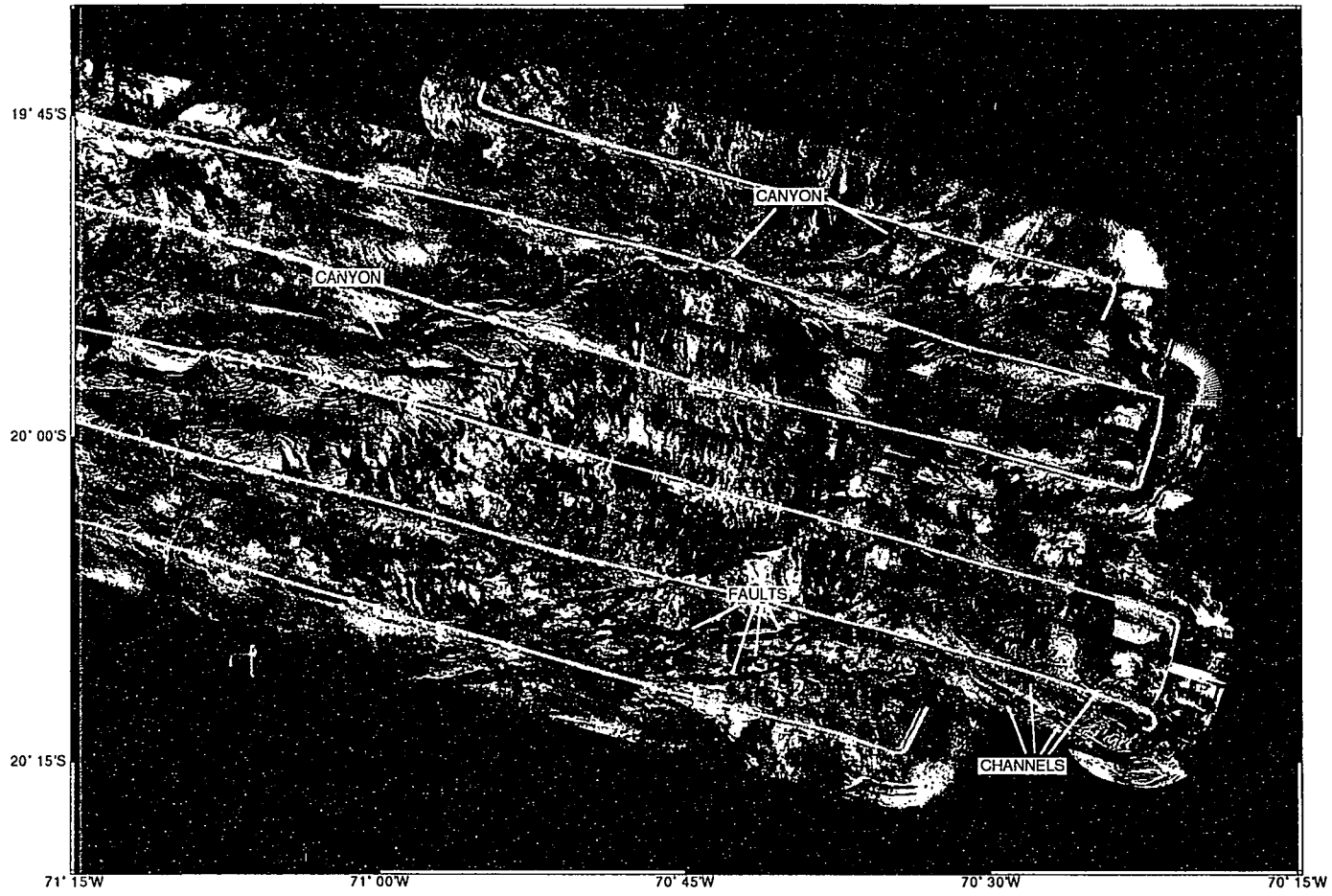
19° 45'S
20° 00'S
20° 15'S
CANYON
CANYON
FAULTS
CHANNELS
71° 15'W
71° 00'W
70° 45'W
70° 30'W
70° 15'W

Surface morphology and structure of the lower and middle forearc slopes

The block faulting visible in seismic reflection profiles across the forearc slope basins in the Arica Bight area is exposed on the seafloor of the lower and middle forearc slopes. Three major fault trends are visible in SeaMARC II side-scan and swath bathymetry images (Figure 5.3).

A series of pronounced north-south trending, west-facing scarps (about 355°) (Figure 5.13) extend from the lower forearc slope, diagonally across the northwest-southeast trend of the forearc, and disappear at the edge of the upper slope basins (Figure 5.14). The relief on these faults is higher than those with other trends and they are clearly visible in the illuminated bathymetry. The north-south trending faults are less obvious on the side-scan images, however, perhaps due to their orientation parallel to the side-scan look direction. They may also be older features that have been overprinted by later faulting and sedimentation.

Faults with a northeast-southwest trend are less pronounced than the north-south trending faults (Figure 5.14), but are somewhat more obvious on the side-scan images. These northeast-southwest trending faults are predominantly east of the north-south trending faults. They also show a systematic change to a more northerly trend as one moves north along the forearc (Figures 5.3 and 5.13). Faults in the Iquique Basin survey area are oriented at about 080°, whereas to the north, in the southern portion of the Arica Bight survey area, the northeast-trending faults have an azimuth of about 012°.

The third and most common fault trend observed in the Arica Bight area consists of faults with a northwest-southeast trend (about 320°), roughly parallel to the trend of the trench off southern Peru (Figure 5.13). For the most part, these faults are of low relief and are not easily observed in the SeaMARC II swath bathymetry (Figure 5.14). They are, however, prominent on the side-scan images (Figure 5.15). Several prominent northwest-

Figure 5.13 Sector diagram and fault azimuth histogram for forearc faults and fractures in the Arica Bight area. Three major fault trends are indicated. Both the sector diagram and histogram are weighted by the lengths of the digitized faults.

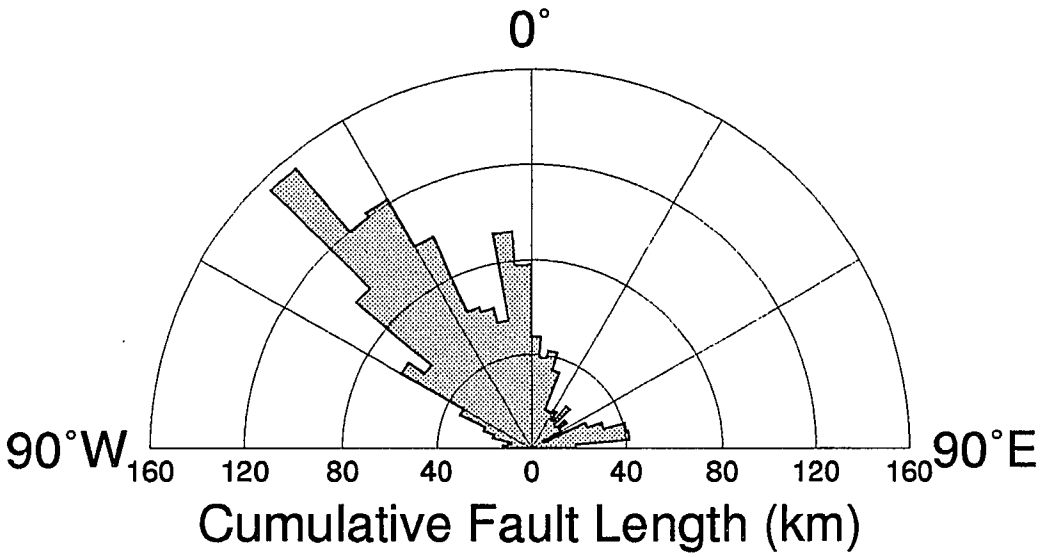
0°
90°W
160
120
80
40
0
40
80
120
160
90°E
Cumulative Fault Length (km)

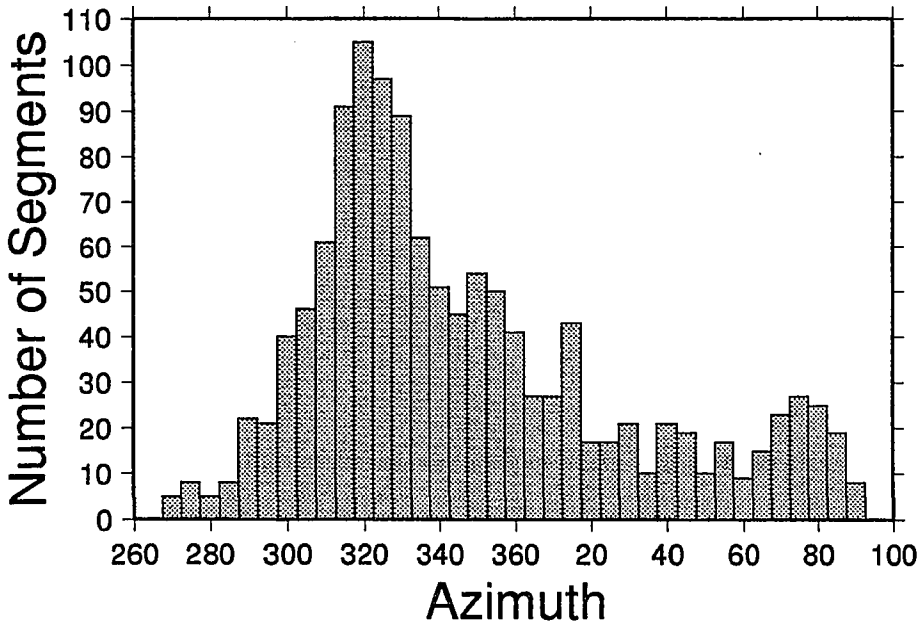
Number of Segments
110
100
90
80
70
60
50
40
30
20
10
0
260
280
300
320
340
360
20
40
60
80
100
Azimuth

Figure 5.14 Color shaded-relief image of SeaMARC II bathymetry in the Arica Bight area. The colors indicate depth and the image is illuminated is from the northeast to bring out the finer detail in the bathymetry.

South
America
Depth (m)
-444
-10000
-20000
-30000
-40000
-50000
-60000
-70000
-7494
18°
19°
20°
73°
72°
71°

Figure 5.15 SeaMARC II side-scan sonar backscatter data across the lower and middle forearc slopes in the Arica Bight area. The surface of the seafloor in this area is broken by faulting with three major trends.

18° 30' S
19° 00'
19° 30'
71°00'
71°30'
72°00 W.

trending faults do appear in the bathymetry on the upper middle slope between the East and West Arequipa Basins, however, where they form deep "V-shaped" fractures in which small linear sedimentary basins have formed (Figure 5.16).

The SeaMARC II bathymetry in the Arica Bight area reveals three embayments in the forearc slope (Figure 5.14). One embayment is located south of the West Arequipa Basin, the second is located south of the East Arequipa Basin, and the third is located southwest of the Arica Basin. The association of these embayments with the forearc slope basins suggests that they are structurally related to the basins. The embayments are probably formed in the same basement graben as the adjacent basin.

Of the three, only the embayment south of the East Arequipa Basin is well-covered by the SeaMARC II survey. The general depth of this embayment is about 4500 m. It is bounded on the north and east by slopes that rise steeply to the edge of the upper forearc slope at about 1800 m. In the western portion of the embayment an isolated high rises to about 2200 m. The steep western boundary of this high is a north-south -trending, west-facing fault scarp with more than 700 m of relief.

Analysis of the structure of this embayment is complicated by Tambo submarine canyon which flows through the area. The canyon enters the embayment from the East Arequipa Basin to the north and is captured by a headward eroding canyon from the southwest that cuts across the isolated structural high at the west side of the embayment (Figure 5.17) [*Bergersen*, 1989]. The remnant of Tambo submarine canyon below this cutoff (the lower slope canyon) continues south along the east side of the isolated structural high before it too turns southwest and continues downslope to the trench axis. The portion of the lower slope canyon confined between the isolated structural high and the upper forearc to the east follows a generally straight north-south course. This north-south section of the canyon is aligned with a major north-south-trending fault to the south, suggesting that the canyon's course is controlled by basement faulting.

Figure 5.16 SeaMARC II side-scan sonar image of small linear basins formed along trench-parallel faults on the middle forearc slope between the East and West Arequipa Basins.

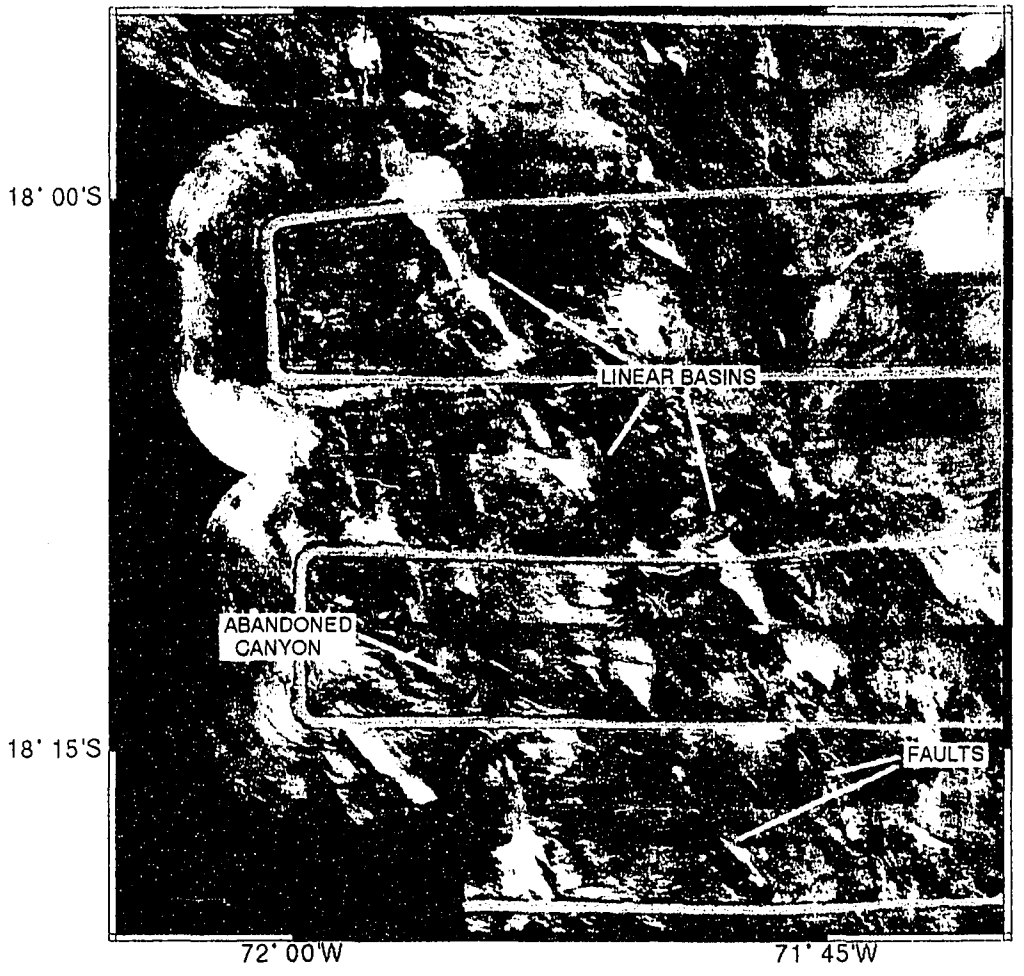
18° 00'S
18° 15'S
LINEAR BASINS
ABANDONED
CANYON
FAULTS
72° 00'W
71° 45'W

Figure 5.17 Block diagram of a portion of the middle forearc in the Arica Bight area. SeaMARC II sidescan is overlain on color bathymetry to produce this perspective view of the embayment south of the East Arequipa Basin. Vertical exaggeration is about 8 x.

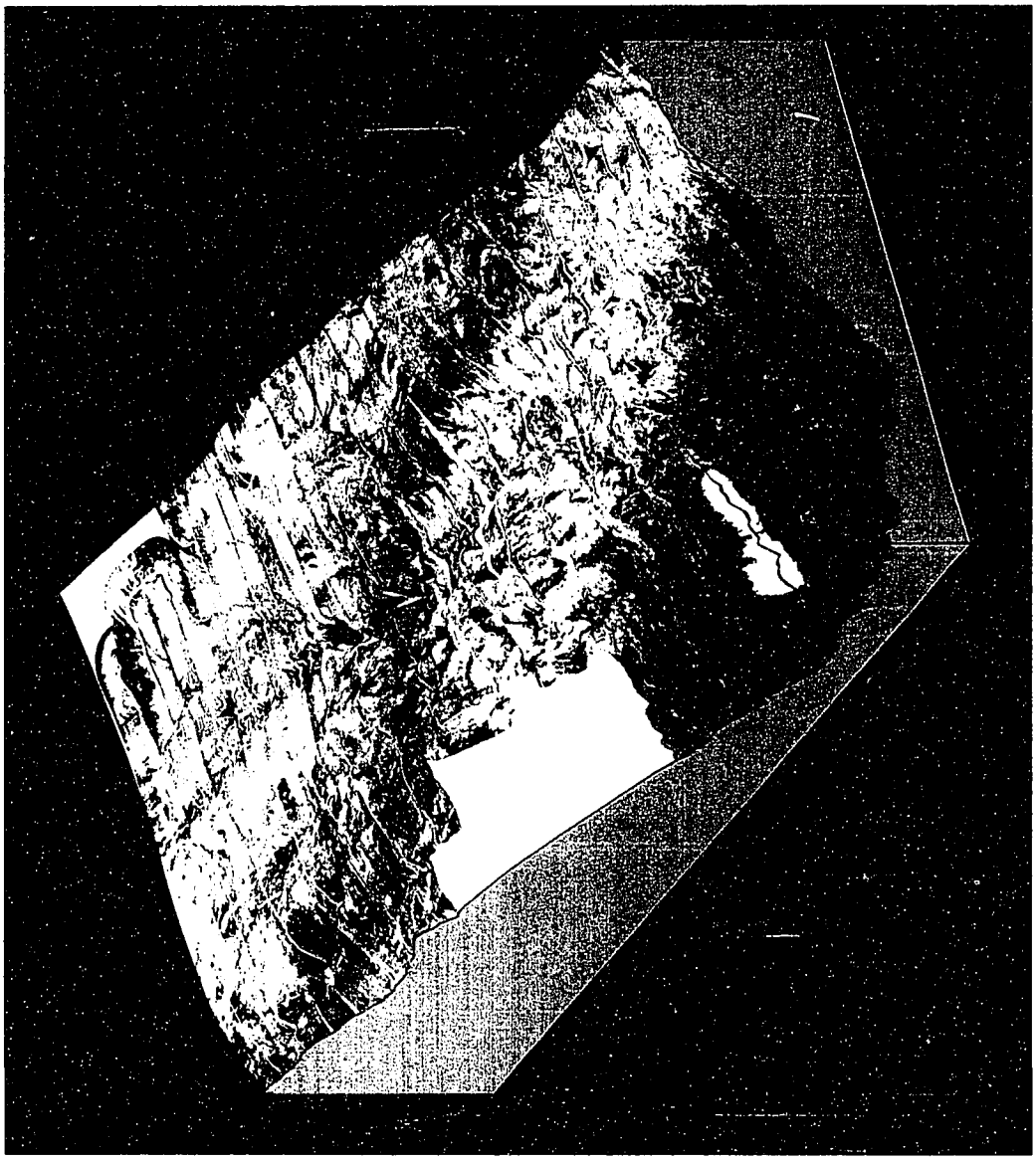

Single-channel seismic reflection profiles reveal little of the subsurface structure of this embayment. Penetration is poor and only a thin veneer of sediment mantles the acoustic basement. Only Line 36 (Figure 5.18) reveals a significant amount of sediment fill ponded between the isolated western high and the upper forearc. Reflectors within this small sediment pond tilt gently eastward, suggesting that the basement block on which they rest has rotated.

Onshore geology and structure in the Arica Bight area

Compressional deformation and thrust faulting are an integral part of the tectonics of the Andes and the sub-Andean belt to the east [*Jordan et al.*, 1983; *Jordan and Alonso*, 1987]. The forearc west of the Andes, however, shows almost no evidence of recent compression. Instead, the area exhibits widespread evidence of extension in the form of normal faulting [*Katz*, 1971; *Mortimer and Saric*, 1975; *Megard and Philip*, 1976; *Hartley et al.*, 1988; *Armijo and Thiele*, 1990]. The Coastal Scarp of northern Chile may in fact be a normal fault scarp caused by this extension [*Paskoff*, 1980; *Armijo and Thiele*, 1990]. North of about 21° 25' S, faults in the Coastal Range have either north-south or east-west trends [*Mortimer and Saric*, 1975]. The east-west-trending faults have a preferred downthrow to the north and appear to be younger than the north-south faults [*Mortimer and Saric*, 1975].

Another prominent structural feature parallel to the coast of northern Chile is the Atacama Fault Zone which extends for more than 1000 km along the eastern margin of the Coastal Range (Figure 5.1). The amount and sense of motion along this fault have been the subject of some disagreement [*St. Amand and Allen*, 1960; *Allen*, 1965; *Arabasz*, 1971; *Naranjo*, 1987]. Several recent studies, however, have found abundant evidence of recent left-lateral strike-slip movement along this fault [*Hervé*, 1987; *Thiele and Pincheira*,

Figure 5.18 Single-channel seismic reflection profiles across the embayment of the middle forearc slope south of the East Arequipa Basin. Profile locations are shown on Figure 5.4.

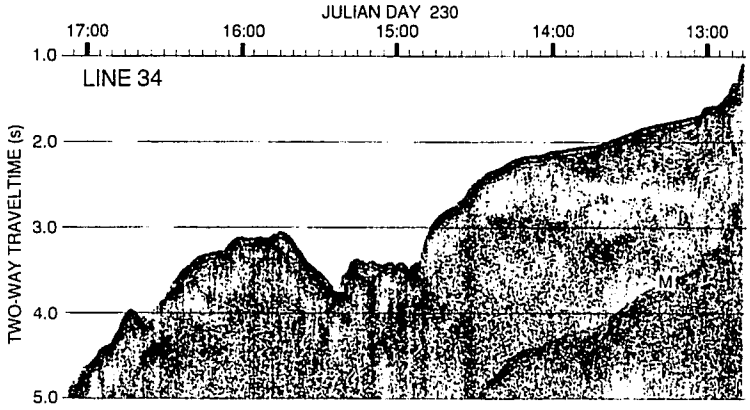
JULIAN DAY 230
17:00
16:00
15:00
14:00
13:00
1.0
LINE 34
TWO-WAY TRAVELTIME (s)
2.0
3.0
4.0
5.0
M

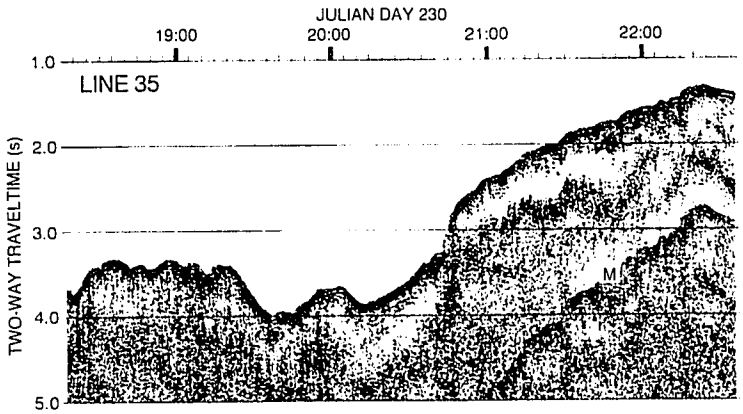
JULIAN DAY 230
19:00
20:00
21:00
22:00
1.0
LINE 35
TWO-WAY TRAVELTIME (s)
2.0
3.0
4.0
5.0
M

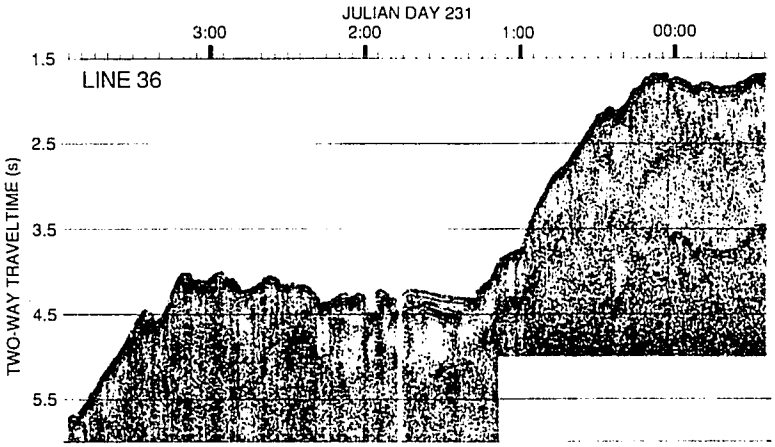
JULIAN DAY 231
3:00
2:00
1:00
00:00
1.5
LINE 36
TWO-WAY TRAVELTIME (s)
2.5
3.5
4.5
5.5

1987; *Armijo and Thiele*, 1990]. This sense of motion conflicts with the right-lateral motion that might be expected if the fault were absorbing the lateral component of the oblique convergence of the Nazca and South American plates in this area [*Jarrard*, 1986]. Armijo and Thiele [*1990*] propose instead that the fault is reflecting clockwise rotation and differential shortening of the orogen south of Arica.

In northern Chile, the Jurassic volcanic arc (exposed in the Coastal Range) and the present trench axis are less than 100 km apart. This is too close for them to have formed in this proximity, given our current knowledge of subduction dynamics and the present dip of the subducting slab. The observed eastward migration of volcanism from the Jurassic arc, now exposed in the Coastal Range, to the present active volcanic arc in the high Andes [*Farrar et al.*, 1970] may have been caused by a reduction in the dip of the subducting Nazca plate [*James et al.*, 1971; *Mortimer and Saric*, 1975; *Jordan et al.*, 1983; *Isacks*, 1988]. This "rollback" of the subduction zone would result from the westward movement of the South American plate over a subducted slab that is anchored in the mantle.

Another process that may also play a role in the development of the Pacific margin of southern Peru and northern Chile is tectonic erosion of the forearc by the subducting plate [*Katz*, 1971; *Rutland*, 1971; *Plafker*, 1972; *Mortimer and Saric*, 1975; *Coulbourn*, 1981]. In the classical view of plate tectonics, a subduction zone results in compression, accretion, and uplift of the over-riding plate. Tectonic erosion, in which convergence at a subduction zone results in the erosion and subduction of material from the edge of the over-riding plate, was proposed as an alternative to the accretionary model to explain the truncation of structures and the apparent absence of significant amounts of young material in some forearcs [*Scholl et al.*, 1970; *Katz*, 1971; *Rutland*, 1971; *Plafker*, 1972].

Structural and stratigraphic relationships among rocks exposed in the Coastal Range of northern Chile indicate that at least half of the Jurassic arc is missing [*Mortimer*, 1972; *Mortimer and Saric*, 1975; *Armijo and Thiele*, 1990]. Precambrian and Paleozoic rocks

and intrusives of the Coastal Batholith exposed along the coast of southern Peru also suggest that a significant amount of material has been removed. Unlike the exotic terranes that have been recognized along the west coast of the United States and Canada, there is no evidence for accretion or lateral movement of exotic terranes along the coast of southern Peru or northern Chile [*Jordan and Gardeweg*, 1989].

Discussion

The tectonic regime of the offshore portion of the forearc of southern Peru and northern Chile appears to be one of extension. Aside from a narrow (15 to 20 km) wedge of accreted material along the lowermost forearc (Figure 5.15), the structure of the forearc is dominated by normal faulting that produces a block faulted basement topography. This structural style continues across the onshore portion of the forearc to the west flank of the Western Cordillera.

A recent study [*Armijo and Thiele*, 1990] of the Mejillones Peninsula, about 500 km south of Arica (Figure 5.2), examined several rift grabens in Paleozoic and Mesozoic basement rocks that contain Neogene sediment. The peninsula itself is an uplifted fault block that is about 50 km long (north-south) and extends 15 to 20 km west of the coastal scarp. The individual fault blocks that make up the peninsula show both eastward and westward tilting, although westward tilting is dominant [*Armijo and Thiele*, 1990]. Offset alluvial fans and Pleistocene shorelines provide abundant morphologic evidence of recent movement on these faults. Figure 5.19 shows Neogene sediment dipping toward a high-angle normal fault that bounds a small rift basin on the peninsula. The structure of this basin is very similar to structures seen on seismic reflection profiles collected offshore in the Arica Bight area, and supports a model of extension in the offshore forearc.

Figure 5.19 Forearc basin sediments exposed in the Mejillones Penninsula. In this figure Neogene marine sediments dip westward toward a steeply dipping normal fault bounding the basin. d = drag fold, u = unconformity. Modified from Armijo and Thiele [*1990*].


d
n
a

In the Arica Bight area, faulting and extension of the upper forearc slope and shelf have created both east- and west-facing half grabens that form small north-south-trending basins. The interaction of three major fault trends on the forearc has apparently caused collapse of sections of the seaward edge of the upper slope. These down-dropped blocks form embayments in the middle and upper forearc slopes that are clearly visible on the bathymetry.

The embayment associated with the East Arequipa Basin (Figures 5.14 and 5.17) is apparently controlled by large north-south-trending faults. A group of west-facing normal faults form the western boundary of a large fault block that includes an isolated structural high. Another large north-south-trending fault defines the eastern boundary of this block. Mass-wasting is apparently widening the embayment to the east as erosion eats upslope into the edge of the basin. Eroded material probably enters the lower slope canyon, which carries it down to the trench axis.

In addition to this surface erosion, large-scale rotational slumping appears to be widening this embayment. Figure 5.20 shows single-channel seismic reflection profiles across a small un-named basin perched on the edge of the upper slope south of the East Arequipa Basin. These profiles show a series of triangular basement blocks. Sediment deposited in small basins between these blocks dips to the east, indicative of rotation along faults bordering the blocks. On the side-scan sonar image (Figure 5.21) the outcropping basement blocks and fault scarps appear as dark bands of high backscatter that form slightly southwest-concave arcs. The northwest and southeast borders of the slump mass are shown by small channels that probably developed along the strike-slip faults that form the lateral boundaries of the slump.

In previous studies of the submarine forearc in the Arica Bight area, Coulbourn and Moberly [*1977*] and Coulbourn [*1979*] noted a landward tilting of reflectors on the seaward sides of the basins and a landward migration of basin depocenters with time. They

Figure 5.20 Single-channel seismic reflection profiles across a small slump basin on the edge of the upper forearc slope south of the East Arequipa Basin. Tilted sediment ponded behind angular basement fault blocks indicates rotational slumping toward the west. Profile locations are shown on Figure 5.4.

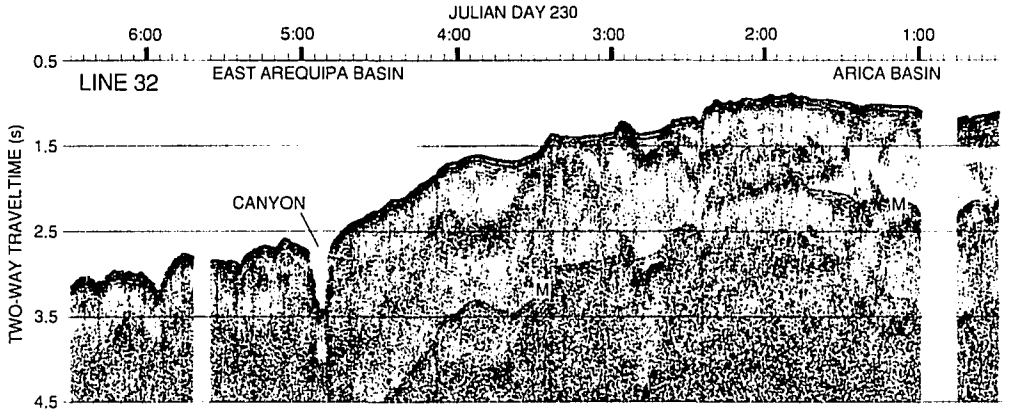
JULIAN DAY 230
6:00
5:00
4:00
3:00
2:00
1:00
0.5
LINE 32
EAST AREQUIPA BASIN
ARICA BASIN
TWO-WAY TRAVELTIME (s)
1.5
2.5
3.5
4.5
CANYON
M
M
M

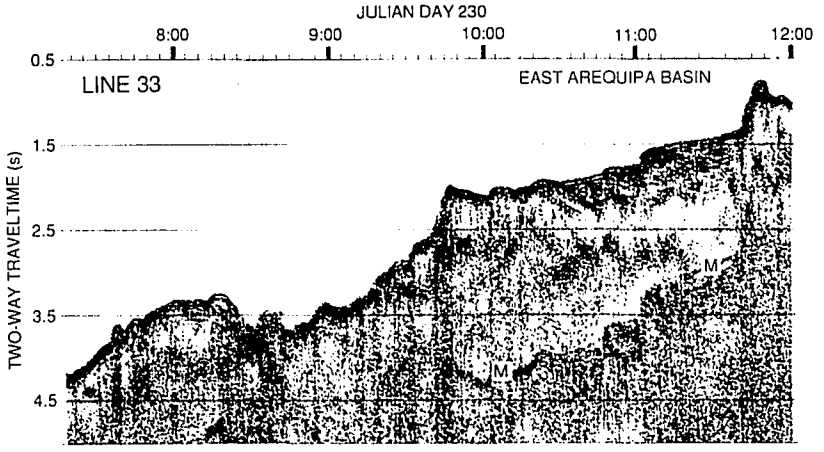
JULIAN DAY 230
8:00
9:00
10:00
11:00
12:00
0.5
LINE 33
EAST AREQUIPA BASIN
TWO-WAY TRAVELTIME (s)
1.5
2.5
3.5
4.5
M
M

Figure 5.21 SeaMARC II side-scan sonar image across the small slump basin. The curving high-backscatter features within the basin are the surface exposures of the block faulted basement and faults. Small channels on the sides of the basin probably developed along the strike-slip faults bounding the slump.

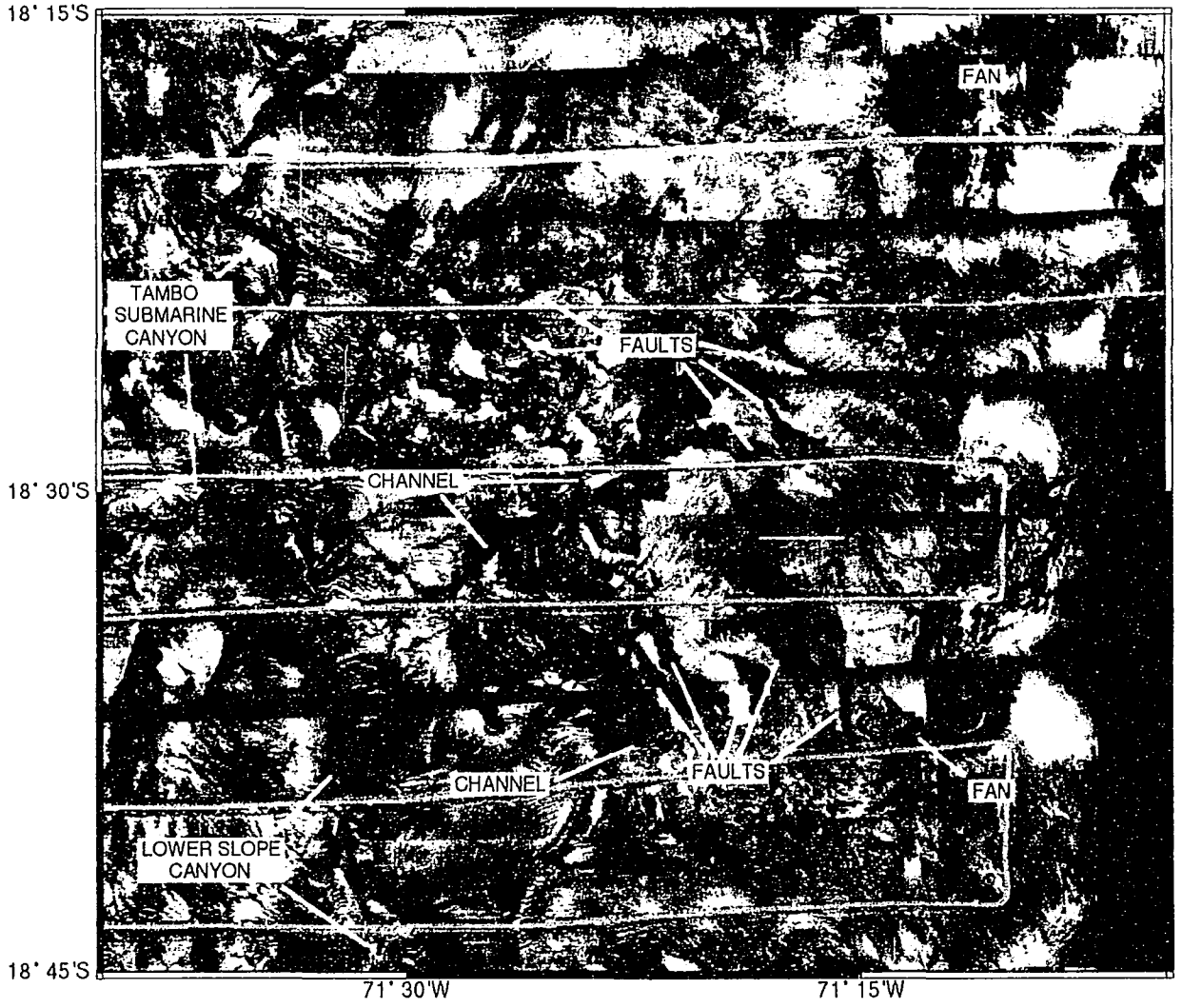
18° 15'S
18° 30'S
18° 45'S
71° 30'W
71° 15'W
FAN
TAMBO
SUBMARINE
CANYON
FAULTS
CHANNEL
CHANNEL
FAULTS
FAN
LOWER SLOPE
CANYON

suggested two possible models to explain these observations: 1) uplift of the structural high bounding the seaward edge of the basin in response to accretion of sediment at the base of the forearc, or 2) subsidence of the basement underlying the basin through sediment loading and downthrow along the seaward side of trench-parallel faults. Unfortunately, all of the seismic profiles from the 1973 and 1974 KANA KEOKI surveys in the Arica Bight area that were used in Coulbourn's study were destroyed in a fire. All that remains are line drawing interpretations that are difficult to correlate with the more recent data. While the landward tilting of reflectors is observed in the more recent profiles, this pattern of basin depocenter migration is not seen everywhere in the Arica Bight area. In some seismic profiles the depocenters appear to have been stationary and the basin strata were then tilted together as a single block. In other profiles the progressive tilting of basin strata and depocenter migration proposed by Coulbourn and Moberly [*1977*] is observed. In many cases adjacent seismic profiles show these different structural styles. Basin formation therefore appears to be variable and is strongly influenced by vertical tectonics.

Although it appears that Coulbourn's observations of migrating basin depocenters may not apply uniformly to all of the offshore basins, the structure of the forearc in the Arica bight area is much as he described, and his ideas for basin formation (described above) are still applicable. Figure 5.22 shows a model for the formation of the East Arequipa Basin. This model should also apply to the other basins in the area, with minor modifications.

In the first stage of the model, the basin formed as a shallow block-faulted depression caused by east-west extension of the forearc. During stage 2, turbidite sedimentation began to fill the basin. Continued motion on some of the basement faults is indicated by fanning reflectors seen in some seismic reflection profiles. In stage 3, the entire basin tilted down to the west and basin sedimentation shifted to the west side of the basin, forming a second major sediment sequence above a basin-wide angular

Figure 5.22 A model showing 4 stages in the evolution of the East Arequipa Basin.

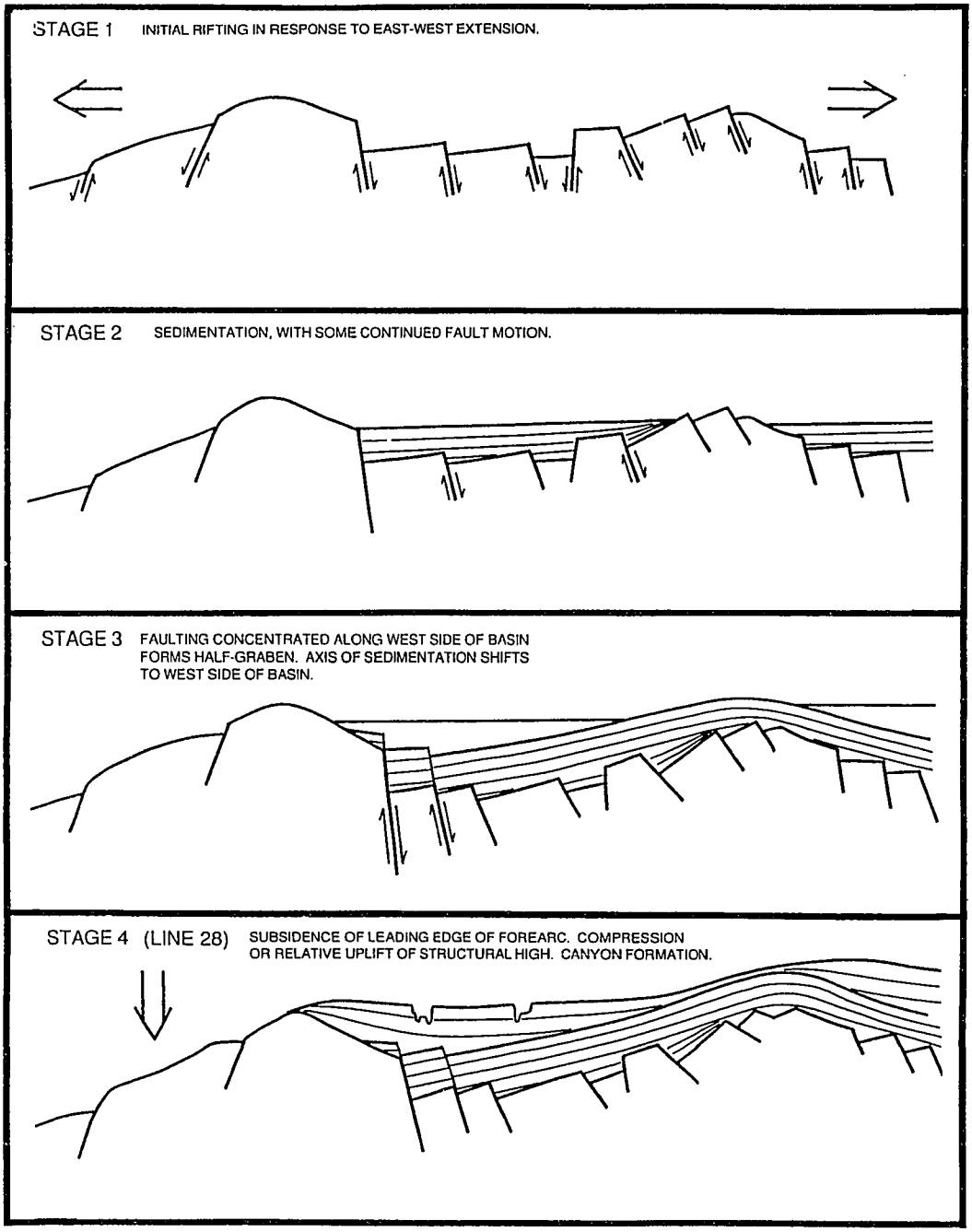
STAGE 1 INITIAL RIFTING IN RESPONSE TO EAST-WEST EXTENSION.
STAGE 2 SEDIMENTATION, WITH SOME CONTINUED FAULT MOTION.
STAGE 3 FAULTING CONCENTRATED ALONG WEST SIDE OF BASIN FORMS HALF-GRABEN. AXIS OF SEDIMENTATION SHIFTS TO WEST SIDE OF BASIN.
STAGE 4 (LINE 28) SUBSIDENCE OF LEADING EDGE OF FOREARC. COMPRESSION OR RELATIVE UPLIFT OF STRUCTURAL HIGH. CANYON FORMATION.

unconformity. Vertical movement during this episode was concentrated along the west side of the basin and resulted in the formation of an east-facing half-graben. In the fourth stage of basin development, continued sedimentation is concentrated along the deep west side of the graben near the large-offset boundary faults. Compaction and loading of the basin sediments and underlying basement cause sediments to dip toward the center of the basin.

Uplift of the structural high bounding the west side of the basin may also be occurring, and could contribute to the landward dip of the reflectors in the western portion of the basin. The structural high bounding the west side of the East Arequipa Basin becomes more pronounced as one moves south along the basin and there is a corresponding increase in the landward dip of basin reflectors that lap onto it (Figure 5.4). Since the structural high becomes closer to the trench as one moves south, it is possible that uplift is occurring in a narrow, trench-parallel zone along the edge of the upper forearc slope. Whether compression and uplift is occurring all along the edge of the forearc, or only locally is difficult to determine. It is possible that, following the period of extension and rifting that formed the forearc slope basins, the forearc in the Arica Bight area has undergone a period of re-adjustment and has experienced accretion of material to the lower forearc and uplift of the edge of the forearc.

What caused the extension and rifting that formed the forearc slope basins in the Arica Bight area? This question is difficult to answer with the available data. Coulbourn [*1981*] presented two possible end-member models for the development of the continental margin in the Arica Bight area (Figure 5.23). The accretionary end-member shows the traditional model of Andean subduction with a thick wedge of deformed sediment accreted against the edge of the continent. In this model, the forearc slope basins straddle the accreted sediment - continental crust boundary and form behind an uplifted structural high. In the non-accretionary (or tectonic erosion) model, a thin covering of hemipelagic

Figure 5.23 Accretionary and erosional end-members for convergent continental margins [*Coulbourn*, 1979].

LEGEND

1 = structural high

2 = forearc basin

3 = block-faulted continental basement

4 = accretionary prism

5 = trench axis turbidites

6 = deformed and dewatered hemipelagic sediments

7 = Mesozoic basement

8 = coastal batholith

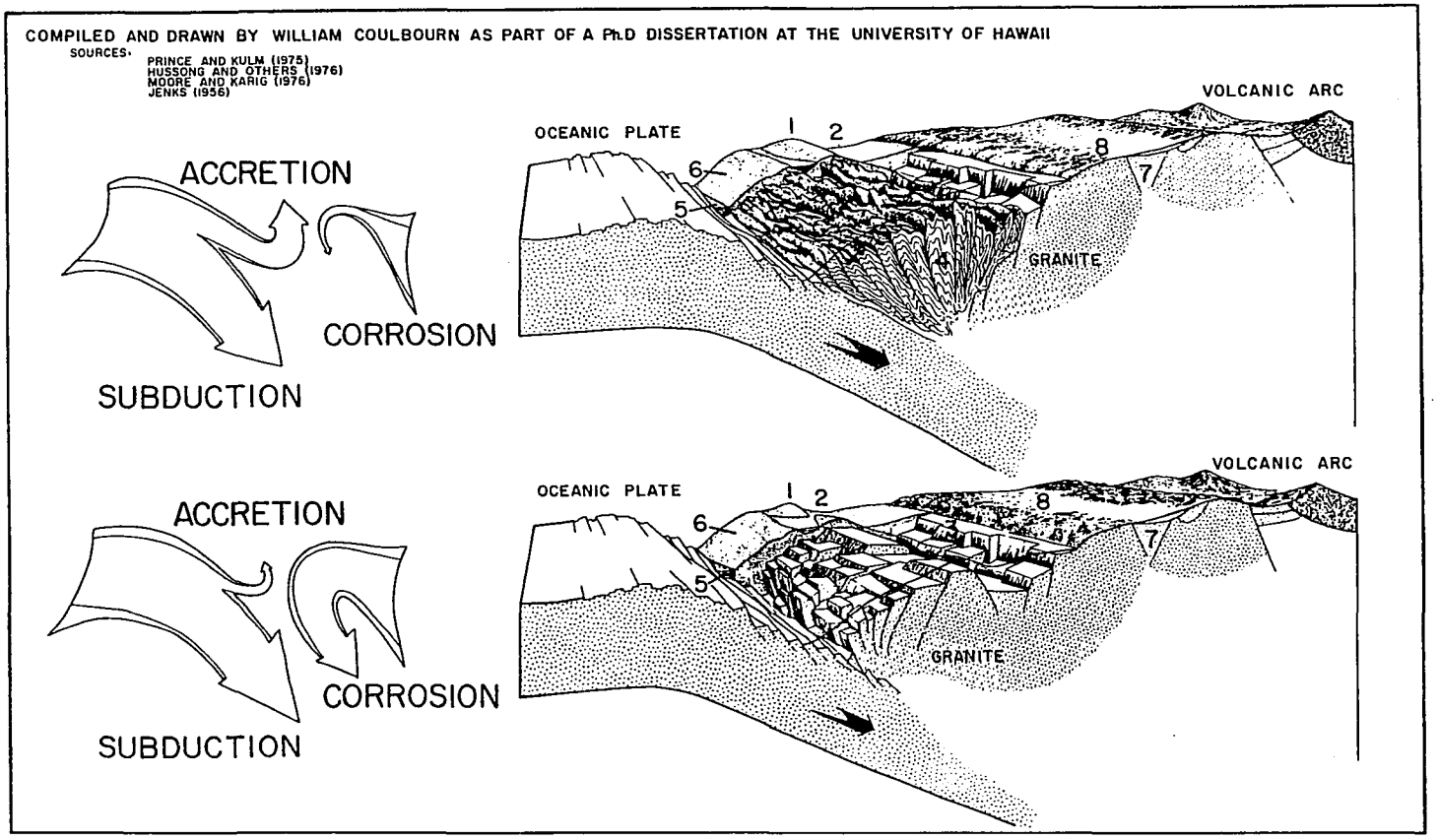
COMPILED AND DRAWN BY WILLIAM COULBOURN AS PART OF A Ph.D DISSERTATION AT THE UNIVERSITY OF HAWAII
SOURCES:
PRINCE AND KULM (1975)
HUSSONG AND OTHERS (1976)
MOORE AND KARIG (1976)
JENKS (1956)
ACCRETION
CORROSION
SUBDUCTION
OCEANIC PLATE
VOLCANIC ARC
GRANITE
1
2
3
4
5
6
7
8
ACCRETION
CORROSION
SUBDUCTION
OCEANIC PLATE
VOLCANIC ARC
GRANITE

sediment overlies the leading edge of the faulted continental crust. In this case, the forearc slope basins form on faulted continental crust. Most of the pelagic and hemipelagic sediment as well as the leading edge of the continental crust is subducted. The model presented in Figure 5.22 for the evolution of the forearc slope basins is consistent with tectonic erosion of the forearc in the Arica Bight area.

Tectonic erosion (or subduction erosion), in which convergence at a subduction zone results in the erosion and subduction of material from the edge of the over-riding plate, was proposed as an alternative to the accretionary model to explain the truncation of structures and the apparent absence of significant amounts of young material in some forearcs, including the Peru-Chile forearc [*Scholl et al.*, 1970; *Katz*, 1971; *Rutland*, 1971; *Plafker*, 1972]. Evaluation of this model was initially difficult due to the general seismic opacity of the lower forearc and the absence of information on sediment types, ages, and vertical tectonics in forearcs [*Scholl et al.*, 1980]. The development and refinement of marine multichannel seismic methods and the drilling of several forearcs by the Deep Sea Drilling Project (DSDP) and the Ocean Drilling Program (ODP) have confirmed tectonic erosion in several areas.

Results from DSDP Legs 56 and 57 on the Japan forearc indicate that most of the sediment entering the trench was subsequently subducted [*von Huene et al.*, 1980]. Seismic and drilling results also indicate that the forearc has subsided as much as 6 km and retreated by about 50 km, implying that material has been removed by tectonic erosion [*Langseth et al.*, 1981]. Multichannel seismic data collected across the Japan forearc show structures indicative of tectonic erosion and gravity collapse at the front of the forearc [*von Huene and Culotta*, 1989].

ODP Leg 112 drilled the forearc of the Peru Trench at latitudes 9° and 11° S. Drilling results showed that rocks of continental affinity extend to the lower slope area. Subsidence of the forearc by at least 3 km and tectonic erosion were also indicated [*von*

Huene et al., 1988]. Multichannel seismic records show that truncated continental basement extends to within 18 to 23 km of the trench near the drill sites [*von Huene et al.*, 1985]. Whereas a small accretionary prism is present, its volume is much less than the amount available during Cenozoic convergence along this margin [*Hussong et al.*, 1976; *Kulm et al.*, 1981; *Shepard and Moberly*, 1981].

The preceding discussion shows that tectonic erosion is well-documented in several forearcs and in at least two locations along the Peru-Chile Trench. This suggests that whether a forearc experiences accretion or tectonic erosion is controlled by regional factors such as subduction geometry or sediment supply, rather than by local factors such as irregularities in the subducting plate, or forearc structure. Therefore, the extension and subsidence of the forearc in the Arica Bight area is not unexpected, and fits into the pattern of tectonic erosion observed at other areas along the Peru-Chile Trench.

Another possible explanation for the extension observed in the offshore forearc in the Arica Bight area is that it results from strike-slip motion. The oblique subduction of the Nazca Plate may cause slivers of the lower forearc to become detached and move laterally along the forearc. The prominent north-south-trending faults that are clearly visible in the SeaMARC II bathymetry on the lower and middle forearc (Figure 5.14), and the trench-parallel faults occupied by the linear basins shown in Figure 5.16, may be right-lateral strike-slip faults as shown in Figure 5.24. The right-lateral offset is suggested by the vertical displacement of the north-south faults on the lowermost forearc, and by the right-lateral offset of the canyon in the West Arequipa Basin (Figure 5.11).

The proposed northward and westward motion of the lower forearc sliver would tend to remove support from the western margin of the upper forearc. The fault-controlled basins of the upper forearc and the bathymetric embayments on the middle forearc could result from the extension and seaward collapse of this unsupported slope.

Figure 5.24 Model for the development of the forearc in the Arica Bight area through strike-slip faulting and lateral motion of lower forearc slivers. The heavy solid lines show the traces of major faults that may have formed by strike-slip motion. Movement of lower forearc slivers along these faults could explain the extensional structure seen beneath the upper slope basins.

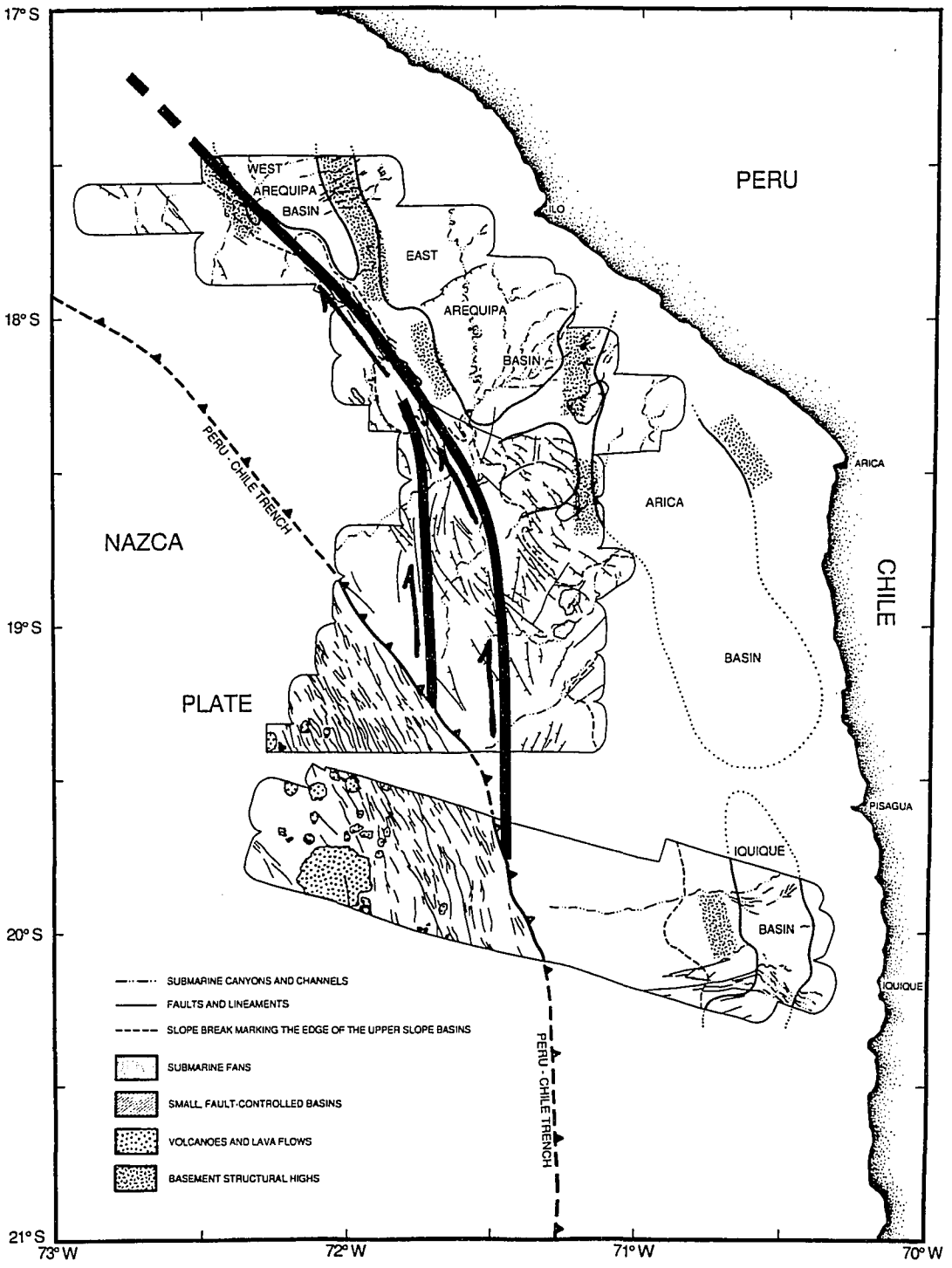
17° S
18° S
19° S
20° S
21° S
73° W
72° W
71° W
70° W
PERU
CHILE
NAZCA
PLATE
WEST
AREQUIPA
BASIN
EAST
AREQUIPA
BASIN
ILO
ARICA
ARICA
BASIN
PISAGUA
IQUIQUE
BASIN
IQUIQUE
PERU - CHILE TRENCH
PERU - CHILE TRENCH
SUBMARINE CANYONS AND CHANNELS
FAULTS AND LINEAMENTS
SLOPE BREAK MARKING THE EDGE OF THE UPPER SLOPE BASINS
SUBMARINE FANS
SMALL, FAULT-CONTROLLED BASINS
VOLCANOES AND LAVA FLOWS
BASEMENT STRUCTURAL HIGHS

Conclusions

In the offshore Arica Bight area, extension of the forearc has created a series of left-stepping en-echelon forearc slope basins that are oriented north-south, oblique to the curving subduction zone. Seismic reflection profiles reveal that these basins have the form of half grabens. The northernmost basin, the West Arequipa Basin, contains up to 1 s of sediment in a west-facing half graben. The east Arequipa Basin and the Arica Basin contain up to 1.6 s and 2.5 s of sediment respectively, in east-facing half grabens. Secondary faulting in all of these basins is dominantly synthetic. The basins are separated by north-south oriented structural highs. The East and West Arequipa Basins are not bounded by structural highs at their southern ends but are truncated by creep and gravitational collapse of sediment down the forearc slope.

The north-south-trending faults that define the forearc slope basins break the middle forearc slope into large blocks that are visible in SeaMARC II side-scan and bathymetry data. The middle forearc is also broken by northwest-southeast, trench-parallel faults and faults with a northeast-southwest trend, creating a complexly faulted terrain. The intersection of these faults has created embayments, visible in the forearc bathymetry. These embayments probably form within the same rift graben as the associated basins.

The embayment south of the East Arequipa Basin is clearly defined by large north-south-trending, west-facing normal faults. Mass-wasting has apparently widened this embayment to the east. In addition to this surface erosion, large-scale rotational collapse has created a small slump basin that is visible on seismic profiles and side-scan images.

A single major unconformity is present in both the East and West Arequipa basins and divides the basin fill into two major sequences. Reflectors beneath the unconformity dip to the west, indicating that the leading edge of the forearc has subsided. A model is proposed in which initial extension of the forearc produced block-faulted basement

depressions in which sediment was deposited. Continued extension across the basin caused continued motion on many of the faults, as evidenced by the fanning of reflectors seen on some seismic profiles. As extension continued, faulting became concentrated at one side of each basin and each basin rotated as it subsided, creating the observed half-graben forms. Basin deposition became concentrated in the deeps along the rift boundary faults. Compaction and sediment loading cause basin sediments to dip toward the axes of the basins. Localized uplift of the bounding structural highs may also contribute to the landward dip of basin sediments.

This model for the evolution of the forearc slope basins fits in well with the pattern of tectonic erosion of the forearc that has been observed along much of the Peru-Chile Trench. The fact that extensional structures are particularly well-developed in the Arica Bight area may be due to the curving subduction zone that enhances extension in the Arica Bight area at the expense of areas to the north and south, as the South America plate advances westward over the subducting slab.

It is also possible that the extension that formed the forearc slope basins resulted from strike-slip motion of lower forearc slivers that removed support at the base of the slope, causing extension and collapse of the middle and upper forearc.

REFERENCES

Allen, C.R., Transcurrent faults in continental areas, *R. Soc. Philos. Trans., 258*, 82-89, 1965.

Arabasz, W.J., Geological and geophysical studies of the Atacama Fault Zone in northern Chile, Unpub. Thesis, California Inst. Tech., 275 p., 1971.

Armijo, R., and Thiele, R., Active faulting in northern Chile: Ramp stacking and lateral decoupling along a subduction plate boundary, *Earth Planet. Sci. Lett., 98*, 40-61, 1990.

Barazangi, M., and Isacks, B.L., Spatial distribution of earthquakes and subduction of the Nazca plate beneath South America, *Geology, 4*, 686-692, 1976.

Barazangi, M., and Isacks, B.L., Subduction of the Nazca plate beneath Peru: evidence from spatial distribution of earthquakes, *Geophys. J. R. Ast. Soc., 57*, 537-555, 1979.

Barnard, W.D., The Washington continental slope: Quaternary tectonics and sedimentation, *Mar. Geol., 27*, 79-114, 1978.

Bartlett, W.A., Peru fore-arc sedimentation: SeaMARC II side-scan interpretation of an active continental margin, *M.S. Thesis*, University of Hawaii, Honolulu, p. 87, 1987.

Beck, M. Jr., Drake, R.E., and Butler, R.F., Paleomagnetism of Cretaceous volcanic rocks from central Chile and implications for the tectonics of the Andes, *Geology, 14*, 132-136, 1986.

Belderson, R.H., and Kenyon, N.H., Long-range sonar views of submarine canyons, *Mar. Geol., 22*, M69-M74, 1976.

Bergersen, D.D., Morphology and sedimentology of a submarine canyon system on the lower trench slope of the Peru-Chile forearc, Masters Thesis, University of Hawaii, 144 pp., 1989.

Bergersen, D.D., Coulbourn, W.T., Hagen, R.A., Izuka, S.K., Matsumoto, H., and Moberly, R., Morphology and sedimentology of a submarine canyon system along the Peru-Chile forearc, *EOS Trans. Am. Geophys. Un., 68*, 1499, 1987.

Blackinton, J.G., Bathymetric mapping with SeaMARC II: An elevation-angle measuring side-scan sonar system, Ph.D. Dissertation, University of Hawaii at Manoa, Honolulu, 1986.

Bourgois, J., Pautot, G., Bandy, W., Boinet, T., Chotin, P., Huchon, P., Mercier de Lepinay, B., Monge, F., Monlau, J., Pelletier, B., Sosson, M., and von Huene, R., Seabeam and seismic reflection imaging of the Andean continental margin off Peru (4° S to 10° S), *Earth Planet. Sci. Lett., 87*, 111-126, 1988.

Bourgois, J., von Huene, R., Pautot, G., and Huchon, P., JEAN CHARCOT Seabeam survey along ODP Leg 112 northern transect, ODP Leg 112, *in* Suess, E., von

Huene, R., et al., *Proc. ODP, Init. Repts.,112,* College Station TX (Ocean Drilling Program), 131-138, 1988.

Bucher, W.H., Submarine valleys and related geologic problems of the North Atlantic, *Bull. Geol. Soc. Am., 51*, 489-512, 1940.

Cande, S.C., Nazca-South America plate interactions since 50 m.y.b.p., Peru-Chile Trench Offshore Peru, in: Hussong, D.M., Dang, S.P., Kulm, L.D., Couch, R.W., and Hilde, T.W.C., eds., Ocean Margin Drilling Program Regional Atlas Ser., No. 9, Marine Science International, Woods Hole, Mass., sheet 4, 1986.

Cande, S.C., LaBrecque, J.L., Larson, R.L., Pitman, I.W.C., Golovchenko, X., and Haxby, W.F., Magnetic Lineations of the World's Ocean Basins, scale 1:27,400,000, Am. Assoc. Petrol. Geol., Tulsa, OK, 1989.

Carlson, P.R., and Karl, H.A., Development of large submarine canyons in the Bering Sea indicated by morphologic, seismic, and sedimentologic characteristics, *Bull. Geol. Soc. Am., 100*, 1594-1615, 1988.

Coira, B., Davidson, J., Mpodozis, C., and Ramos, V., Tectonic and magmatic evolution of the Andes of northern Argentina and Chile, *Earth Sci. Rev., 18*, 303-332, 1982.

Cooper, P., and Taylor, B., Seismicity and focal mechanisms at the New Britain Trench related to deformation of the lithosphere, *Tectonophysics, 164*, 25-40, 1989.

Couch, R., and Whitsett, R.M., Structures of the Nazca Ridge and the continental shelf and slope of southern Peru, *Mem. Geol. Soc. Am.,154,* 569-586, 1981.

Coulbourn, W.T., Tectonics and sediments of the Peru-Chile trench and continental margin at the Arica Bight, Ph.D. Dissertation, Univ. of Hawaii, 243 p., 1977.

Coulbourn, W.T., Deposition and erosion in a submarine canyon system, Arequipa fore-arc basin off southern Peru, *Geol. Soc. Am. Annual Meeting Abstracts with Program, 20,* A197, 1988.

Coulbourn, W.T., and Moberly, R., Structural evidence of the evolution of fore-arc basins off South America, *Can. J. Earth Sci.,14,* 102-116, 1977.

Coulbourn, W.T., Tectonics of the Nazca plate and the continental margin of western South America, 18° S to 23° S, *Mem. Geol. Soc. Am., 154,* 587-618, 1981.

Cutler, S.T., Geophysical investigation of the Nazca ridge, *M.S Thesis,* University of Hawaii, Honolulu, p. 83, 1977.

Daly, R.A., Origin of submarine canyons, *Am. Jour. Sci., 31,* 401-420, 1936.

Damuth, J.E., Flood, R.D., Kowsmann, R.O., Belderson, R.H., and Goroni, M.A., Anatomy and growth pattern of Amazon deep-sea fan as revealed by long-range side-scan sonar (GLORIA) and high-resolution seismic studies, *AAPG Bull., 72,* 885-911, 1988.

Dewey, J.F., and Bird, J.M., Mountain belts and the new global tectonics, *J. Geophys. Res., 75*, 2625-2647, 1970.

Dickinson, W.R., and Seely, D.R., Structure and stratigraphy of forearc regions, *Bull. Am. Assoc. Petr. Geol., 63*, 2-31, 1979.

Dill, R.F., Contemporary submarine erosion in Scripps Submarine Canyon, Ph.D. Dissertation, Univ. of California, Scripps Inst. Oceanography, 248 pp., 1964.

Erlandson, D.L., Hussong, D.M., and Campbell, J.F., Sediment and associated structure of the northern Nazca plate, *Mem. Geol. Soc. Am.,154,* 295-314, 1981.

Farrar, E., Clark, A.H., Haynes, S.J., Quint, G.S., Conn, H., and Zentilli, M., K-Ar evidence for the post-Paleozoic migration of granitic intrusion foci in the Andes of northern Chile, *Earth Planet. Sci. Lett., 10*, 60-66, 1970.

Farre, J.A., McGregor, B.A., Ryan, W.B.F., and Robb, J.M., Breaching the shelfbreak: Passage from youthful to mature phase in submarine canyon evolution, *in* Staley, D.J. and Moore, J.C., eds., The shelfbreak: Society of Economic Paleontologists and Mineralogists Special Publication no. 33, 25-39, 1983.

Fisher, R.L., Middle America Trench: Topography and structure, *Bull. Geol. Soc. Am., 72*, 703-720, 1961.

Fisher, R.L., and Hess, H.H., Trenches, *in* Hill, M.N., ed., The Sea, v. 3, Wiley, N.Y., 411-436, 1963.

Fisher, R.L., and Raitt, R.W., Topography and structure of the Peru--Chile trench, *Deep-Sea Res., 4,* 423-443, 1962.

Flint, S., Turner, P., and Jolley, E.J., Depositional archetecture of Quaternary fan-delta deposits of the Andean forearc: Relative sea-level changes as a response to aseismic ridge subduction, *Spec. Publs. Int. Ass. Sediment., 12*, 91-103, 1991.

Flood, R.D., and Damuth, J.E., Quantitative characteristics of sinuous distributary channels on the Amazon deep-sea fan, *Bull. Geol. Soc. Am., 98*, 728-738, 1987.

Galli-Olivier, C., Climate: A primary control of sedimentation in the Peru-Chile trench, *Bull. Geol. Soc. Am., 80,* 1849--1852, 1969.

Gates, O., and Gibson, W., Interpretation of the configuration of the Aleutian Ridge, *Bull. Geol. Soc. Am., 67*, 127-146, 1956.

Gnibidenko, H.S., and Svarichevskaya, L.V., The submarine canyons of Kamchatka, *Mar. Geol., 54*, 277-307, 1984.

Gould, H.R., Turbidity Currents, *In* Smith, W.O., Vetter, C.P., and Cummings, G.B., (Eds.), Comprehensive Survey of Sedimentation in Lake Mead, 1948-49, *USGS Prof. Paper 295*, 201-207, 1960.

Greene, H.G., Stubblefield, W.L., and Theberge, A.H. Jr., Geology of the Monterey Submarine Canyon system and adjacent areas, offshore central California, *USGS Open-File Report 89-221*, 30 p., 1989.

Hagen, R.A., Tectonic effects of a subducting aseismic ridge: The subduction of the Nazca Ridge at the Peru Trench, *EOS Trans. Am. Geophys. Un., 72*, 459, 1991.

Handschumacher, D.W., Post Eocene plate tectonics of the eastern Pacific, *in,* The Geophysics of the Pacific Ocean Basin and its Margin, *Am. Geophys. Union Monogr. 19,* 117-202, 1976.

Hartley, A.J., Turner, P., Williams, G.D., and Flint, S., Paleomagnetism of the Cordillera de la Costa, northern Chile: Evidence for local forearc rotation, *Earth Planet. Sci. Lett., 89*, 375-386, 1988.

Heki, K., Hamano, Y., Kinoshita, H., Taira, A., and Kono, M., Paleomagnetic study of Cretaceous rocks of Peru, South America: Evidence for rotation of the Andes, *Tectonophysics, 108*, 267-281, 1984.

Hervé, M., Movimiento sinistral en el Cretácico inferior de la Zona de Falla de Atacama, al norte de Paposo (24° S), *Rev. Geol. Chile, 31*, 37-42, 1987.

Hilde, T.W.C., Sediment subduction versus accretion around the Pacific, *Tectonophysics, 99*, 381-397, 1983.

Hilde, T.W.C., and Warsi, W.E.K., Magnetic anomaly profiles along ship tracks and lineations, Peru-Chile Trench Offshore Peru, Atlas 9, sheet 4, Ocean Margin Drilling Program Reg. Atlas Ser., edited by D.M. Hussong et al., Marine Science International, Woods Hole, Mass., 1986.

Honza, E., Basic framework of the island arc systems in the NW Pacific margin, (abstr.) Int. Geodyn. Conf., Tokyo, 54, 1978.

Huchon, P., and Bourgois, J., Subduction-induced fragmentation of the Nazca plate off Peru: Mendaña fracture zone and Trujillo trough revisited, *J. Geophys. Res., 95*, 8419-8436, 1990.

Hussong, D.M., Edwards, P.B., Johnson, S.H., Campbell, J.F., and Sutton, G.H., Crustal structure of the Peru--Chile Trench: 8--12S latitude, *in* Sutton, G.H., Manghnani, M.H., and Moberly, R., eds., *The Geophysics of the Pacific Ocean Basin and its Margin, Amer. Geophys. Union, Geophysical Monograph 19,* 71-85, 1976.

Hussong, D.M., Reed, T.B. IV., and Bartlett, W.A., SeaMARC II sonar imagery and bathymetry of the Nazca plate and Peru forearc, ODP Leg 112, *in* Suess, E., von Huene, R., et al., *Proc. ODP, Init. Repts.,112,* College Station TX (Ocean Drilling Program), 125-130, 1988.

Isacks, B.L., Uplift of the central Andean plateau and bending of the Bolivian orocline, *J. Geophys. Res., 93*, 3211-3231, 1988.

James, D.E., Plate tectonic model for the evolution of the central Andes, *Bull. Geol. Soc. Am., 82*, 3325-3346, 1971.

Jarrard, R.D., Terrane motion by strike-slip faulting of forearc slivers, *Geology, 14*, 780-783, 1986.

Johnson, D.W., The Origin of Submarine Canyons: A Critical Review of Hypotheses, Columbia Univ. Press, New York, N.Y., 126 pp., 1939.

Johnson, P.H., Helferty, M., The geological interpretation of side-scan sonar, *Rev. of Geophys., 28*, 357-380, 1990.

Johnson, S.H., and Ness, G., Shallow structure of the Peru margin 12° S - 18° S, *Mem. Geol. Soc. Am., 154,* 525-544, 1981.

Jones, G.M., Hilde, T.W.C., Sharman, G.F., and Agnew, D.C., Fault patterns in outer trench walls and their tectonic significance, *J. Phys. Earth, 26,* Suppl., S85-S101, 1978.

Jordan, T.E., and Alonso, R.N., Cenozoic stratigraphy and basin tectonics of the Andes mountains, 20° - 28° south latitude, *Bull. Am. Assoc. Petrol. Geol., 71*, 49-64, 1987.

Jordan, T.E., and Gardeweg, M.P., Tectonic evolution of the late Cenezoic central Andes (20° - 33°S), in: *The Evolution of the Pacific Ocean Margins, Oxford Monographs*

on Geology and Geophysics, No. 8, Oxford Univ. Press, Inc., New York, 193-207, 1989.

Jordan, T.E., Isacks, B.L., Allmendinger, R.W., Brewer, J.A., Ramos, V.A., and Ando, C.J., Andean tectonics related to geometry of subducted Nazca plate, *Geol. Soc. Am. Bull., 94*, 341-361, 1983.

Katz, H.R., Continental margin in Chile-Is tectonic style compressional or extensional?, *Amer. Assoc. Petrol. Geol. Bull., 55*, 1753-1758, 1971.

Kenyon, N.H., Belderson, R.H., and Stride, A.H., Channels, canyons and slump folds on the continental slope between south-west Ireland and Spain, *Oceanol. Acta, 1*, 369-380, 1978.

Klaus, A., and Taylor, B., Submarine canyon development in the Izu-Bonin forearc: A SeaMARC II and seismic survey of Aoga Shima Canyon, *Mar. Geophys. Res., 13*, 131-152, 1991.

Knebel, H.H., Wood, S.A., and Spiker, E.C., Hudson River: Evidence for extensive migration on the exposed continental shelf during Pleistocene time, *Geology, 7*, 254-258, 1979.

Kono, M., Heki, K., and Hamano, Y., Paleomagnetic study of the central Andes: Counterclockwise rotation of the Peruvian block, *J. Geodyn., 2*, 193-209, 1985.

Kulm, L.D., Prince, R.A., French, W., Johnson, S., and Masias, A., Crustal structure and tectonics of the central Peru continental margin and trench, *Geol. Soc. Am., Memoir 154,* 445-468, 1981.

Kulm, L.D., Schweller, W., and Masias, A., A preliminary analysis of the subduction process along the Andean continental margin 6° to 45° S, *in* Talwani, M., and Pitman, W.C. III, eds., Island arcs, deep sea trenches, and back-arc basins: *Am. Geophys. Union, Maurice Ewing Series, v. 1,* 285-301, 1977.

Kulm, L.D., Thornberg, T.M., Schrader, H., Masias, A., Resig, J.M., and Johnson, L., Late Cenozoic carbonates on the Peru continental margin: Lithostratigraphy, biostratigraphy, and tectonic history, *Mem. Geol. Soc. Am., 154,* 469-507, 1981.

Kulm, L.D., Thornburg, T.M., Suess, E., Resig, J., and Fryer, P., Clastic, diagenetic, and metamorphic lithologies of a subsiding continental block: Central Peru forearc, *in* Suess, E., von Huene, R., et al., *Proc. ODP, Init. Repts.,112,* College Station TX (Ocean Drilling Program), 91-107, 1988.

Lambert, A.M., Kelts, K.R., and Marshall, N.F., Measurements of density underflows from Walensee, Switzerland, *Sedimentology,, 23,* 87-105, 1976.

Langseth, M.G., von Huene, R., Nasu, N., and Okada, H., Subsidence of the Japan Trench forearc region of northern Honshu, *Oceanologica Acta, 4, supplement,* 173-179, 1981.

Leopold, L.B., and Longbein, W.B., River meanders, *Sci. American, 214*, 60-70, 1966.

Leopold, L.B., and Wolman, M.G., River channel patterns: Braided, meandering and straight, *USGS Prof. Paper 282-B*, 39-85, 1957.

Leopold, L.B., and Wolman, M.G., River meanders, *Bull. Geol. Soc. Am., 71*, 769-794, 1960.

Ludwig, W.J., Ewing, J.I., Ewing, M., Murauchi, S., Den, N., Asano, S., Hotta, H., Hayakawa, M., Asanuma, T., Ichikawa, K, and Noguchi, I., Sediments and structure of the Japan trench, *J. Geophys. Res., 71*, 2121-2137, 1966.

Masson, D.G., Fault patterns at outer trench walls, *Marine Geophys. Res., 13,* 209-225, 1991.

Matsumoto, H., Characteristics of SeaMARC II phase data, *IEEE J. Ocean. Eng., 15*, 350-360, 1990.

McGregor, B.A., Stubblefield, W.L., Ryan, W.B.F., and Twichell, D.C., Wilmington Submarine Canyon: A marine fluvial-like system, *Geology, 10*, 27-30, 1982.

McHargue, T.R., and Webb, J.E., Internal geometry, seismic facies, and petroleum potential of canyons and inner fan channels of the Indus submarine fan, *Bull. Am. Assoc. Petrol. Geol., 70*, 161-180, 1986.

Megard, F., The evolution of the Pacific Ocean margin in South America north of Arica elbow (18°S), in: *The Evolution of the Pacific Ocean Margins, Oxford Monographs on Geology and Geophysics, No. 8*, Oxford Univ. Press, Inc., New York, 208-230, 1989.

Megard, F., and Philip, H., Plio-Quaternary tectono-magmatic zonation and plate tectonics in the central Andes, *Earth Planet. Sci. Lett., 33*, 231-238, 1976.

Moore, G.F., Curray, J.R., and Emmel, F.J., Sedimentation in the Sunda Trench and forearc region, *in* Leggett, J.K., ed., Trench-forearc Geology, Oxford, England, Blackwell, 245-258, 1982.

Moore, G.F., and Sender, K.L., Structure of the southwest Panama deformed belt, *in* P. Mann, ed., Geologic and Tectonic Development of the Caribbean Plate Boundary in Southern Central America, *Geol. Soc. Am. Spec. Paper*, in press.

Moore, G.F., and Taylor, B., Structure of the Peru forearc from multichannel seismic reflection data, *in* Suess, E., von Huene, R., et al., *Proc. ODP, Init. Repts.,112*, College Station TX (Ocean Drilling Program), 71-76, 1988.

Mordojovich, C., Sedimentary basins of Chilean-Pacific offshore, *AAPG Studies in Geology, 12*, 63-82, 1981.

Mortimer, C., The evolution of the continental margin of northern Chile, *Proc. of the 24th Int. Geol. Congress, Montreall, Canada, Sect. 8*, 48-52, 1972.

Mortimer, C., and Saric, N., Cenozoic studies in northernmost Chile, *Geol. Rundschau, 64*, 395-420, 1975.

Naranjo, J.A., Interpretación de la actividad cenozoica superior a lo largo de la Zona de Falla Atacama, norte de Chile, *Rev. Geol. Chile, 31*, 43-55, 1987.

Paskoff, R.P., Late Cenozoic crustal movements and sea level variations in the coastal area of northern Chile, *in* Mörner, N.A., ed., *Earth Rheology, Isostacy and Eustasy*, Wiley, New York, N.Y., 487-495, 1980.

Pilger, R.H., and Handschumacher, D.W., The fixed hotspot hypothesis and the origin of the Easter-Sala y Gomez- Nazca trace, *Bull. Geol. Soc. Am., 92*, 437-446, 1981.

Plafker, G., Alaskan earthquake of 1964 and Chilean earthquake of 1960: Implications for arc tectonics, *J. Geophys. Res., 77*, 901-925, 1972.

Raitt, R.W., Fisher, R.L., and Mason, R.G., Tonga Trench, *in* Crust of the Earth, Geol. Soc. Am. Spec. Paper 62, 237-254, 1955.

Rutland, R.W.R., Andean orogeny and ocean floor spreading, *Nature, 233*, 252-255, 1971.

Ryan, W.B.F., Cita, M.B., Miller, E.L., Hanselman, D., Nesteroff, W.D., Hecker, B., and Nibbelink, M., Bedrock geology in New England submarine canyons, *Oceanol. Acta, 1*, 233-254, 1978.

Scanlon, K.M., The continental slope off New England: A long-range sidescan-sonar perspective, *Geo-Marine Lett., 4*, 1-4, 1984.

Scholl, D.W., Christensen, M.N., von Huene, R., and Marlow, H.S., Peru-Chile trench sediments and sea-floor spreading, *Geol. Soc. Amer. Bull., 81*, 1339-1360, 1970.

Scholl, D.W., von Huene, R., Vallier, T.L., and Howell, D.G., Sedimentary masses and concepts about tectonic processes at underthrust ocean margins, *Geology, 8*, 564-568, 1980.

Schumm, S.A., The Fluvial System, John Wiley & Sons, New York, N.Y., 338 pp., 1977.

Schumm, S.A., and Khan, H.R., Experimental study of channel patterns, *Bull. Geol. Soc. Am., 83*, 1755-1770, 1972.

Schumm, S.A., and Khan, H.R., Winkley, B.R., and Robins, L.G., Variability of river patterns, *Nature, Physical Science, 237*, 75-76, 1972.

Schweller, W.J., and Kulm, L.D., Extensional rupture of oceanic crust in the Chile trench, *Marine Geol., 28*, 271-291, 1978.

Schweller, W.J., Kulm, L.D., and Prince, R.A., Tectonics, structure, and sedimentary framework of the Peru-Chile trench, *Mem. Geol. Soc. Am., 154*, 323--349, 1981.

Searle, R.C., Submarine central volcanoes on the Nazca Plate - High-resolution sonar observations, Mar. Geol., 53, 77-102, 1983.

Sender, K.L., Shor, A.N., and Hagen, R.A., SeaMARC II side-scan processing techniques, *EOS Trans. Am. Geophys. Union, 70:43,* 1304, 1989.

Shepard, F.P., Canyons beneath the seas, *Scientific Monthly, 37,* 31-39, 1933.

Shepard, F.P., and Dill, R.F., Submarine Canyons and Other Sea Valleys, McNally, Chicago, Il, 397 pp., 1966.

Shepard, F.P., Marshall, N.F., McLoughlin, P.A., and Sullivan, G.G., Currents in submarine canyons and other seavalleys, AAPG Studies in Geology No. 8, Am. Assoc. Petrol. Geologists, Tulsa, OK, 173 pp., 1979.

Shepard, G.L., and Moberly, R., Coastal structure of the continental margin, northwest Peru and southwest Ecuador, *Geol. Soc. Am. Memoir 154,* 351-391, 1981.

Shor, A.N., SeaMARC II seafloor mapping system: Seven years of Pacific research, *Proc. Pac. Rim 90 Congress, v. III,* 49-59, 1990.

Spencer, J.W., Submarine valleys off the American coasts and in the North Atlantic, *Bull. Geol. Soc. Am., 14,* 207-226, 1903.

St. Amand, P., and Allen, C.R., Strike-slip faulting in northern Chile, (abstr.), *Bull. Geol. Soc. Am., 71,* 1965, 1960.

Stetson, H.C., Geology and paleontology of the Georges Bank canyons, *Bull. Geol. Soc. Am., 47*, 339-366, 1936.

Stubblefield, W.L., McGregor, B.A., Forde, E.B., Lambert, D.N., and Merrill, G.F., Reconnaissance in DSRV ALVIN of a "fluvial-like" meander system in Wilmington Canyon and slump features in south Wilmington Canyon, *Geology, 10*, 31-36, 1982.

Suarez, G., Molnar, P., and Burchfiel, B.C., Seismicity, fault plane solutions, depth of faulting, and active tectonics of the Andes of Peru, Ecuador, and southern Columbia, *J. Geophys. Res., 88*, 10403-10428, 1983.

Suess, E., von Huene, R., and Leg 112 Shipboard Scientists, Ocean drilling program Leg 112, Peru continental margin: Part 2, Sedimentary history and diagenesis in a coastal upwelling environment, *Geology, 16*, 939-943, 1988.

Taylor, B., and Smoot, N.C., Morphology of Bonin fore-arc submarine canyons, *Geology, 12*, 724-727, 1984.

Thiele, R., and Pincheira, M., Tectónica transpresiva y movimiento de desgarre en el segmento sur de la Zona de Falla Atacama, *Chile, Rev. Geol. Chile, 31*, 77-94, 1987.

Thornburg, T., and Kulm, L.D., Sedimentary basins of the Peru continental margin: Structure, stratigraphy, and Cenozoic tectonics from 6° S to 16° S latitude, *Geol. Soc. Am. Memoir 154*, 393-422, 1981.

Thornburg, T.M., Kulm, L.D., and Hussong, D.M., Submarine fan development in the southern Chile Trench: A dynamic interplay of tectonics and sedimentation, *Bull. Geol. Soc. Am., 102*, 1658-1680, 1990.

Tosdal, R.M., Clark, A.H., and Farrar, E., Cenozoic polyphase landscape and tectonic evolution of the Cordillera Occidental, southernmost Peru, *Bull. Geol. Soc. Am., 95*, 1318-1332, 1984.

Turner, P., Clemmey, H., and Flint, S., Paleomagnetic studies of a Cretaceous molasse sequence in the Central Andes (Coloso Formation, northern Chile), *J. Geol. Soc. London, 141*, 869-876, 1984.

Twichell, D.C., and Roberts, D.G., Morphology, distribution, and development of submarine canyons on the United States Atlantic continental slope between Hudson and Baltimore canyons, *Geology, 10*, 408-412, 1982.

Uyeda, S., Subduction zones: An introduction to comparative subductology, *Tectonophysics, 81*, 133-159, 1982.

Veatch, A.C., and Smith, P.A., Atlantic submarine valleys of the United States and the Congo submarine valley, *Geol. Soc. Am. Special Paper 7*, 101 pp., 1939.

von Huene, R., A sedimentary and tectonic history of Lima Basin, an offshore contemporary of Pisco Basin, *in press.*

von Huene, R., Bourgois, J., Miller, J., and Pautot, G., A large tsunamogenic landslide and debris flow along the Peru Trench, *J. Geophys. Res., 94*, 1703-1714, 1989.

von Huene, R., and Culotta, R., Tectonic erosion at the front of the Japan Trench convergent margin,*Tectonophysics, 160,* 75-90, 1989.

von Huene, R., Kulm, L.D., and Miller, J., Structure of the frontal part of the Andean convergent margin, *J. Geophys. Res., 90,* 5429-5442, 1985.

von Huene, R., and Lallemand, S., Tectonic erosion along the Japan and Peru convergent margins, *Geol. Soc. Am. Bull., 102*, 704-720, 1990.

von Huene, R., Langseth, M., Nasu, N., and Okada, H., Summary, Japan Trench transect, *in* Lee, M., Stout L., et al., *Init. Repts. DSDP, 56, 57, part 1,* Washington (U.S. Govt. Printing Office), 473-488, 1980.

von Huene, R., and Miller, J., Migrated multichannel seismic reflection records across the Peru continental margin, *n* Suess, E., von Huene, R., et al., *Proc. ODP, Init. Repts.,112,* College Station TX (Ocean Drilling Program), 109-124, 1988.

von Huene, R., Suess, E., and Shipboard Scientific Party, Ocean Drilling Program Leg 112, Peru continental margin: Part 1, tectonic history, *Geology, 16*, 934-938, 1988.

Warsi, W.E.K., Hilde, T.W.C., and Searle, R.C., Convergence structures of the Peru trench between 10° S and 14° S,*Tectonophysics, 99,* 313-329, 1983.

Whitaker, J.H. McD., Ancient submarine canyons and fan valleys, *in* Dott, R.H. Sr., and Shaver, R.H., eds., Modern and Ancient Geosynclinal Sedimentation, *Soc. Econ. Paleontol. and Mineral. Spec. Pub. 19,* 106-125, 1974.

Zeng, J., Lowe, D.R., Prior, D.B., Wiseman, W.J. Jr., Bornhold, B.D., Flow properties of turbidity currents in Bute Inlet, British Columbia, Sedimentology, 38, 975-996, 1991.

Ziegler, J.M., Athern, W.D., and Small, H., Profiles across the Peru-Chile trench, *Deep-Sea Res., 4,* 238-249, 1957.

Ziel, W., The Andes: A Geological Review, Gebrüder Borntraeger, Berlin-Stuttgart, Germany, 260 p., 1979.